APPLICATION OF THE MNA DESIGN METHOD TO A NON-LINEAR TURBOFAN ENGINE

by

Dr. Gary Leininger

AUTOMATIC CONTROL CENTER

SCHOOL OF MECHANICAL ENGINEERING

January 1981

PURDUE UNIVERSITY
WEST LAFAYETTE, INDIANA
47907

FORWARD

This document represents the final report to the National Aeronautics and Space Administration for work performed under Grant number NSG-3171. The NASA technical monitor was Dr. Bruce Lehtinen, NASA Lewis Research Center, Cleveland, Ohio.

TABLE OF CONTENTS

Page

Chapter I - Introduction. 1

Chapter II - Multivariable Nyquist Array Method. 7

A - Background and Notation 8

B - Perspectives. 14

C - Design Procedure. 22

D - Summary 33

Chapter III - MNA Applied to QCSEE Engine 34

A - QCSEE Turbofan Engine 35

B - Non-Linear QCSEE Simulation and Linear Models 41

C - MNA Design. 46

References. 96

Appendix A - Linear Operating Point Models 99

CHAPTER I

INTRODUCTION

To meet the performance demands of future military and commercial aircraft, propulsion system requirements will make necessary the design and development of substantially more complex engine configurations. These new propulsion systems will dictate the need for advanced multivariable control system design methodologies capable of interrelating the design goals with the physical limitations of the turbomachinery. This means that although steady state operating line conditions will retain their importance in the design specifications further emphasis will be placed on the short term transient performance of the engine. To satisfy these performance requirements, more control variables will be introduced and more output variables will be monitored to evaluate engine performance.

In the early years of jet aircraft propulsion, single-spool turbojets were used almost exclusively. The first control systems for these engines wre hydromechanical and used the principle of the flyball governor extensively

for fuel-rotor speed control [1]. As tubojet engine performance demands increased, a second compressor-turbine section was added to drive a fan to remove energy from the primary jet airstream, thus reducing engine airflow velocity and increasing cycle efficiency. The addition of this second compressor-turbine section enabled greater flexibility of compressor performance at high discharge to intake pressure ratios, but required the control of two mechanically independent turboshafts. Turbofans now power most modern subsonic aircraft and, with afterburners, many high performance supersonic military aircrafts as well.

The turbofan engines in use today are basically fixed-geometry designs. The control system modulates one or two variables and is configured as a set of single loop controllers which are scheduled in an open loop manner according to aerodynamic and environmental conditions. The majority of the control systems have been designed using single-input single-output (SISO) classical frequency response techniques. The resulting control configurations have typically been implemented using hydromechanical or electronic analog components.

As aircraft turbine engines become more complex, additional requirements for the control system will result. Operational requirements will become more stringent thus

necessitating increased control system capability in terms of computational accuracy and static and dynamic response. As performance requirements increase, more variables must be controlled and more engine parameters must be monitored. SISO control system design methods will no longer be appropriate as cross-coupled system interactions must be taken into consideration. Open-loop, trajectory-dependent control designs will yield to closed loop design procedures as the now-standard, analog/hydromechanical devices yield to full authority digital electronic control packages.

Some research and development activity for turbofan engine control systems using modern control theory has been reported by Michael and Farrar [2,3], Stone and co-workers [4], Weinberg [5], and Merrill and Leininger [6]. The most comprehensive application of modern control theory to aircraft propulsion system design was performed by Systems Control Inc. on the Pratt and Whitney F100-PW-100 turbofan engine [7-11]. This LQR control design was successfully tested in an altitude chamber at NASA-LeRC by Lehtinen and co-workers [12,13]. The results of this test demonstrate the effectiveness of modern control theory for highly non-linear sophisticated turbofan applications in addition to providing an evaluation of digital electronic devices for turbofan engine control systems.

In 1977, the F100 sea level static condition was used as the theme problem to explore alternatives for linear multivariable control in a symposium sponsored by the National Engineering Consortium. The results reported in [14] demonstrate the successful application of multivariable frequency domain control system design methods to the F100 design problem.

During the period 1974-1979, the General Electric Corporation, under contract to NASA, designed, developed, and tested an experimental commercial aircraft engine [15,16]. This new Quiet Clean Shorthaul Experimental Engine (QCSEE) incorporates performance and structural characteristics unlike those in any turbofan engine in production today. The QCSEE program introduced high bypass ratios for turbomachinery noise suppression, reversible pitch fan blades for rapid thrust response, total digital electronic engine controls, and extensive use of composites for drag reduction and weight considerations. In addition to fuel flow and fan blade pitch angle, variable nozzle area control is also provided. To incorporate all of these characteristics into a single propulsion system, represents a significant breakthrough in turbofan engine technology.

During the period of development and testing of the QCSEE engine, NASA developed a highly non-linear, accurate,

real-time digital simulation of the engine at sea-level static conditions. This non-linear model was used in extensive tests at the NASA-Ames in-flight simulator facility for test pilot evaluations of integrated engine airframe combinations [17].

Using the non-linear digital simulation as a representative model of the dynamic operation of the QCSEE turbofan engine, a feedback control system is designed in this report by multivariable frequency domain design techniques. Transfer function matrices are generated at each of five power lever settings covering the range of operation from approach power to full throttle, i.e., 62.5% to 100% full power. These transfer functions are then used by an interactive control system design synthesis program to provide a closed loop feedback control using the multivariable Nyquist array (MNA) method [18-20] and the recent extensions to multivariable Bode diagrams (MBD) and Nichols Charts (MNC) [21-22].

The QCSEE design is initially performed holding nozzle area full open with fixed fan blade pitch angle at the power setting of 62.5% of full power. This SISO design is evaluated at other power settings and tested in the non-linear simulation to evaluate engine performance during a power slam from 62.5% to full power (100%).

The second phase of the MNA design uses fuel flow and fan blade pitch angle in realizing a two input two output feedback design. These results are extended to the three input three output system with nozzle area as the third input. This variable is used to provide additional control over inlet-Mach number for noise suppression. In each case, the MNA design is compared with the Standard QCSEE control.

The next chapter details the basic concepts associated with the Multivariable Nyquist Array Method and introduces several recent extensions to the theory. Chapter 3 then uses this design philosophy to determine the closed loop feedback control system for the QCSEE turbofan engine. The successful application of the MNA method clearly demonstrates the effectiveness and utility of the multivariable classical frequency design procedure.

CHAPTER II

MULTIVARIABLE NYQUIST ARRAY METHOD

The Multivariable Nyquist Array (MNA) method is composed of two Nyquist array design procedures: one procedure for the direct polar plane (DNA) and one for the inverse polar plane (INA). Both methods have identical design objectives and are founded upon a common mathematical structure. The principal point of departure is the use and interpretation of the multivariable Nyquist stability criterion in achieving the final system design.

The INA method was first introduced in 1968 [23] based upon the premise that compensator selection to achieve the desired diagonal dominance condition was easier to obtain in the inverse polar plane. In 1974, a more comprehensive description of the INA method became available [24] which also provided the forum for the introduction of the DNA method. Until recently these design methods were considered to be mutually exclusive in the sense that once the open loop design conditions were met in a specific polar plane the closed loop design analysis was restricted to that polar plane. Thus an INA design could not at that time be projected into

the more favored direct polar plane. This led Fisher et al [25] in a comprehensive application study to indicate a preference for the DNA method over the INA method whereas the INA method is used most frequently in Europe.

In this chapter the MNA design objective is briefly reviewed. New theoretical concepts are presented which eliminate the polar plane dependency and establish a foundation for finite frequency range designs. A new graphical design procedure is then introduced which utilizes the fundamental ideas of Bode and Nichols in multi-loop systems.

A. MNA Background and Notation

For the system in Figure 1a, G(s) represents an mxm transfer matrix relating the output vector y(s) to the system input vector u(s). The vector $y_{ref}(s)$ denotes the reference output vector. The design objective is to determine the input vector u(s) such that the system output vector follows the reference vector with dynamics acceptable to the system designer. If, for example, $y_{ref}(s)$ represents a desired set point operation then y(t) should achieve the desired level within prespecified rise time, settling time, and percent overshoot requirements.

To the system of Figure 1a, three square compensators are used to close the feedback loop as in Figure 1b. For reasons which will be apparent later in the development L and F(s) are assumed to be diagonal and K is assumed to be an arbitrary constant matrix. All matrices are assumed to be of rank m. Shifting the constant diagonal matrix L to the left side of the summing junction Figure 1c is obtained. Re-arranging Figure 1c and letting

$$\begin{aligned} Z_{ref} &= L\, y_{ref} \\ Z(t) &= L\, y(t) \end{aligned} \tag{1}$$

the standard MNA block diagram of Figure 1d is obtained.

Let F(s) equal the identity matrix and define

$$Q(s) = L\, G(s) K \tag{2}$$

Following Rosenbrock [24], K and L must be selected such that Q(s) and/or

$$\hat{Q}(s) = \hat{K}\, \hat{G}(s) \hat{L} \tag{3}$$

is diagonal dominant by rows or columns for all s on the standard Nyquist D contour.

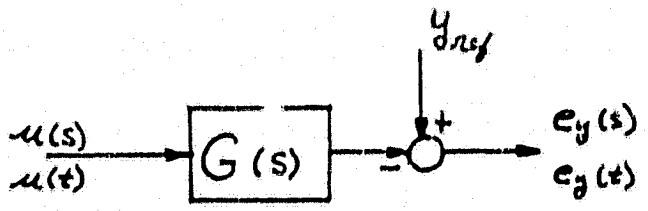

FIGURE 1A: OPEN LOOP SYSTEM

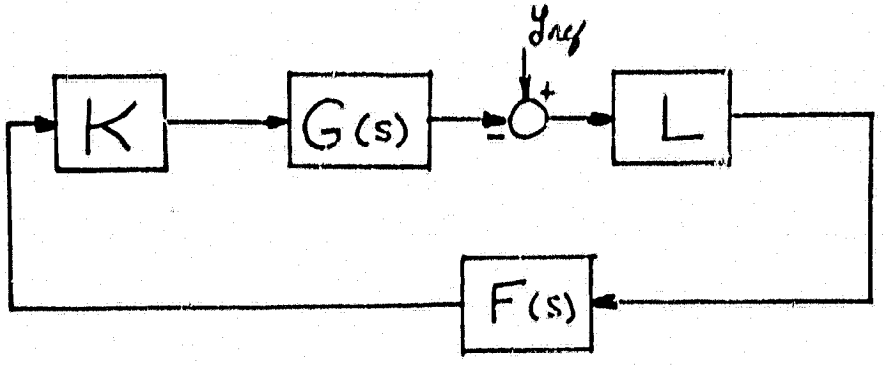

FIGURE 1B: CLOSED LOOP CONFIGURATION 1

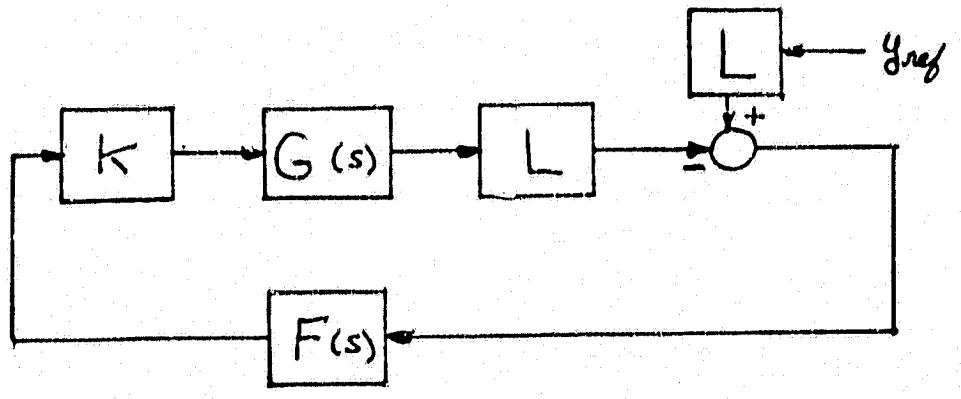

FIGURE 1C: CLOSED LOOP CONFIGURATION 2

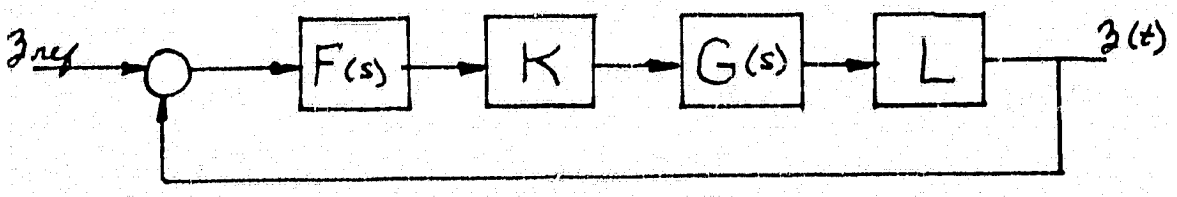

FIGURE 1D: CLOSED LOOP CONFIGURATION 3

The concept of diagonal dominant matrices is well documented [18,23,24] and is defined as follows for the DNA method:

Definition: Let Q(s) be a complex square matrix of dimension m. Then Q(s) is diagonal dominant if either or both of the following conditions exist for all $s \in D$

$$\theta_i^r = \underset{s \in D}{\text{Max}} \sum_{\substack{j=1 \\ j \neq i}}^{m} |q_{ij}(s)|/|q_{ii}(s)| < 1.0 \qquad (4)$$

$$\theta_i^c = \underset{s \in D}{\text{Max}} \sum_{\substack{j=1 \\ j \neq 1}}^{m} |q_{ji}(s)|/|q_{ii}(s)| < 1.0 \qquad (5)$$

where (4) utilizes the rows of Q(s) (row dominance) and (5) uses the columns of Q(s) (column dominance).

Clearly if Q(s) in (2) (or $\hat{Q}(s)$ in (3)) is purely diagonal, then m feedback controllers (and m loop gains) can be designed independently for the uncoupled system. To achieve this degree of independence, K and L would of necessity be complicated functions of s and could result in severe implementation problems. Rosenbrock questioned the need for a purely diagonal open loop transfer matrix Q(s)

and developed a procedure wherein the off-diagonal entries in Q(s) were allowed to be non-zero but of sufficiently small moduli to permit design synthesis by single loop methods. By relaxing the diagonality condition of Q(s) to that of a diagonal dominant Q(s), the compensator matrices K and L in most cases remain constant thus significantly improving the implementation requirements.

Using the above definition for diagonal dominance, Rosenbrock was able to extend the classical SISO Nyquist Criterion to the multivariable case. This development led to a graphical interpretation of the multi-input multi-output (MIMO) Nyquist design objective where the traditional Nyquist curve is replaced by a band of circles. The radii of the circles (called the Gershgorin circles) consist of the sum of the moduli of the off-diagonal terms in Q(s) by rows or by columns. For the DNA method the Gershgorin radii for (4) and (5) become

$$d_i^r(s) = \sum_{\substack{j=1 \\ j\neq i}}^{m} |q_{ij}(s)| \qquad (6)$$

$$d_i^c(s) = \sum_{\substack{j=1 \\ j\neq i}}^{m} |q_{ji}(s)| \qquad (7)$$

Hence, the dominance levels can be written as

$$\theta_i^r = \underset{s\in D}{\text{Max}}\ d_i^r(s)/|q_{ii}(s)| \tag{8}$$

$$\theta_i^c = \underset{s\in D}{\text{Max}}\ d_i^c(s)/|q_{ii}(s)| \tag{9}$$

To determine the elements of K and L, an optimization procedure was developed by Leininger [18,19] based upon the dominance levels in (8) and (9). Fundamentally, the optimization objective is to secure the lowest level of dominance in the respective rows (or columns) using a constant compensator structure. This method of achieving dominance can be used in conjunction with any of the twelve MNA forms and thus significantly reduces the time required to obtain dominance from several weeks (or months) using previous trial and error procedures [24] to several CPU seconds.

Once the compensator pairs have been selected in accordance with the above concepts, the respective control loops can then be designed independently using classical SISO design procedures. The resulting closed loop design configuration can be further reviewed on an individual loop basis through the utilization of Ostrowski's theorem [26].

This theorem provides for the reduction of the Gershgorin radii in loop i based upon the feedback configurations in loops $j \neq i$. Thus a more accurate assessment of the respective phase margins and gain margins can be made.

It is useful at this point in the development to digress from the formalities of the MNA design procedure to closely examine the closed loop structure that has been created above. This analysis will place the MNA design procedure in proper perspective and provide the foundation for subsequent designs using multivariable Bode and Nichols methods.

B. MNA - Perspectives

In most applications of the MNA design method Q(s) (or $\hat{Q}(s)$) cannot be made diagonal dominant when L is the identity matrix and K is constrained to be a constant matrix. The alternatives are therefore to either insert a constant postcompensator matrix or allow K to be a dynamic function of s. To design a K(s) for open loop dominance over a large frequency range would be an extremely cumbersome and tedious task. It is also questionable whether the end result (i.e, dominance of Q(s)) could justify the means by which it was achieved. That is, if

dynamics are to be introduced into the feedforward path, it should be to the benefit of the closed loop design rather than achieving a particular open loop configuration. The problem of inserting loop dynamics to meet design specifications will be addressed in the next subsection.

Consider the utilization of a postcompensator matrix L as indicated in Figure 1-C. Note that the shift of matrix L to the left side of the summing junction completely changes the characteristics of the design problem unless L is constrained to be diagonal. For a non-diagonal L the design problem becomes one in which a linear combination of the system outputs, L y(t), are expected to track a linear combination of the reference values, L y_{ref}. The error vector for this case is thus a linear combination of the output errors,

$$e_y(t) = L(y_{ref} - y(t)) \tag{10}$$

and may become zero for conditions other than

$$y(t) \Longrightarrow y_{ref} \tag{11}$$

However, when L is diagonal the error vector in (10) becomes zero if and only if (11) is satisfied. We therefore, impose this constraint on L and utilize the concept of dominance sharing [19,20] to achieve the desired dominance condition for Q(s) (or $\hat{Q}(s)$).

In Figure 1d, assume F(s) is the identity matrix, L is diagonal, and K and L are constant matrices which have been determined such that Q(s) in (2) is column diagonal dominant. A common misconception associated with MNA methods concerns an alleged modification of the relationship between y(t) and u(t). Clearly, this relationship is always dictated by G(s) and remains intact regardless of the selection of K and L. What is dependent upon K and L, however, is the relationship between the corresponding entries in z(t) and $e_z(t)$,

$$z(s) = Q(s)\ e_z(s) \tag{12}$$

When Q(s) is diagonal dominant, $z_i(s)$ is primarily dependent upon the i th error signal

$$e_{z_i}(t) = z_{ref} - z_i(t) \tag{13}$$

with cross-coupled error signal ($i \neq j$) interactions determined by the degree of dominance achieved and respective loop gains (inherent within the elements of Q(s)).

The i th element in (12) can be written as

$$z_i(s) = q_{ii}(s)\ e_{z_i}(s) + \sum_{\substack{j=1 \\ j\neq i}}^{m} q_{ij}(s)\ e_{z_j}(s) \tag{14}$$

where i = 1, 2, ..., m. Note that although we assumed Q(s) column dominant, it is the row elements of Q(s) which contribute to the interaction terms in (14). To examine this anomaly further, let m = 2 and postmultiply (2) by F as in Figure 1d

$$Q(s)F = L\ G(s)K\ F \tag{15}$$

where F is a diagonal constant gain matrix. Since Q(s) is assumed column dominant, the dominance levels of Q(s) are unaffected by the moduli of the elements of F. Thus (12) becomes

$$z_1(s) = q_{11}(s)\ f_1\ e_{z_1}(s) + q_{12}(s)\ f_2\ e_{z_2}(s) \tag{16}$$

$$z_2(s) = q_{21}(s)\ f_1\ e_{z_1}(s) + q_{22}(s)\ f_2\ e_{z_2}(s) \tag{17}$$

With $|q_{ii}(s)| > |q_{ji}(s)|$ for all $s \in D$ it is clear that the error term $e_{z_i}(s)$ has proportionally more influence on $z_i(s)$ than on $z_j(s)$, $i \neq j$. But note what happens as the gain f_2 is increased with f_1 fixed. The interaction of $e_{z_2}(s)$ on $z_1(s)$ increases while the effect of $e_{z_1}(s)$ on $z_2(s)$ decreases. This interaction influence of the gain matrix F is independent of the respective dominance levels.

Thus low levels of dominance associated with each diagonal entry in Q(s) are not sufficient to insure low inter-

action levels unless the impact of the respective loop gains has been properly addressed. This analysis explains why the DNA (or INA) bands may be very narrow (low dominance levels) yet the closed loop time domain responses indicate high levels of cross-coupled interactions.

To pursue this analysis further, consider the closed loop system of Figure 1d and assume that K and L have been determined for column dominance of Q(s). Shift the diagonal L matrix around the loop as in Figure 2 recognizing that this is the most probable implementation configuration since our interest is in the y(t) vector and not necessarily z(t) where

$$z(t) = L\, y(t) \tag{18}$$

From Figure 1d, the closed loop relationship is

$$Z(s) = (I + LGKF)^{-1}\, LGKF\, Z_{ref}(s) \tag{19}$$

or

$$Z(s) = P(s)\, Z_{ref}(s) \tag{20}$$

with

$$\begin{aligned} P(s) &\triangleq (I + LGKF)^{-1}\, LGKF \\ &= (I + Q(s)F)^{-1}\, Q(s)F \end{aligned} \tag{21}$$

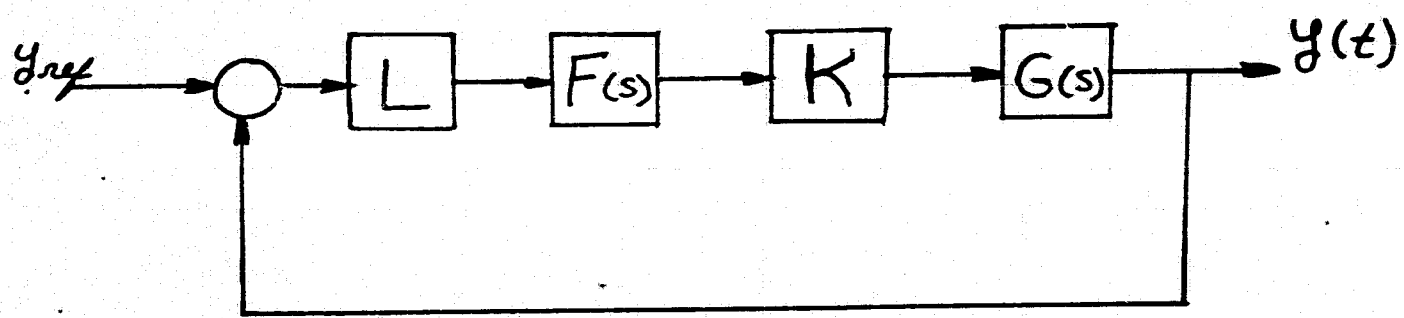

FIGURE 2: CLOSED LOOP SYSTEM WITH L MATRIX SHIFTED

Using Figure 2 the closed loop system is described by

$$y(s) = (I + G(s)\ KFL)^{-1}\ G(s)\ KFL\ y_{ref}(s) \tag{22}$$

or

$$y(s) = H(s)\ y_{ref}(s) \tag{23}$$

$$H(s) = (I + L^{-1}\ Q(s)\ FL)^{-1}\ L^{-1}\ Q(s)\ FL \tag{24}$$

Comparing (21) with (24) if follows that

$$H(s) = L^{-1}\ P(s)\ L \tag{25}$$

or

$$H(s) = \begin{bmatrix} P_{11}(s) & \frac{\ell_2}{\ell_1} P_{12}(s) & \cdots & \frac{\ell_m}{\ell_1} P_{1m}(s) \\ \frac{\ell_1}{\ell_2} P_{21}(s) & P_{22}(s) & & \\ \vdots & & \ddots & \\ \frac{\ell_1}{\ell_m} P_{m1}(s) & \cdots & & P_{mm}(s) \end{bmatrix} \tag{26}$$

Hence, the diagonal elements of the closed loop transfer function matrix are unaffected by the compensator shift. Further, if each control loop is designed for a small steady state error condition (i.e., high loop gains), then the off-diagonal terms in (26) tend to zero and y(t) tracks y_{ref}. If the gain in loop i decreases, then the degree of interaction in loop i from the remaining high gain loops will increase. This interaction effect is not easily detected from the Nyquist array diagrams as it is independent of the dominance levels when using a DNA column or an INA row dominant design objective.

The concerns associated with closed loop interaction levels and system dominance can be resolved simultaneously when using a DNA row and/or an INA column dominance objective. For these MNA design configuration the m^2 elements of K, m elements of L, and the m dynamic compensators of F(s) must be simultaneously selected. In this way, system dominance, loop gains, and response shaping for all loops are addressed simultaneously since they are highly interconnected. As a result of the complexity of these design formats, they have never been seriously considered as viable design procedures.

In the following section recent extensions to the MNA design technique are briefly described.

C. New Design Procedures

The MNA method as originally conceived by Rosenbrock was composed of two design procedures. Each design procedure was relegated to the specific complex plane in which the diagonal dominance conditions was obtained. Stability theorems based upon the extended Nyquist criterion were then developed for each design procedure.

In a typical application of the MNA design methods, $Q(s)$ and $\hat{Q}(s)$ are not, in general, simultaneously diagonal dominant in the Gershgorin sense for all s on the Nyquist D contour. This is due to the fact that

$$\hat{q}_{ij}(s) \neq q_{ij}^{-1}(s) \tag{27}$$

for i, j, and s on D. Hence it was thought that the MNA forms were not compatible, i.e., DNA compensation methods could not be used when INA dominance was obtained and visa versa. This limitation of the MNA design philosophies is removed by introducing a conformally mapped image process.

The details of the imaging process are contained in [20] and will be briefly reviewed.

Assume $\hat{Q}(s)$ is Gershgorin dominant in the inverse polar plane Z where the origin is exterior to the respective Gershgorin bands. Let

$$W = 1/Z \tag{28}$$

represent the conformal mapping from the inverse polar plane to the direct polar plane W. Thus under (28) there exists a one-to-one correspondence between the points $z(s) = x(s) + j\, y(s)$ in the Z plane and the points $w(s) = u(s) + j\, y(s)$ in the W plane. Since (28) is a conformal mapping circles in the Z plane map to circles in the W plane.

Let d(s) represent the radii of the cirlces in the Z plane and r(s) represent the radii of the image circles in the W plane. Then the image center point and image radii are given by

$$u(s) = \frac{x(s)}{x^2(s) + y^2(s) - d^2(s)} \tag{29}$$

$$v(s) = \frac{y(s)}{x^2(s) + y^2(s) - d^2(s)} \tag{30}$$

$$r(s) = \frac{d(s)}{x^2(s) + y^2(s) - d^2(s)} \tag{31}$$

Since the origin is not an interior point of the Z plane circles, the interior of these circles map to the interior of the image circles. Furthermore, the relationship between respective circles in the W plane will be maintained

since (28) is conformal. Hence, any gain and/or phase margins measured with respect to the Gershgorin circles (or envelope) in the Z plane will be retained in the image plane.

This mapping procedure works equally as well when Q(s) is diagonal dominant and the Gershgorin bands are projected into the inverse plane. Note that the imaging process is independent of Gershgorin dominance levels in the image mode as the imaging process retains the dominance levels from the projected domain.

Stability theorems for the image bands as well as further insights into the imaging process are contained in Appendix A. The significance of this theoretical development will become more apparent when the Bode and Nichols methods are discussed for MIMO systems later in this section.

A second limitation of the MNA design methods as proposed by Rosenbrock was the requirement of diagonal dominance for Q(s) or $\hat{Q}(s)$ by rows or by columns over the entire Nyquist D contour. This condition was imposed to ensure that the stability theorems of Rosenbrock would remain valid. For if the system lost diagonal dominance, then the theorems neither confirm nor deny stability.

Since all real systems are band limited (i.e., strictly proper in Rosenbrock's terms), the search for dominance only needs to be checked as w proceeds up the imaginary axis on the D contour. Although this simplifies the search to the customary range of $0 \leq w \leq \infty$ it imposes an excessive burden on the system designer if he knows that frequencies beyond some finite value, w_o, are not likely to contribute to the system response.

In response to this concern, a new theoretical development was introduced wherein the contribution to the MNA or image bands for all frequencies beyond w_o could be properly accounted for. The specific mechanism for finite frequency domain design evaluation and related stability theorems are detailed in [20].

Fundamentally, the contribution to the dynamic response for frequencies beyond some w_o are contained within a circle centered about the origin in the complex plane. The radius of this circle is determined by the moduli of the elements in $Q(s)$ or $\hat{Q}(s)$ at $s = jw_o$. As w_o increases the corresponding circle radii decrease for the DNA method and increase for the INA method. The feedback gains are then selected in accordance with the appropriate array bands and origin centered circles.

The origin-centered circles associated with a finite frequency range evaluation can be conformally mapped to the image plane. In this case the origin is contained within the circle, hence under the mapping principal the interior of the circle in one domain maps to the exterior of the circle in the image domain.

The two new theoretical developments discussed above provide the basis for the equivalence between the multivariable Nyquist array design procedures. As a result, closed loop compensator design analysis and synthesis is no longer restricted to the polar plane in which the desired diagonal dominance condition was obtained. Thus, DNA designs can be used for INA dominance conditions and the desirable INA minor loop synthesis procedures can be used when DNA dominance has been achieved. In addition the theory is now complete for finite frequency dominance.

With this equivalence principal we are now in a position to extend the design synthesis procedure to the magnitude/frequency and phase/frequency planes. The resulting graphical display will allow for design analysis and compensator synthesis using standard Bode techniques. Using the magnitude/phase angle plane, a graphical display for each control loop can be reviewed by the familiar Nichols chart methods.

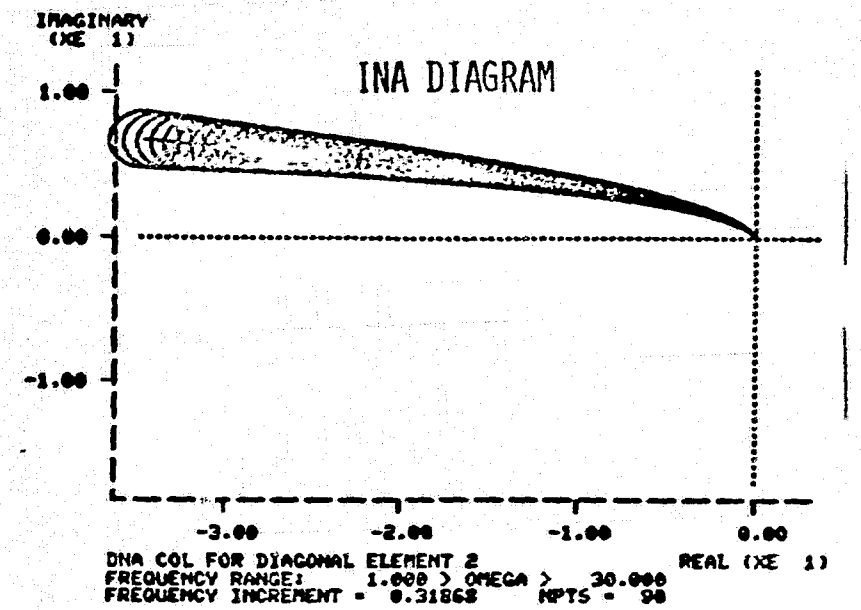

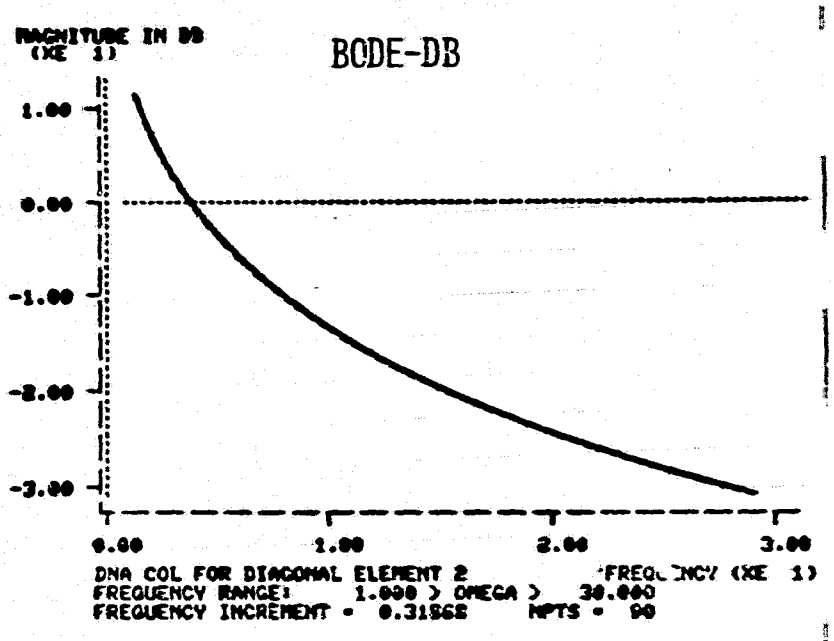

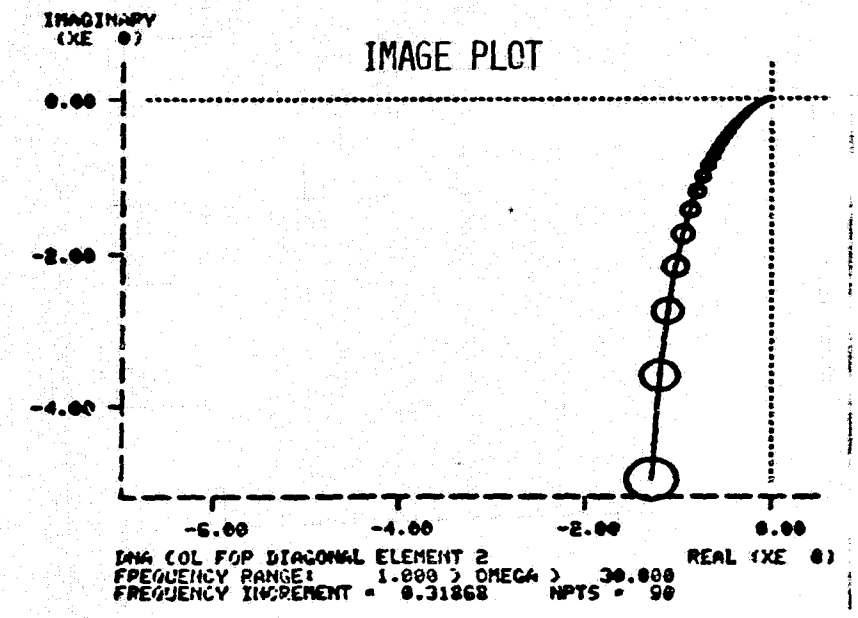

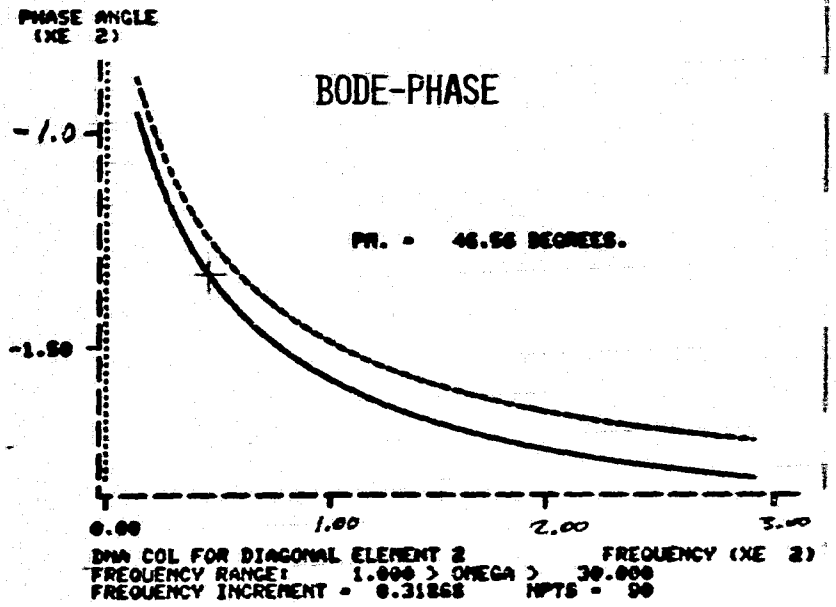

FIGURE 3: TYPICAL INA-IMAGE - BODE-MNA PLOTS

The fundamental concept of multivariable Bode Plots and Nichols Charts to be presented below are described in more detail in [21]. Reference [22] describes a computer aided design suite for closed loop system design and includes all of the graphical procedures referred to in this chapter.

The multivariable Bode diagrams are constructed directly from the data used to calculate a direct polar plane Nyquist diagram. If the OLTF matrix is DNA dominant, the envelope curves [27] of the corresponding Gershgorin radii are each converted to polar form and independently drafted as a function of frequency. When system dominance is obtained in the inverse polar plane, it is necessary to first form the equivalent set of image bands in the direct polar plane. The envelope of the image bands are then used to construct the multivariable Bode diagrams.

Figure 3a represents an INA diagram which is dominant over the finite frequency range $0 \leq w \leq 30$. Figure 3b contains the corresponding image band for Figure 3a with Figures 3c and 3d displaying the Bode information.

Since the mapping between the respective complex polar planes is conformal, it is not necessary to actually compute and/or display the image circles. The envelope curves for the image domain can be computed directly from the envelope curves in the domain in which dominance was achieved.

Theorem

Let $c_1(w)$ and $c_2(w)$ represent the envelope curves for an MNA diagram. The envelope curves, $C_1(w)$ and $C_2(w)$, to the corresponding image circles in the image plane are given by,

$$C_1(w) = [c_1(w)]^{-1} \text{ and } C_2(w) = [c_2(w)]^{-1} \qquad (32)$$

Proof:

The relationships in (32) follow directly from the conformality of the mapping $W = 1/Z$ between the respective polar planes.

Q.E.D.

Thus for an INA system dominant condition, the Bode diagrams can be calculated based upon the inverse of the INA Gershgorin bands. The multivariable Nichols chart is then obtained directly from the data used to construct the Bode diagrams and is presented in Figure 4 for the conditions detailed in Figure 3.

With the graphical analysis procedures described above, system output response shaping can be considered by any of the standard SISO methods. Since INA and DNA design methods are described elsewhere, the remainder of this section will be restricted to the Bode design form.

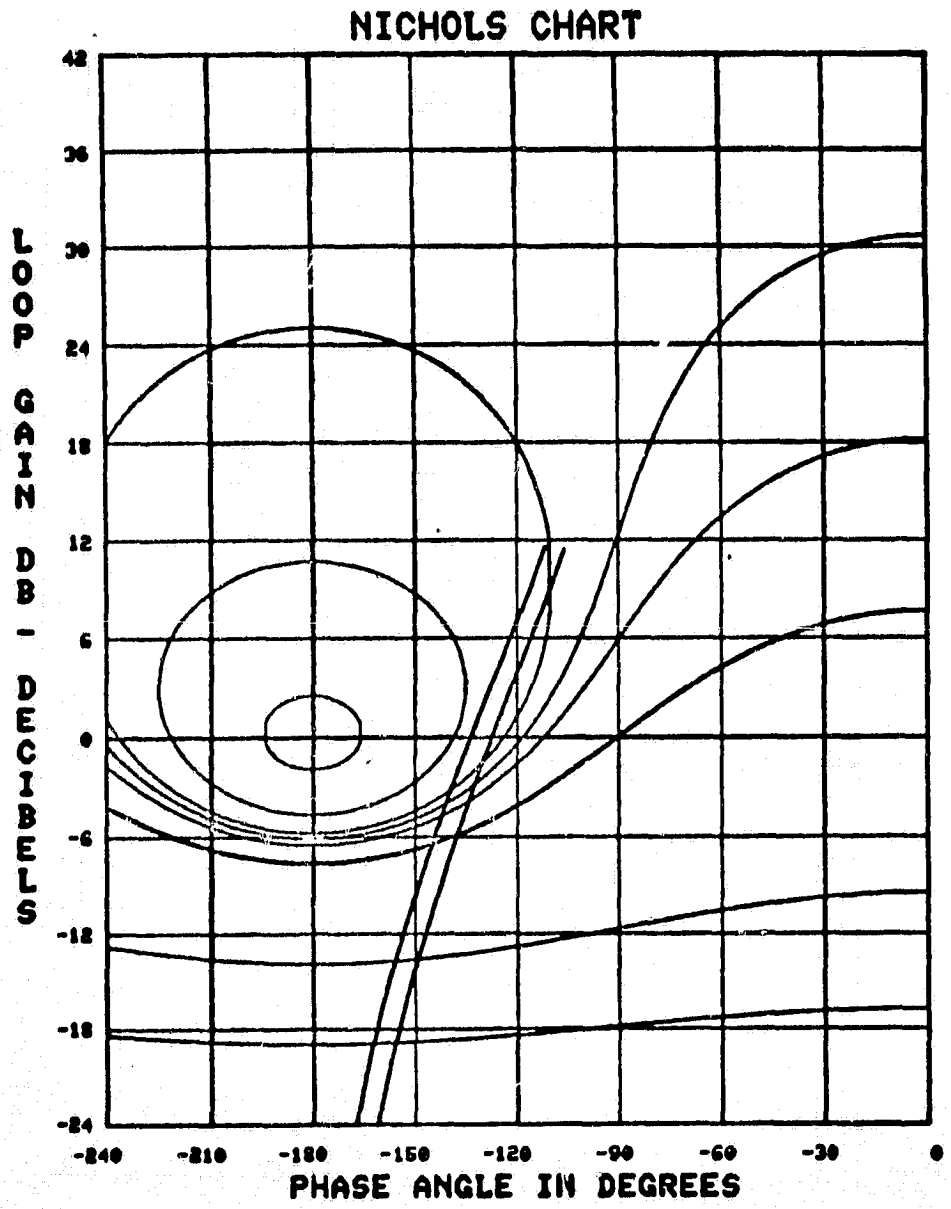

FIGURE 4: NICHOLS CHART FOR FIGURE 3

Consider a DNA column dominant condition for Q(s) in (2), and assume the system is type o. Since the loop gain determined at w = 0 may be low, a reasonably large steady state error could be expected. If the design specification will accept an error no greater than 10%, we may compute the required gain increase using

$$e_{ss} = \frac{1}{1 + f_i \, P_i(0)} \qquad (33)$$

where $P_i(0)$ is the value of the i th Gershgorin envelope (or image DNA envelope) closest to the origin at w = 0. Using this value in (33) ensures that the steady state error will always be less than the required minimum level. Thus

$$f_i = \left[\frac{1 - e_{ss}}{e_{ss}}\right] P_i(0) \qquad i = 1, 2, \ldots, m \qquad (34)$$

Similar relationships can be obtained for type 1 or higher systems.

Inserting (34) into the system will only shift the magnitude curve of the Bode diagram. As the curve is shifted, the closed loop bandwidth of the system (-3 db point on magnitude curve) will be simultaneously affected.

It is also possible the system dominance may be lost as a result of the gain change. This is apparent for those cases in which the 180° phase angle information corresponding to the new zero db crossover point is contained within the phase envelope curves.

This condition, however, does not present any serious complications since we can easily synthesize an appropriate compensator to shift the -180° point outside the phase angle bands at the crossover frequency. This can be accomplished using standard lead, lag, or lead-lag methods. The details of the compensation procedure are described in [21, 22]. Similar procedures apply for type n systems.

It is now apparent that the multivariable Bode diagrams and Nichols chart can play an important role in the effective design of multivariable closed loop systems. In addition, it provides an effective measure of the frequency range over which dominance was obtained. If the desired closed loop bandwidth is beyond the range in which dominance was obtained, new efforts are required to compensate for this deficiency. At the other end of the spectrum, if the zero db crossover frequency is well within the dynamic range, this could reflect too conservative of a frequency range

(i.e., frequency range too large) for dominance acquisition. New design efforts over a reduced range may provide less interaction levels in the bandwidth regions of interest and could improve the overall design significantly.

D. Summary

In this chapter the MNA design procedure was briefly reviewed and new design tactics were introduced. The Image bands play an important role in establishing the equivalence of the INA and DNA design methods and provide the theoretical foundation for viewing the INA Gershgorin envelope curves in the Bode and Nichols domain. The finite frequency development provides the theory needed to reduce the computational burden for the diagonal dominance search. The multivariable Bode diagrams provide a new view of the system design where SISO compensator design procedures can be used effectively to secure dominance and simultaneously achieve the desired closed loop performance. The corresponding multivariable Nichols chart displays the Bode information in a familiar form which again is suitable for design analysis and control system synthesis.

The next chapter utilizes the design procedures and theoretical developments of this chapter to design a closed loop control for the General Electric QCSEE turbofan engine.

CHAPTER III

MNA APPLIED TO QCSEE ENGINE

The turbofan engine selected for the MNA control design study was the quiet clean shorthaul experimental engine (QCSEE) [16]. The QCSEE engine program was a NASA sponsored effort to design, build, and test two experimental engines which would serve as test beds for advanced propulsion technology evaluation. One engine was designed for under-the-wing (UTW) mounting while the second design was developed for an over-the-wing (OTW) mounting. This study was limited to the UTW design.

Turbofan engines of the QCSEE design are under consideration to power shorthaul aircraft of the STOL configuration. These aircraft would operate from small airports located near major urban communities. In this way large transports could land at metropolitan airports many miles from the urban center with passengers and cargo transported to the civic centers via low noise and high reliability STOL aircraft.

To provide these services, primary propulsion requirements for the aircraft are those of low noise levels

and exhaust emissions at all operating levels, rapid thrust response capability including reverse thrust and low weight. The design challenges were met by the General Electric Company.

In the next section the specific design for the QCSEE UTW engine is detailed with principal emphasis placed on the control system design requirements. The following section describes the non-linear digital simulation program developed by NASA from which the linear operating point models for the MNA design are obtained. The last section discusses the results of the control system design study performed using the multivariable frequency domain design procedure.

A. QCSEE Turbofan Engine

A cross-section of the under-the-wing QCSEE turbofan engine design is detailed in Figure 5. The design incorporates performance and structural characteristics unlike those in any engine in production today and includes:

1. An extremely high by-pass ratio (12:1) and a high throat Mach number inlet for noise suppression.
2. Reversible pitch fan blades for rapid thrust response.

QCSEE UTW ENGINE

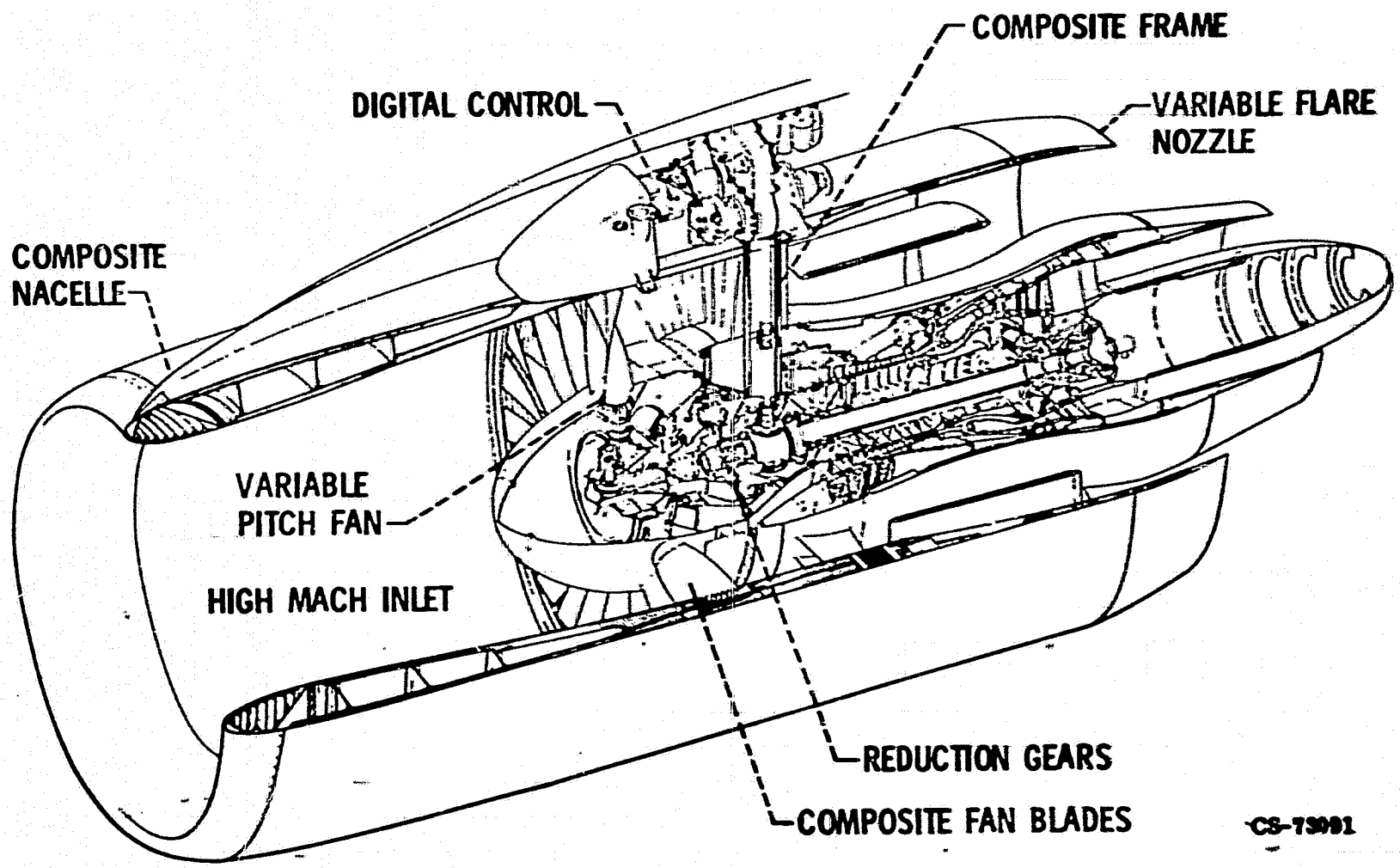

FIGURE 5: QCSEE-UTH ENGINE

3. Geared turbine/fan combination for low fan tip speeds with a high thrust rating.

4. Digital electronic engine controls.

5. Extensive use of composites for drag reduction and weight considerations.

The engine also incorporates a variable area fan duct exhaust and variable compressor stator blades. The fan is driven by the low pressure turbine through reduction gears to achieve an efficient low pressure ratio, low tip speed operation. The variable pitch mechanism is capable of moving the blades from a forward thrust position to a full reverse thrust position in less than one second. In the reverse thrust position, the hydraulically actuated fan duct exhaust nozzle is opened to a flare position to serve as an efficient inlet.

The power requirements of a shorthaul aircraft system dictated the design specifications which had to be met by the QCSEE control. The primary specifications were:

1. to allow the pilot to command percent rated thrust,

2. to assure engine operation at all times within safe engine limits,

3. to control inlet Mach number to meet noise suppression levels,

4. to achieve rapid thrust response (in both forward and reverse modes).

These requirements all relate mainly to safety and noise emission considerations. The first requirement resulted from the desire to decrease pilot work load in a STOL environment. This can be achieved by closing the feedback loops using a parameter closely related to thrust (such as engine pressure ratio) instead of using a parameter indirectly related to thrust (such as spool speed). This reduces the time the pilot must spend adjusting the throttle to achieve the desired thrust level.

The second requirement meant that logic must be incorporated to prevent compressor and fan overspeeds and turbine overtemperature. To meet noise suppression specifications, a high inlet throat Mach number is required to significantly reduce noise radiation from the inlet duct. The requirement for rapid thrust response arises from the need to insure safe STOL operation. In particular, to have a safe go-around capability, thrust changes from 62% (approach power) to 95% of full power must be achieved within one second. This is two to four times as fast as is possible with current production engines.

The above control system requirements were met by the engine manufacturer by using an engine mounted digital control system shown in Figure 5. All primary control

functions are programmed on the digital control computer. Digital command signals are sent directly to the three input actuators:

1. fuel flow actuator,
2. fan pitch actuator,
3. nozzle area actuator.

A hydromechanical control provides fuel flow limiting and is also used to provide the command to the compressor variable stator actuators.

An important consideration in the manufacturer's design process was the control mode selection. This is the process of pairing the four control variables with four output variables. The mode selection was made such that at key, selected steady-state operating conditions, primary (unmeasurable) performance variables such as thrust, specific fuel consumption, and stall margins are relatively insensitive to small sensor inaccuracies. The result of the mode selection process for the QCSEE UTW engine control was to pair fan speed with fan pitch angle, engine pressure ratio (P_{S3}/P_{T0}) with fuel flow and inlet Mach number with fan duct nozzle area. The core stators were controlled essentially independently, being scheduled (according to standard practice) as a function of corrected core compressor speed.

The steady state operation of the QCSEE engine is determined by a set of demand schedules. These schedules command optimum values of engine pressure ratio (EPR), inlet Mach number and fan speed as functions of the pilot's power request and ambient conditions. In particular, the EPR schedule is a monotonic increasing function of the power request. The inlet Mach number is scheduled to be a constant 0.79; however, at low power (less than 70% of maximum), the nozzle is full open and the Mach number then varies with power request. The fan speed is scheduled as a constant value for power requests above 55%. Below that value, fan pitch is at its minimum allowable setting and hence fan speed varies with power request. Keeping fan speed constant means that thrust can be rapidly modulated without the necessity of waiting for the rotor speeds to change. This is especially important when attempting to meet the stringent thrust response requirement of one second between a 62% to 95% power request change.

In addition to the steady state schedules, a number of limit schedules are incorporated for engine protection. Fuel flow is limited by maximum fan speed, core speed, and fan turbine inlet temperature schedules. Also fan pitch and nozzle area controls have maximum and minimum limit schedules. And finally, closed loop proportional plus integral control

was implemented on EPR, fan speed and inlet static pressure (inlet Mach number) to insure that these three outputs follow their respective demand schedules.

The QCSEE control designed using the Multivariable Nyquist Array (MNA) method (described in Chapter 2) makes use of much of the control logic described above. In particular, demand schedules and limit logic designed by the engine manufacturer are used with the MNA design as are the max and min limit logic. However, the MNA design replaces the three independently designed uncoupled servo loops on EPR, fan speed, and Mach number with an MNA-designed pre-compensator matrix, which provides cross-coupling between the command schedules for optimum overall control performance.

In the next section the non-linear digital simulation for the QCSEE engine is described. This simulation is then used to obtain linear models for the MNA design method.

B. Non-Linear QCSEE Simulation and Linear Models

During the hardware test of the UTW engine at the NASA Lewis Research Center, NASA developed a highly non-linear accurate real-time digital simulation of the QCSEE engine at sea-level static conditions. This non-linear model was used in extensive tests at the NASA-Ames in-flight simulator facility for test pilot evaluations of integrated engine airframe STOL configurations [17].

The digital simulation of the QCSEE UTW engine, shown in Figure 7, was based on both steady state, flow-pressure-temperature relationships (maps) for each component (fan, compressor, combustor, etc.) and on dynamic relationships. These relationships are based upon continuity considerations for mass, momentum, and energy.

Maps of pressure and temperature ratio as functions of corrected rotor speed and weight flow are used to model fan tip and also high pressure compressor performance. Compressor variable stators were assumed to be on schedule at all times. Fan hub performance is a polynomial function of fan tip performance. The inlet throat and duct are modeled by static pressure loss relationships. The combustor is represented by a heat addition and a pressure drop, with combustor volume dynamics neglected. Both high and low pressure turbines are represented by maps of flow and enthalpy drop which are functions of pressure ratios across the turbines and corrected speeds. Compressor speed is computed by forming a torque balance between torque generated by the turbine and absorbed by the high pressure compressor. The same procedure is followed to compute fan speed.

The complete non-linear simulation is programmed in Fortran and uses a modified Euler method for integration. It runs much faster than real-time, having a problem time to CPU time ratio of approximately 25 to one on a UNIVAC 1100-40.

The MNA control system design procedure requires linear operating point models. These models can be generated directly from the non-linear digital simulation through the use of a perturbation technique. This procedure (also used to obtain the F100 linear models) [28] produces matrices A, B, C, and D for the standard state variable form model:

$$\dot{x} = Ax + Bu \tag{35}$$

$$y = Cx + Du \tag{36}$$

where x is the system state vector of dimension eight, u is a third order control vector, and y is an eighth order output vector.

For the QCSEE UTW engine the physical variables indicated in Table I were used to define the linear state models. Note that several of the variables in the y(t) vector are not measurable.

To obtain linear models, the following procedure was followed:

1. Run the simulation to steady state operating point conditions.
2. Disconnect integrator inputs and perturb each state variable $x_j(t)$ in turn ($j = 1, \ldots, 8$) by a small amount $\Delta x_j(t)$ from its steady state level.

3. Note the corresponding change in the state derivatives ($\Delta\dot{x}_j(t)$) and outputs $\Delta y_j(t)$. Compute elements of A and C using

$$A_{ij} = \Delta\dot{x}_i/\Delta x_j$$

$$C_{ij} = \Delta y_i/\Delta x_j$$

4. Compute steady state gain relationships between u_j and x_i and y_i by perturbing u_j in turn (j = 1, 2, 3) and allowing the simulation to reach steady state. Note the steady state relationships as

$$\Delta x(\infty) = K_x\ \Delta u(\infty)$$

$$\Delta y(\infty) = K_y\ \Delta u(\infty)$$

5. Determine the B and D matrices as

$$B = -AK_x$$

$$D = K_y - CK_x$$

Following this procedure linear models were obtained for five power demand values, i.e., 62.5, 70, 80, 90, and 100 percent power. The matrices obtained are indicated in Appendix A.

TABLE I

VARIABLES QCSEE-UTW LINEAR MODELS

State Variables

P_{12} - Fan inlet duct total pressure

P_{13} - Fan discharge total pressure

P_4 - Compressor discharge pressure

P_8 - Core nozzle total pressure

NL - Fan speed

NH - Compressor speed

T_3 - Compressor discharge temperature

T_4 - Combustor discharge temperature

Input Variables

XMV - Fuel metering valve position

X18 - Fan nozzle area actuator position

Theta I - Fan pitch mechanism drive motor position

Output Variables

PS_{11} - Engine inlet static pressure

P_{13} - Fan discharge total pressure

P_4 - Combustor pressure

P_8 - Core nozzle total pressure

NL - Fan rotor speed

NH - Compressor speed

T41C - Calculated turbine temperature

FN - Net thrust

C. MNA Design

The MNA control systems designs to be discussed in this section utilize the state equations of Appendix A augmented by one state variable for each integrated input variable. This integral control action eliminates steady state offset and conforms to the standard QCSEE control form. Since all control loops utilize integral control action, the entries in the transfer function matrix, G(s), were modified appropriately. Thus, the resulting MNA designs could be implemented directly in the non-linear simulation for design evaluation.

The first MNA design for the QCSEE-UTW engine assumes nozzle area to be fixed at the full open position and fan pitch angle fixed at the 62.5% of full power position. With these two control inputs fixed at their respective values, the only input variable to be determined then is fuel metering valve position. For this SISO condition, combustor exit pressure (P_4) was selected as the output variable to be controlled as it is most representative of system thrust response.

From the linear models of Appendix A, transfer functions augmented with integral control action for P_4/X_{mv} at each operating point are obtained. For the 62.5% condition, the Nyquist, inverse Nyquist, and Bode diagrams are indicated

in Figure 6 for a feedback gain of 0.04. The phase margin is 29.90 degrees with an infinite gain margin. The closed loop bandwidth at this design point is approximately 10. radians with the feedback control

$$X_{mv} = -.04\ P_4 \tag{37}$$

To examine the effect of this control at each of the other four operating points (70%, 80%, 90%, and 100%) the composite Nichols chart of Figure 7 may be used. Here each curve represents the respective Nichols plot for each P_4/X_{mv} transfer function with a gain of 0.04. The 62.5% power curve and the 70% power curve coincide. As the power level increases, the corresponding curves move to the right. This signifies an improvement in phase margin (to 50° at 100% power) with a corresponding decrease in loop bandwidth.

The transient responses of the nonlinear simulation to the SISO design discussed above for a power change from 62% to 70% are indicated in Figures 8A-8D. For reference purposes the transient responses of the simulation using the full GE QCSEE control are also indicated in the figures.

Over the power range 62.5-80% power, the full GE control consists of a SISO X_{mv} control and sufficient control logic (i.e., constraints) to impede movement of X_{18} (nozzle area)

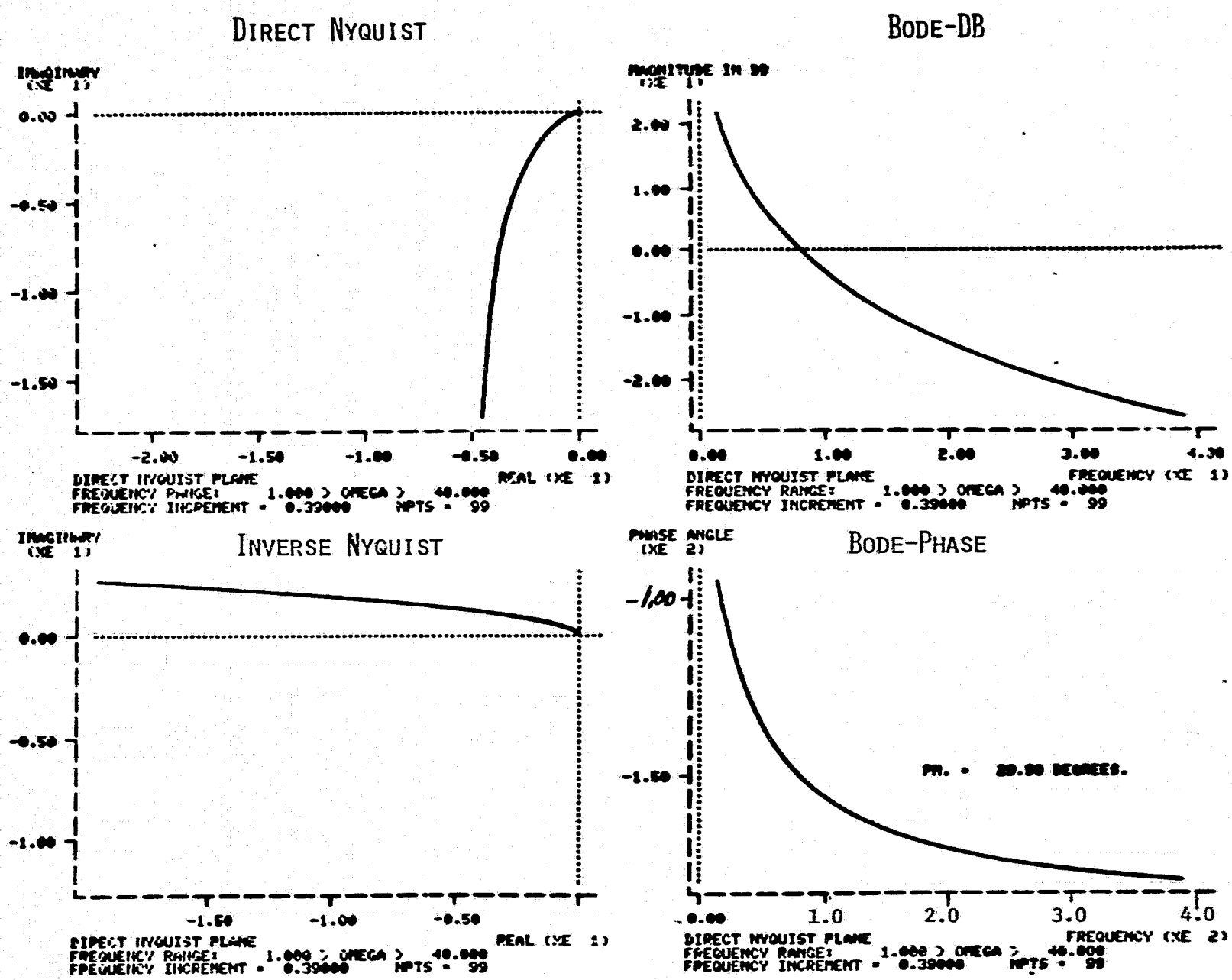

FIGURE 6: SISO-MNA DESIGN-62.5% POWER

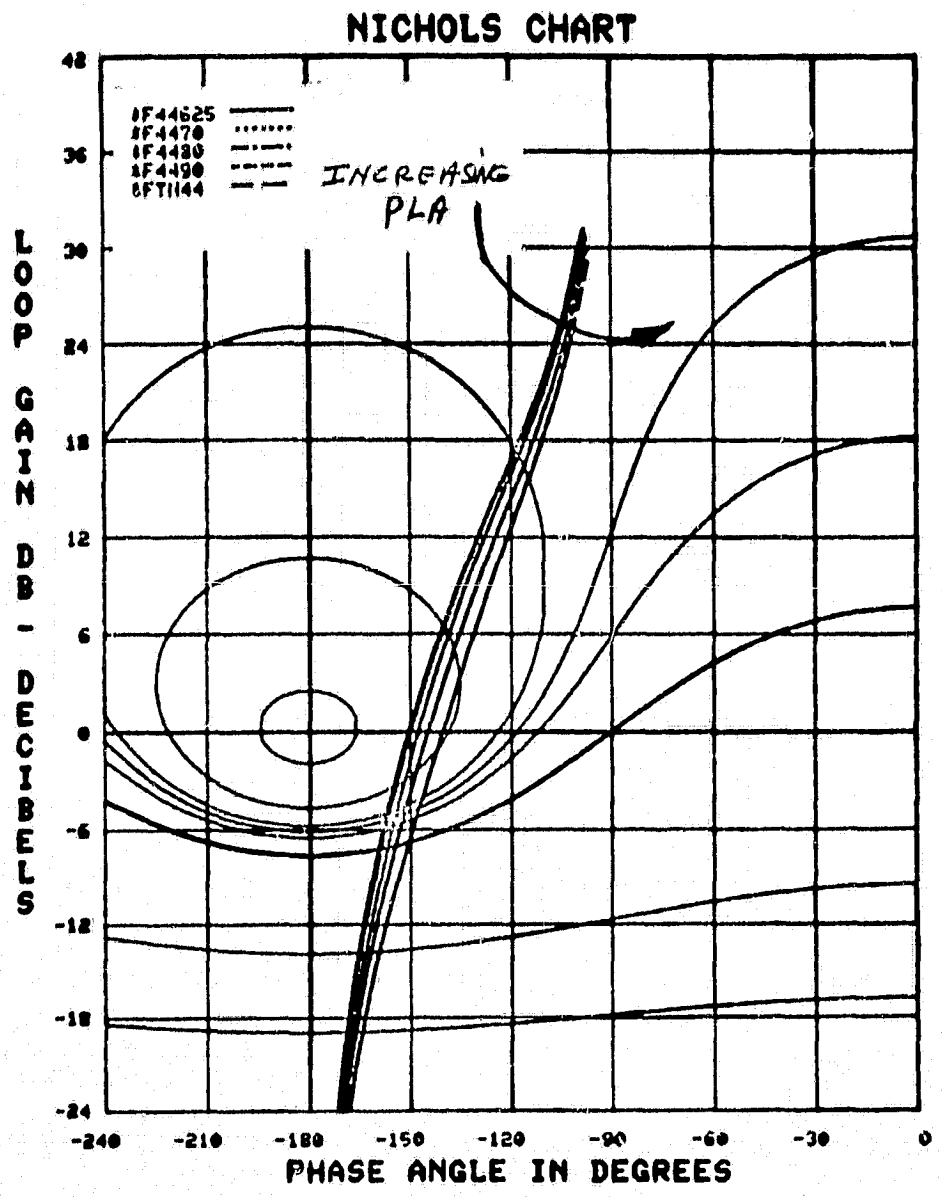

FIGURE 7: NICHOLS CHART FOR SISO DESIGN AS A FUNCTION OF POWER SETTING

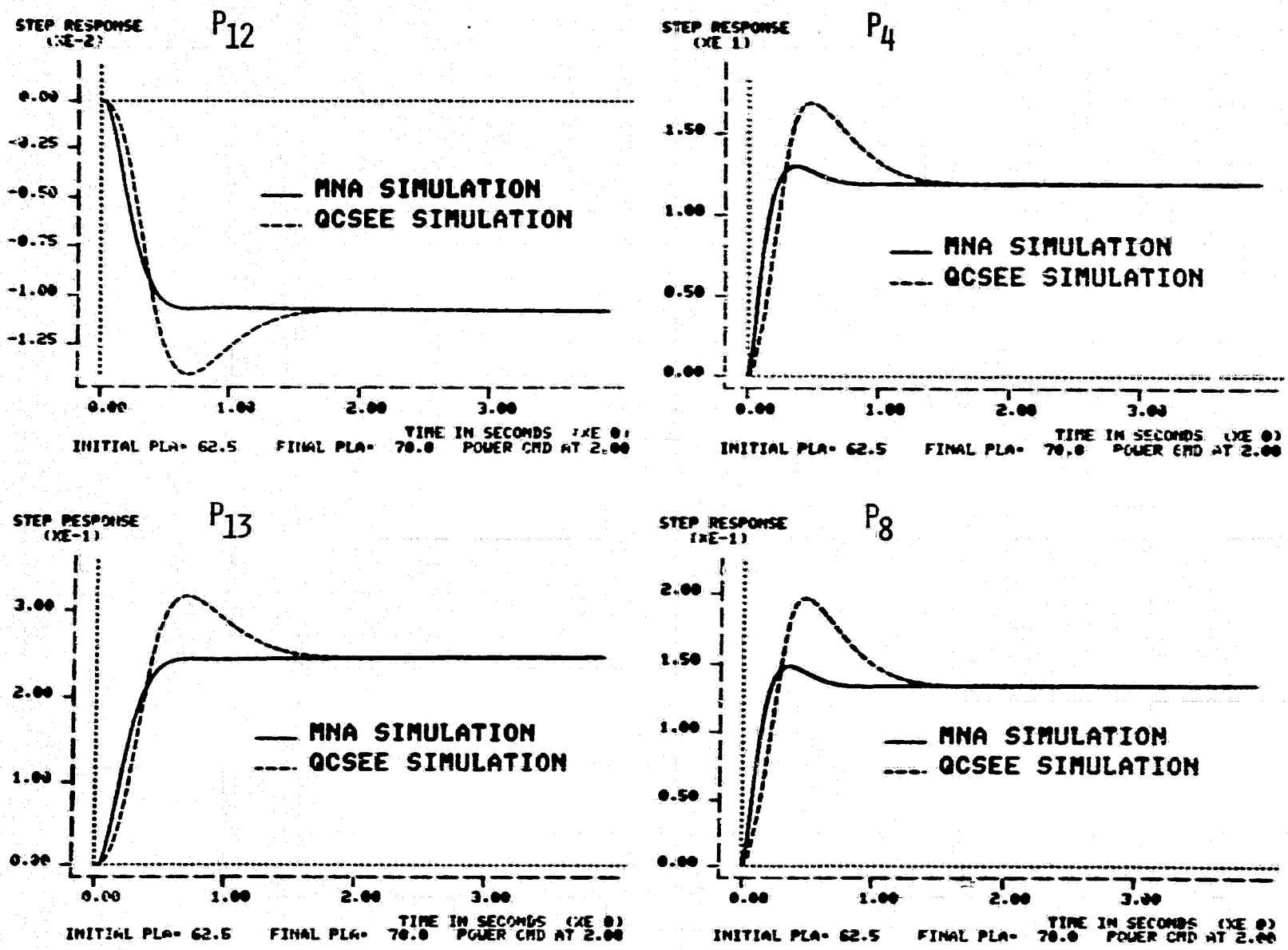

FIGURE 8A: SISO MNA - FULL GE-QCSEE 62.5-70%

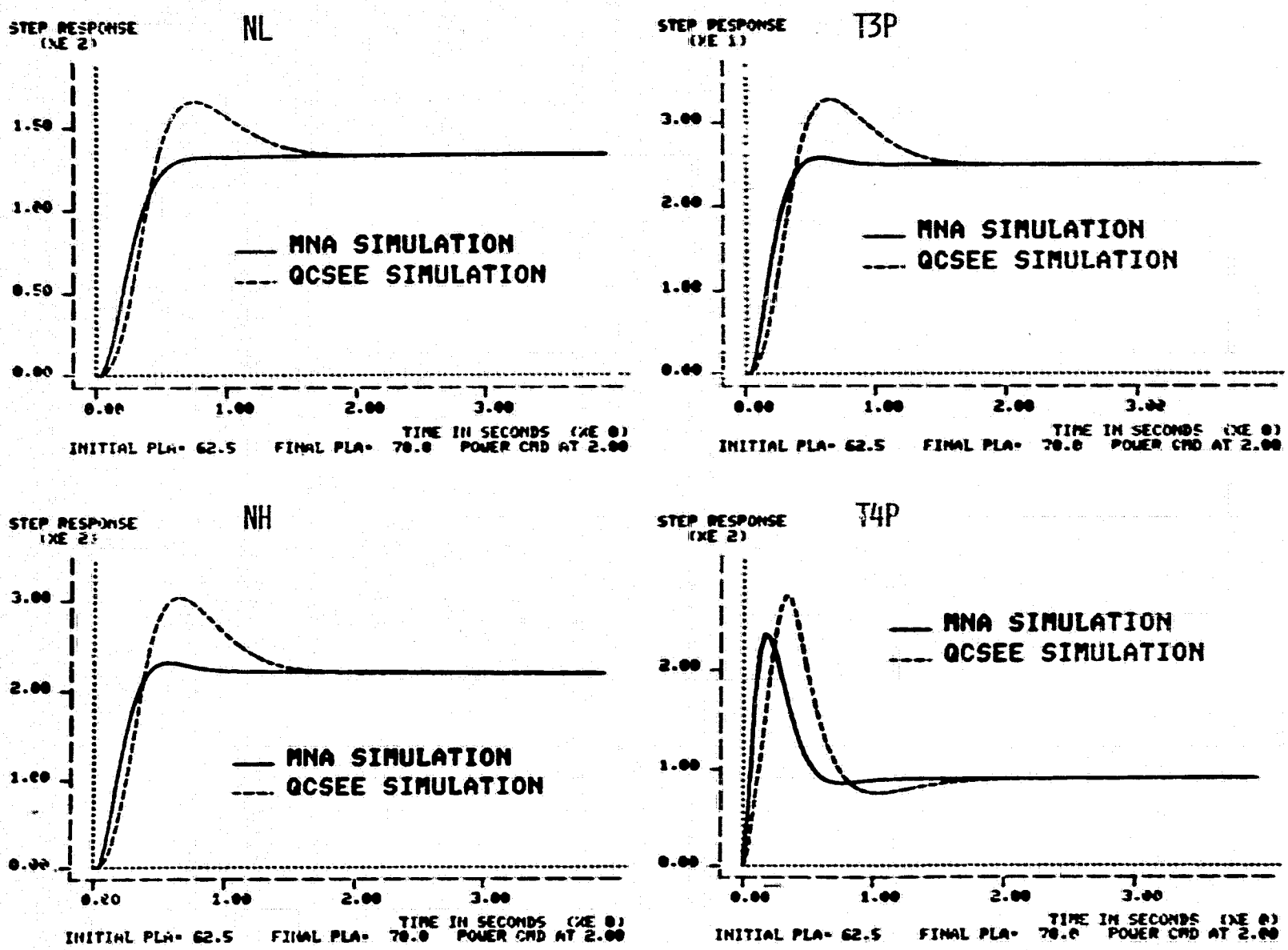

FIGURE 8B: SISO MNA - FULL GE-QCSEE 62.5-70%

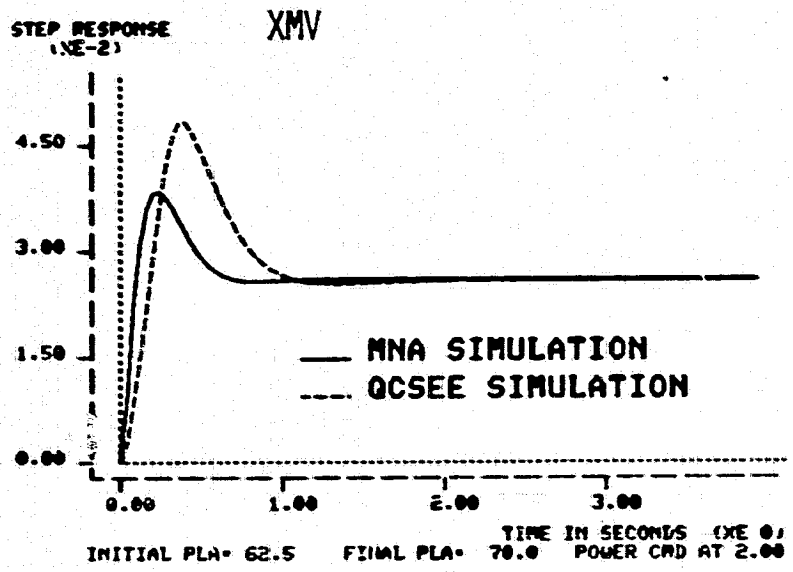

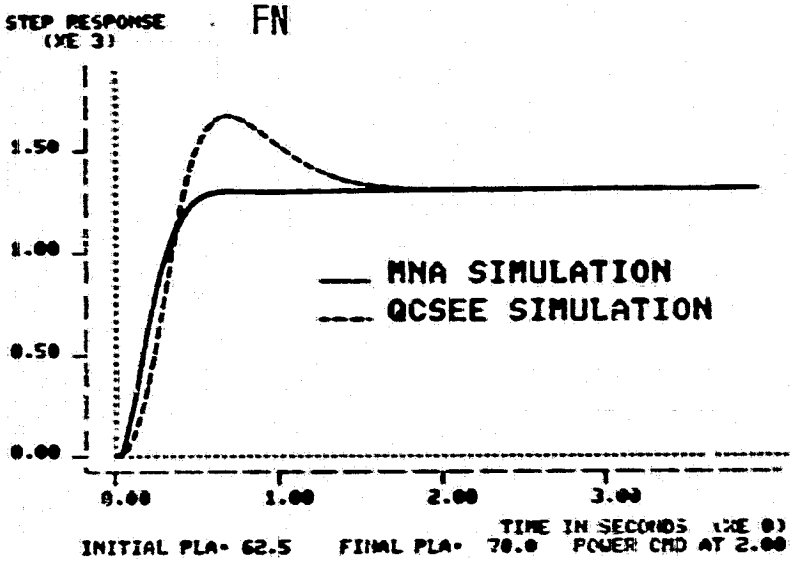

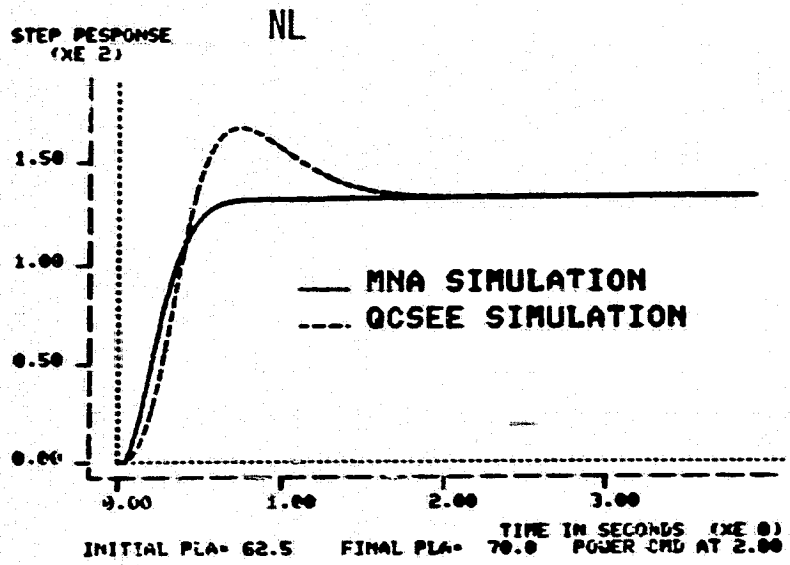

No Change in THETA I or X18.

Figure 8C: SISO MMA - Full GE-QCSEE 62.5-70%

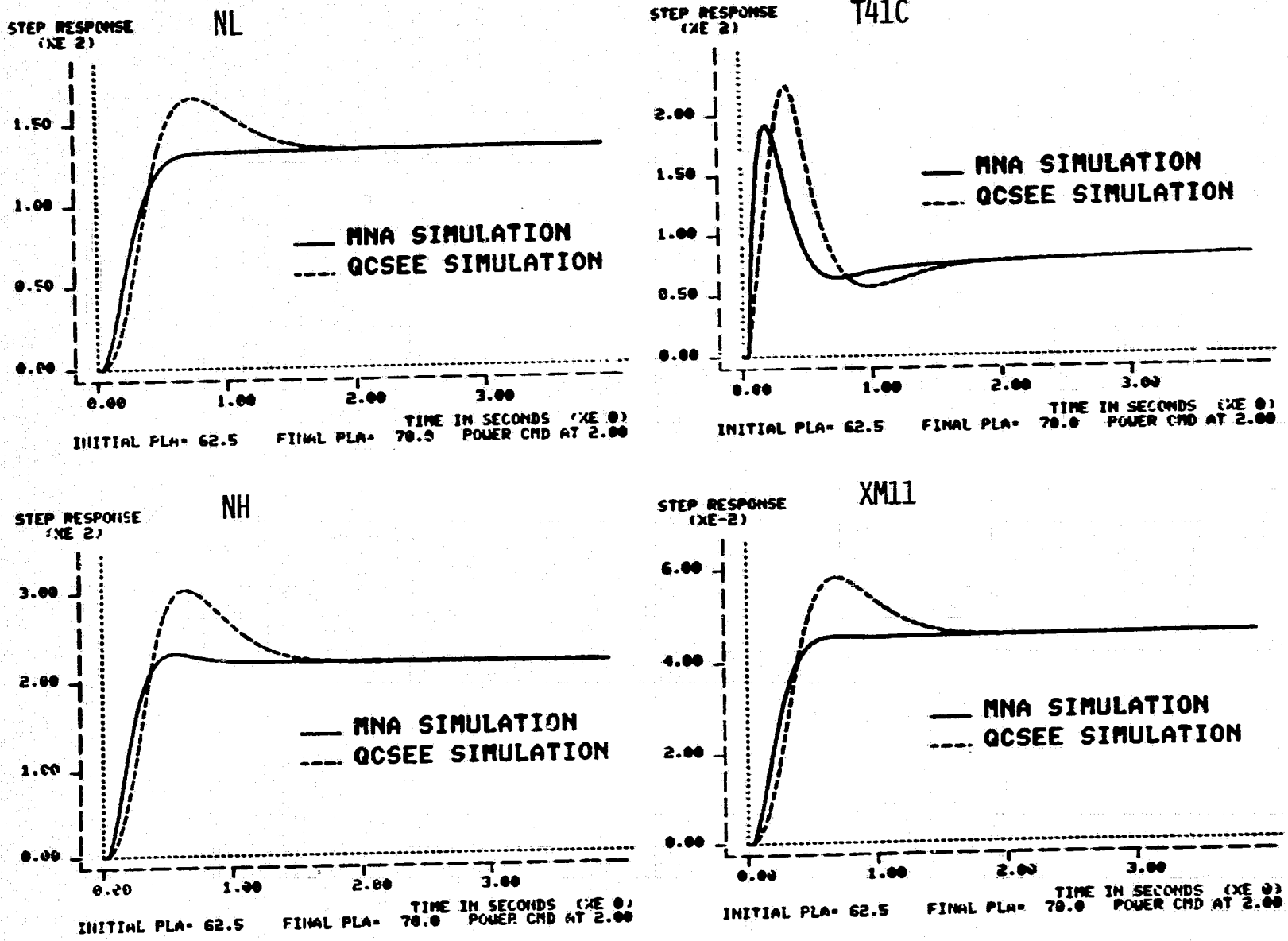

FIGURE 8D: SISO MNA - FULL GE-QCSEE 62.5-70%

and Theta I (fan pitch angle). When the environmental conditions near 80% power are realized, the GE control logic permits Theta I to change, at or near 90% power conditions X_{18} is permitted to vary. It is not surprising, therefore, that the steady state conditions for the SISO MNA and full QCSEE control responses are identical over 62.5-70% full power.

What is surprising, however, is the improved responses for X_{mv}, thrust (FN), and fan speed (NL) of Figure 8C. Since total fuel consumption is the area under the X_{mv} curve, it appears that the MNA control of (37) is more fuel efficient at this operating condition.

To examine the impact of the constant gain control of (37), in light of the Nichols chart of Figure 7, a non-linear simulation run was made for a power slam situation, i.e., 62.5% to 100% full power. Here the engine command setting of 100% full power was requested from the 62.5% operating point condition. The corresponding transient responses for the MNA-SISO and full GE controls are indicated in Figures 9A-9D.

From these responses it can be seen that fan speed (NL) and inlet duct pressure (P_{12}) are significantly higher for the MNA-SISO design than for the full GE QCSEE control. However, engine thrust (FN) and total fuel consumption (area

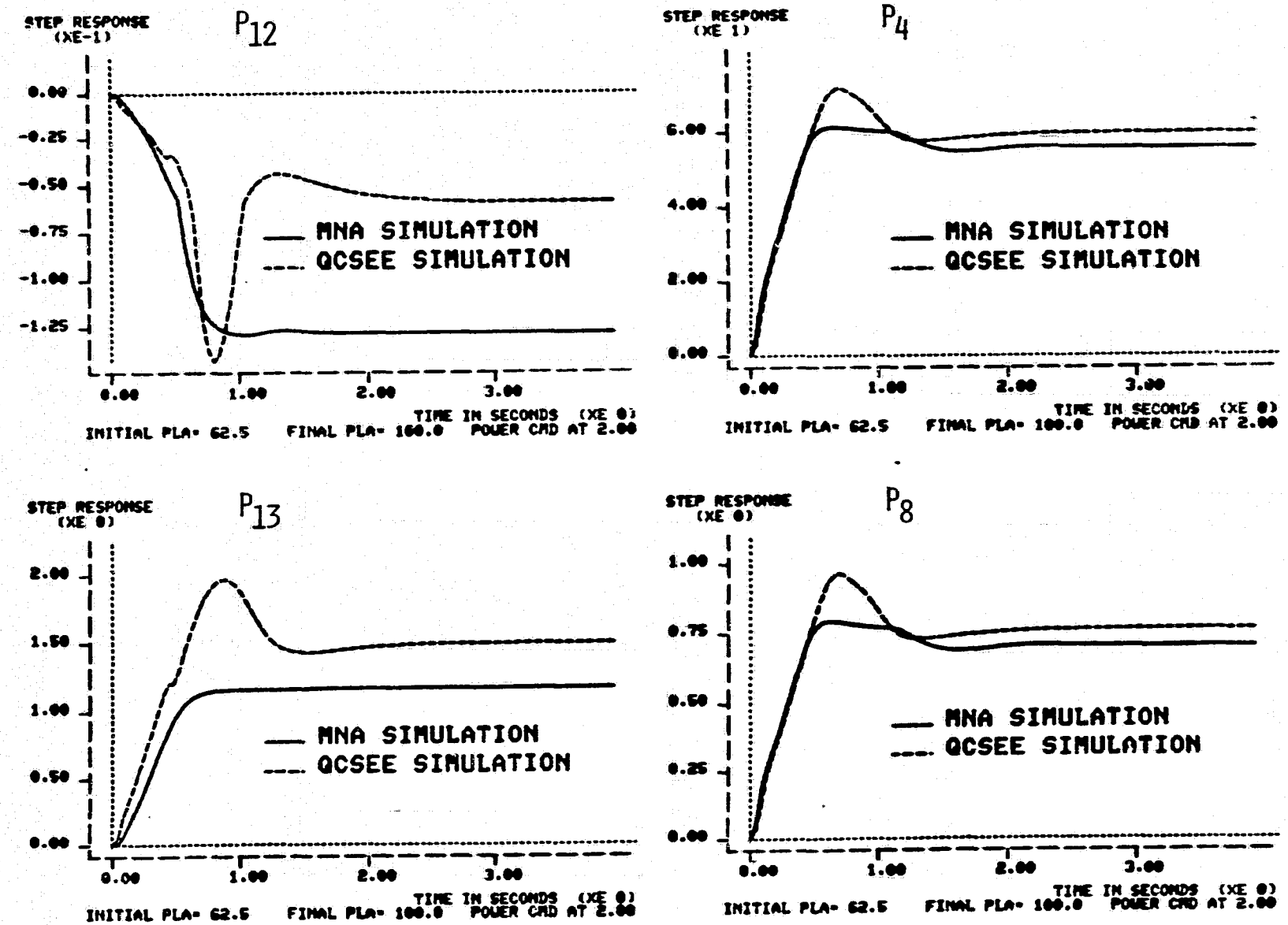

FIGURE 9A: SISO MNA - FULL GE-QCSEE 62.5-100%

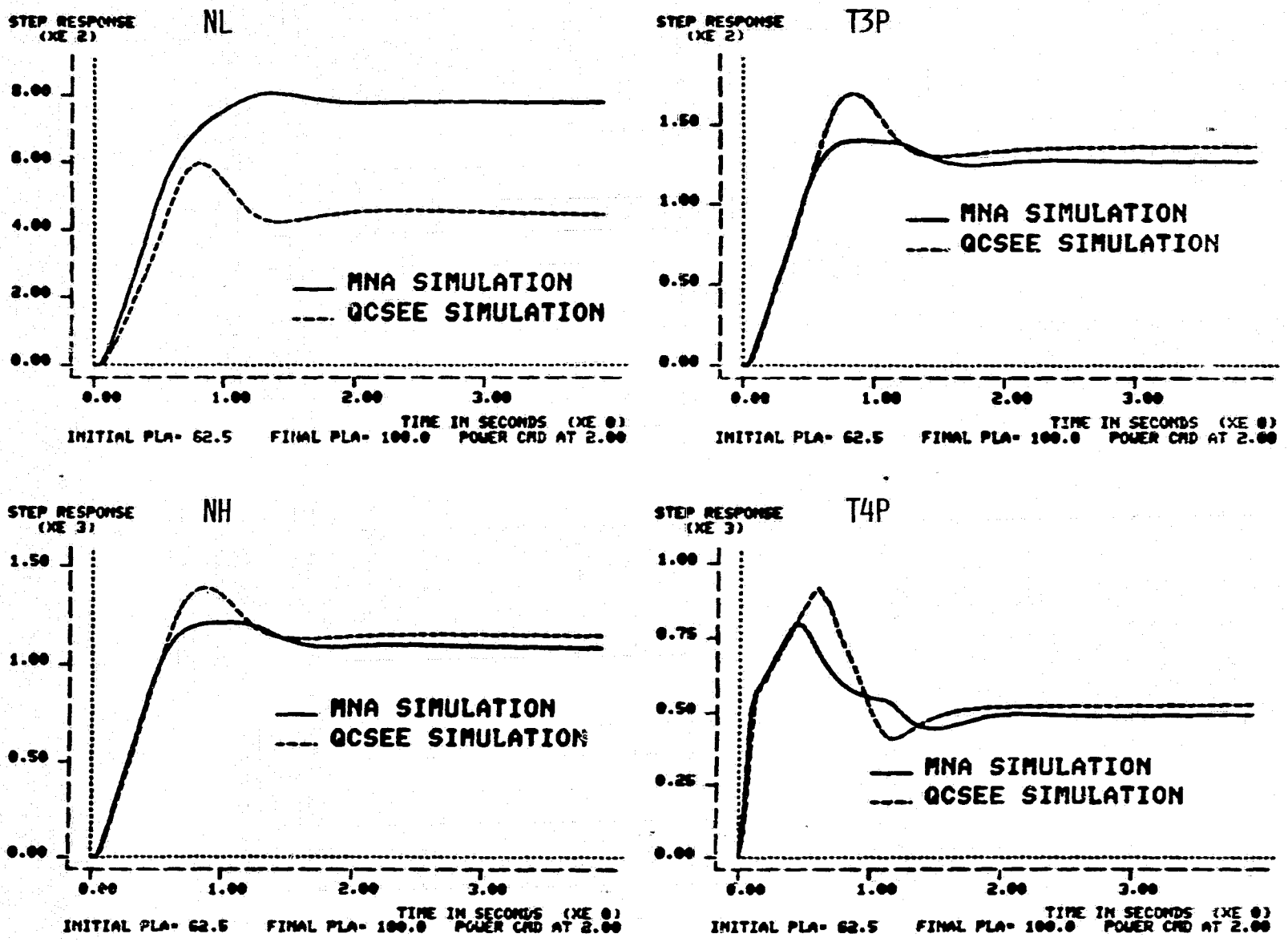

FIGURE 9B: SISO MNA - FULL GE-QCSEE 62.5-100%

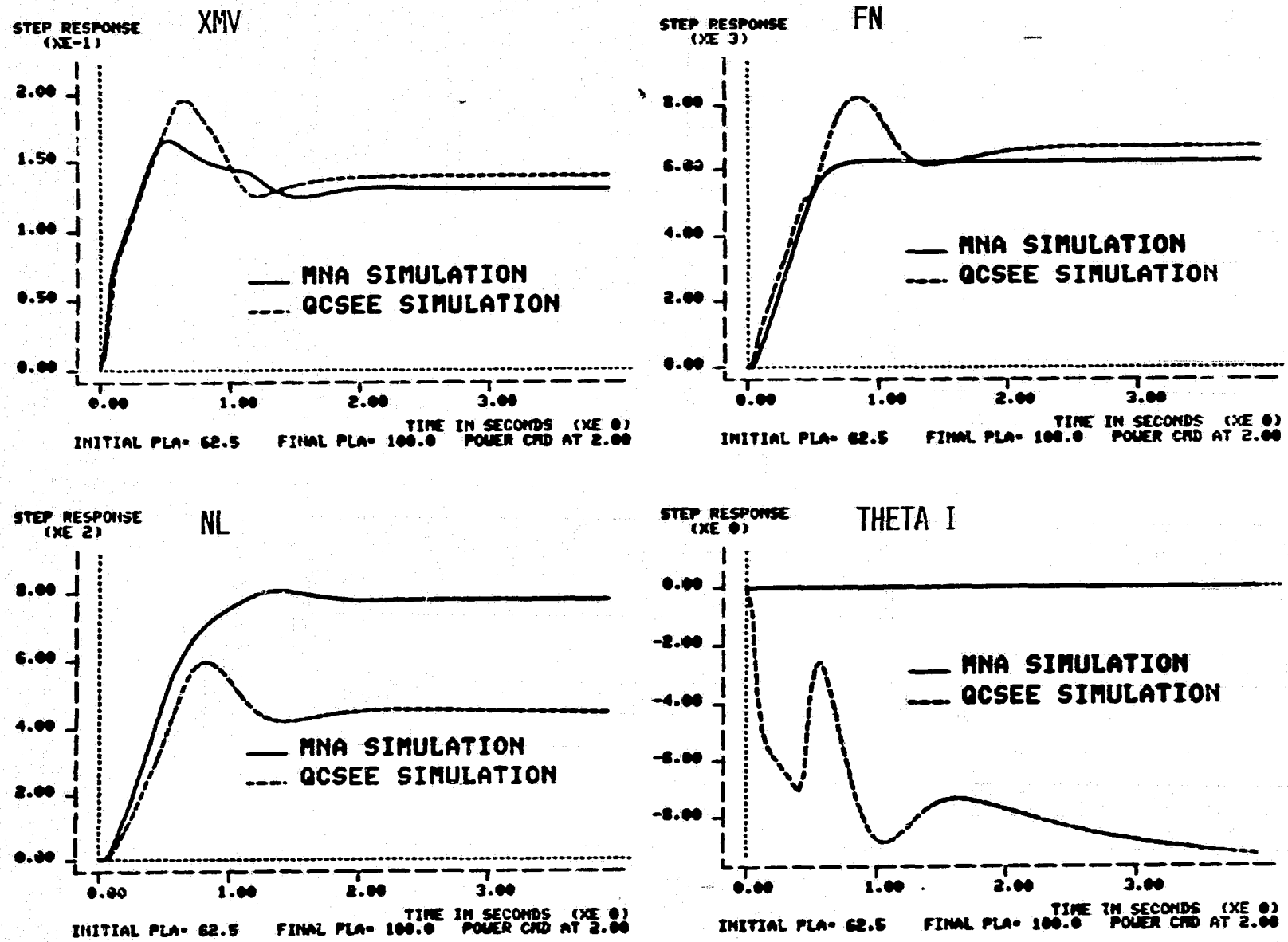

FIGURE 9C: SISO MNA - FULL GE-QCSEE 62.5-100%

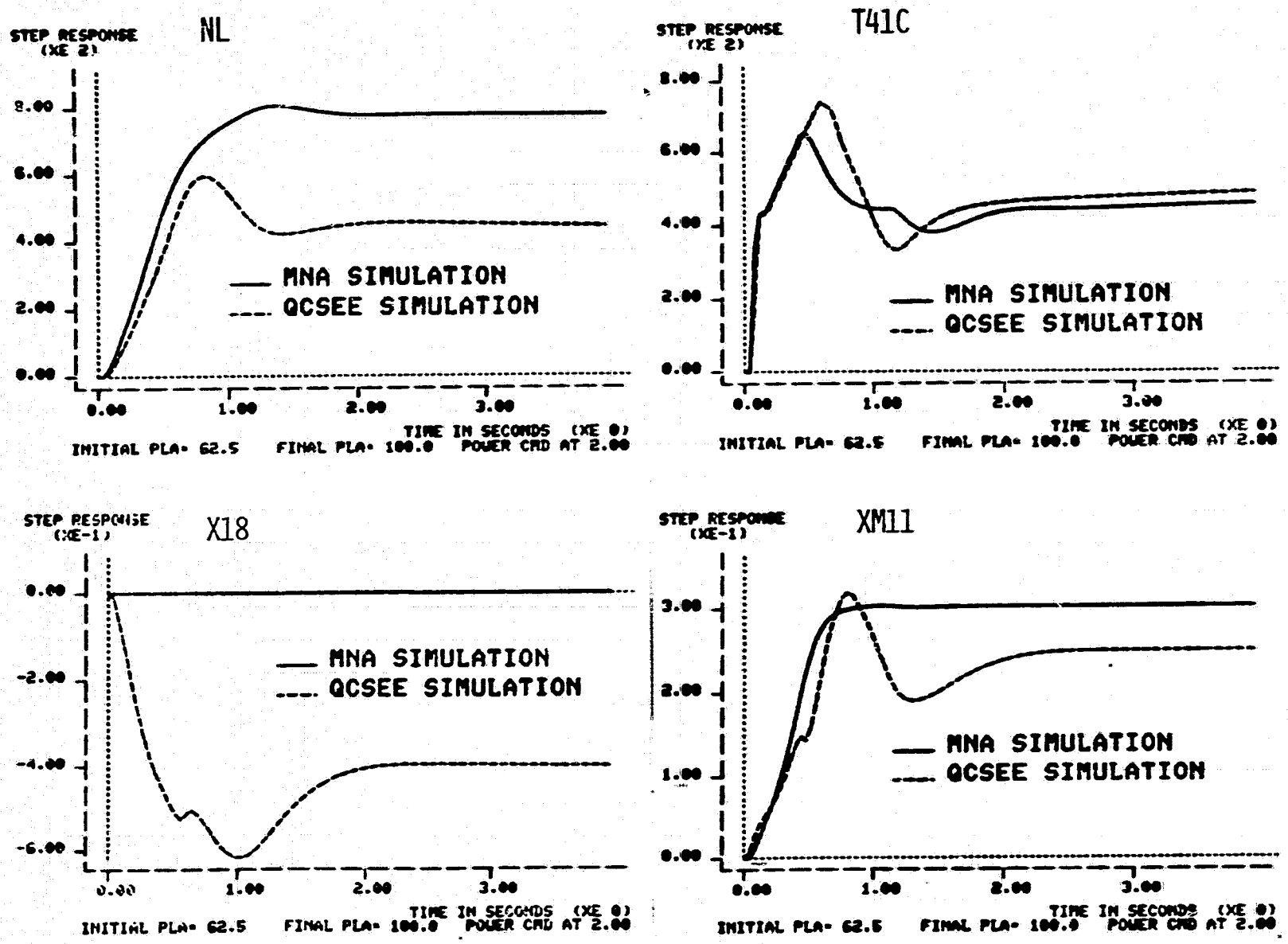

FIGURE 9D: SISO MNA - FULL GE-QCSEE 62.5-100%

under X_{mv} curve) for the MNA SISO could be considered an improvement over the corresponding full GE control responses. It appears, therefore, that both X_{18} and Theta I (fan pitch angle are used for noise suppression in the full GE control and not (as stated in (15)) "primarily to provide rapid thrust response." Except for the obvious reduction in NL, the impact of Theta I of Figure 9C is unclear.

For a more meaningful comparison, the GE controls on nozzle area (X_{18}) and fan pitch angle (Theta I) were held fixed at the 62.5% full power position. This condition is then equivalent to the MNA SISO design and is presented in Figures 10A-10D for a transient power slam to 100% power. The two designs are comparable in transient and steady state performance. The control logic to implement (37) is considerably simpler than the logic in [15, 16].

As indicated in Figures 8A-8D, good system performance is obtained at the 62.5% power point by a SISO control design. The design point at which two controls are simultaneously used by the GE QCSEE control occurs at the 80% power point. Using the linearized model corresponding to 80% power, a two input two output condition was configured for an MNA design attempt. The inputs selected were X_{mv} and Theta I with

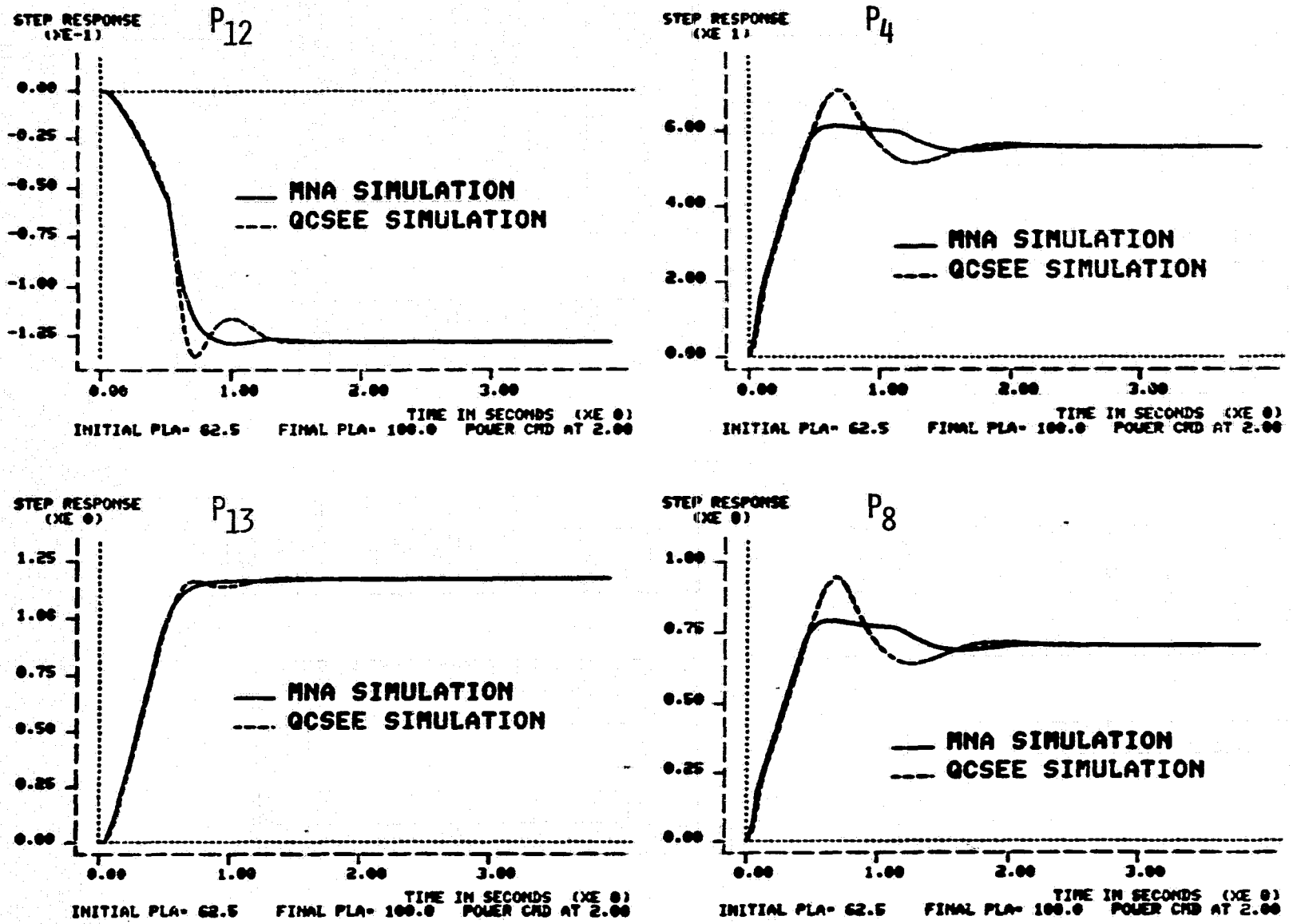

FIGURE 10A: SISO MNA - SISO GE-QCSEE 62.5-100%

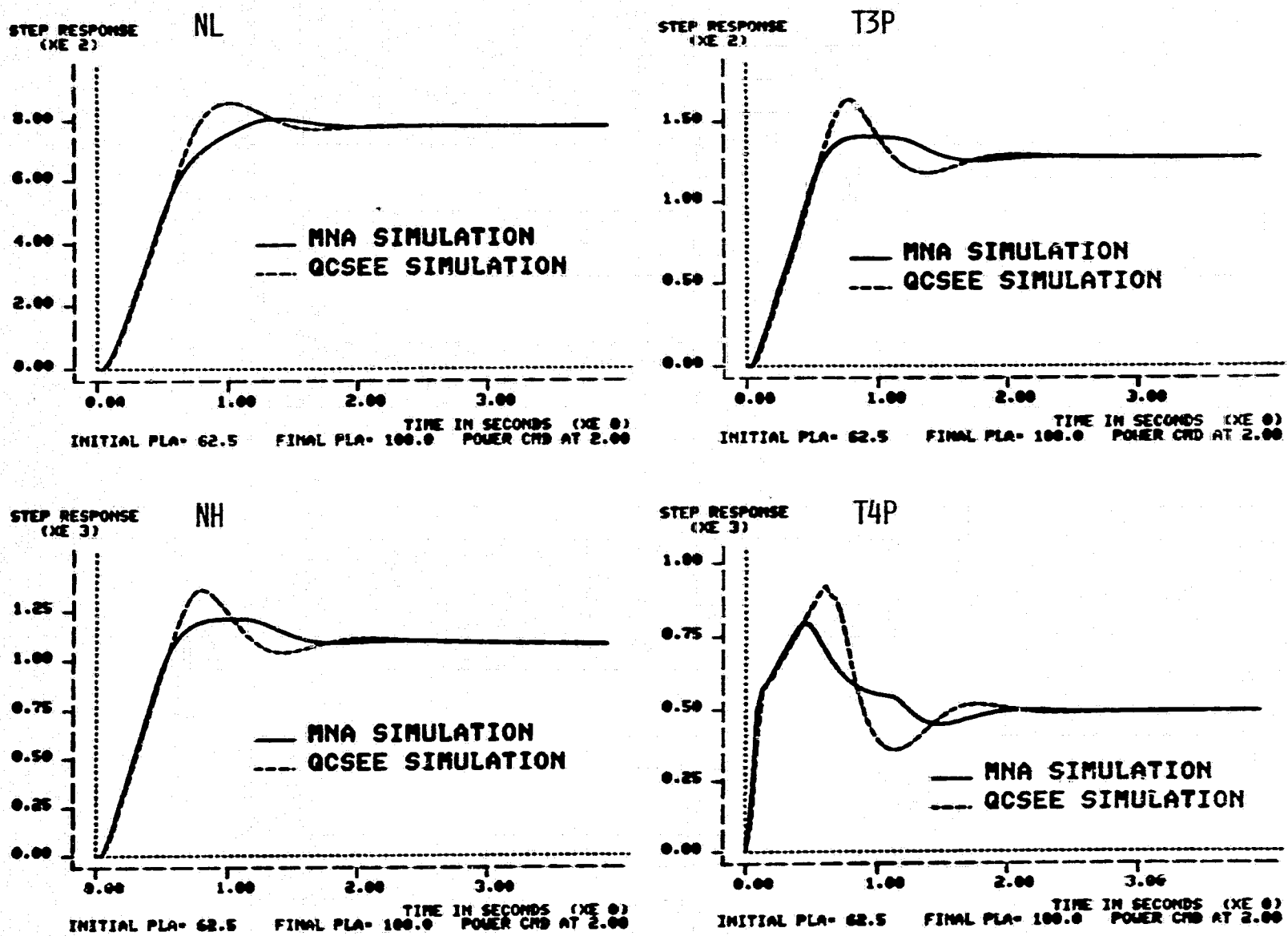

FIGURE 10B: SISO MNA - SISO GE-QCSEE 62.5-100%

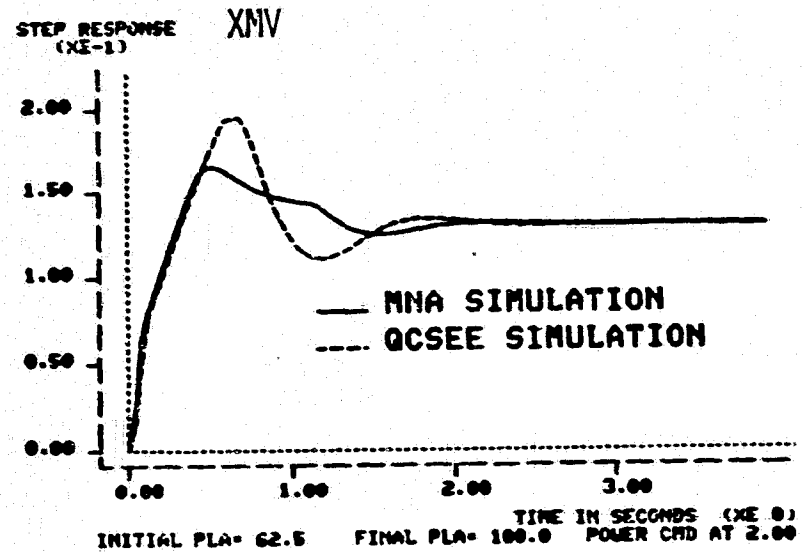

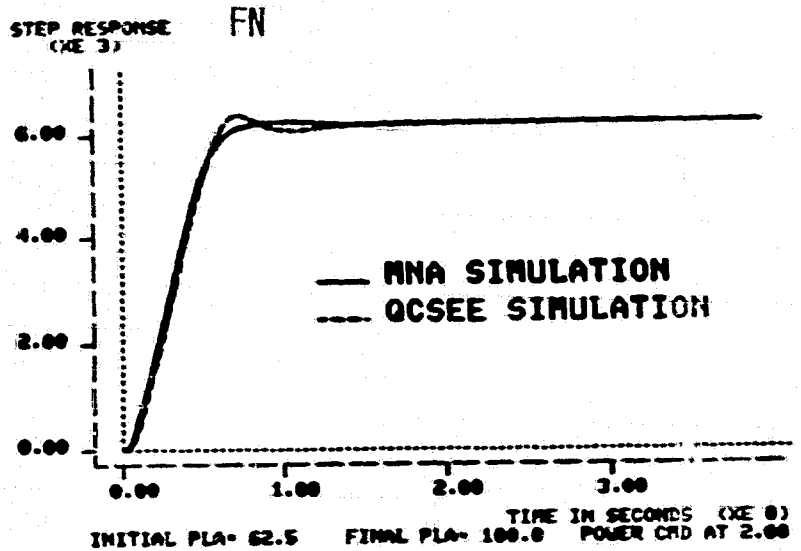

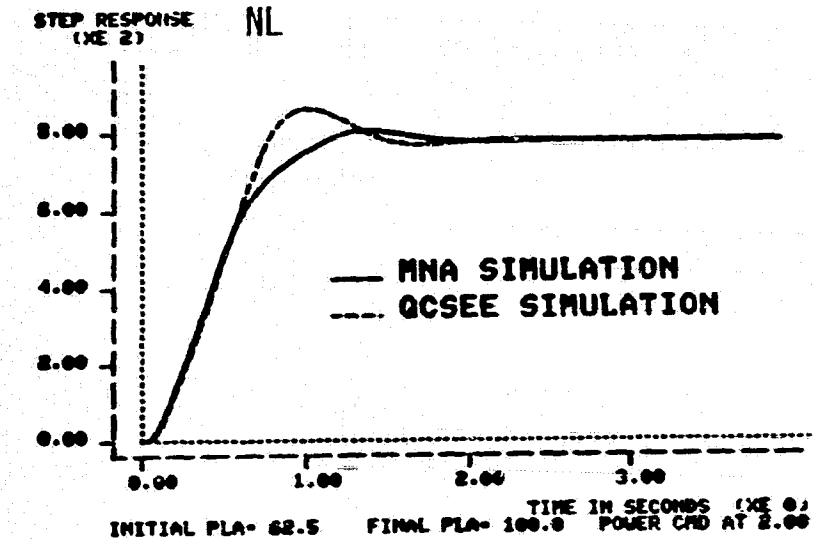

THETA I HELD AT 62.5% POSITION.

X18 HELD AT 62.5% POSITION.

FIGURE 10C: SISO MNA - SISO GE-QCSEE 62.5-100%

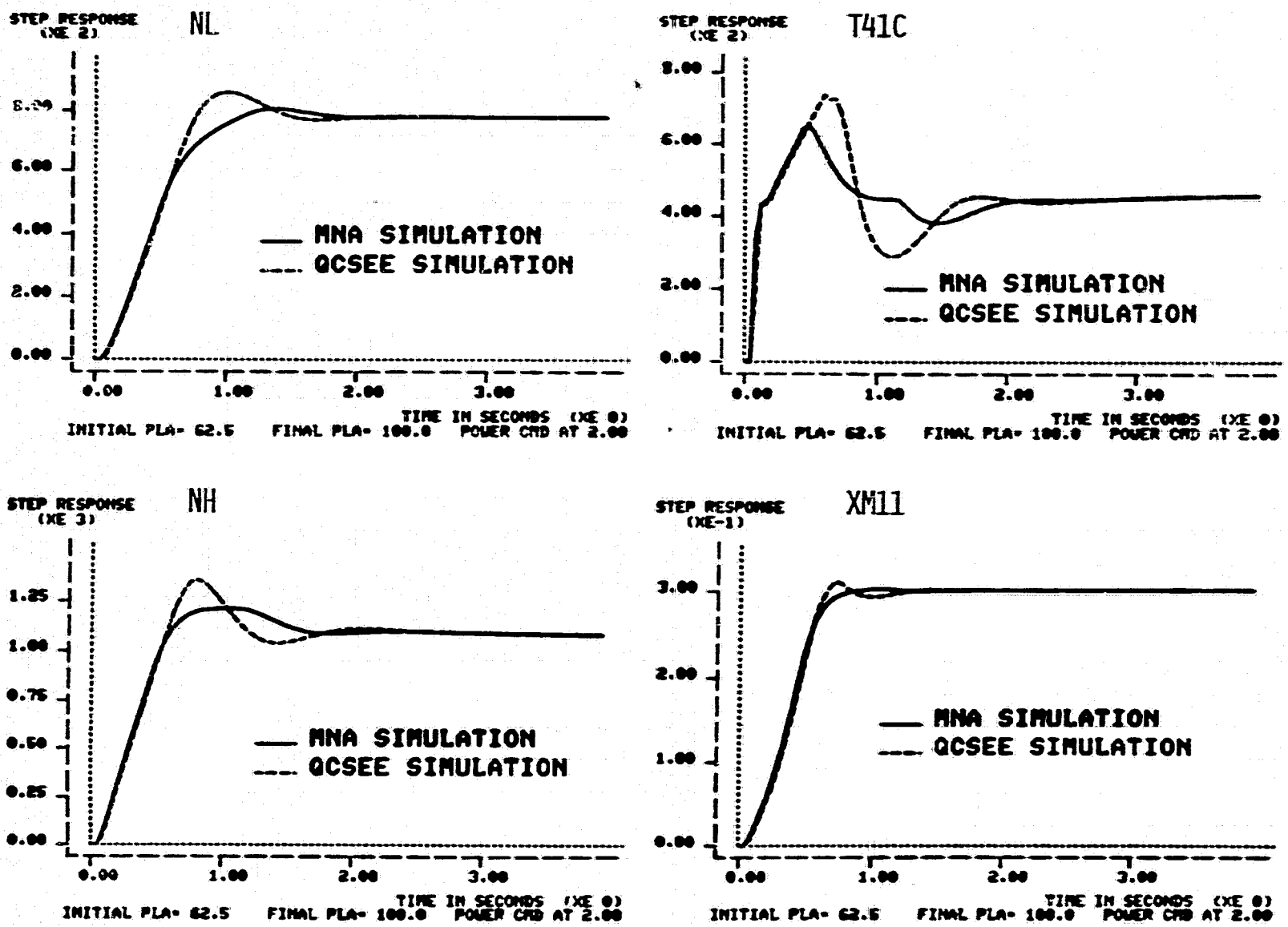

FIGURE 10D: SISO MNA - SISO GE-QCSEE 62.5-100%

outputs P_4 and NL,

$$\begin{bmatrix} NL \\ P_4 \end{bmatrix} = \begin{bmatrix} G_{11}(s) & G_{12}(s) \\ G_{21}(s) & G_{22}(s) \end{bmatrix} \begin{bmatrix} X_{mv} \\ \text{Theta I} \end{bmatrix}$$

Here nozzle area (X_{18}) was fixed at its full open position (62.5% power).

Application of the MNA design suite described in [22] to the corresponding transfer function matrix at 80% power yielded system dominance over the range 0.1 to 50 radians. The resulting constant compensators are

$$K = \begin{bmatrix} 1.1 & 80163.5 \\ 23361.1 & -2.1263(10^7) \end{bmatrix} \tag{38}$$

$$L = \begin{bmatrix} 0.5161 & 0.0 \\ 0.0 & 13.8743 \end{bmatrix} \tag{39}$$

$$F = \begin{bmatrix} 3.0(10^5) & 0.0 \\ 0.0 & 1.1(10^{-8}) \end{bmatrix} \tag{40}$$

The DNA, INA, Bode, and Nichols plots appears as Figures 11-14. Transient responses to a power step from 80% to 90%

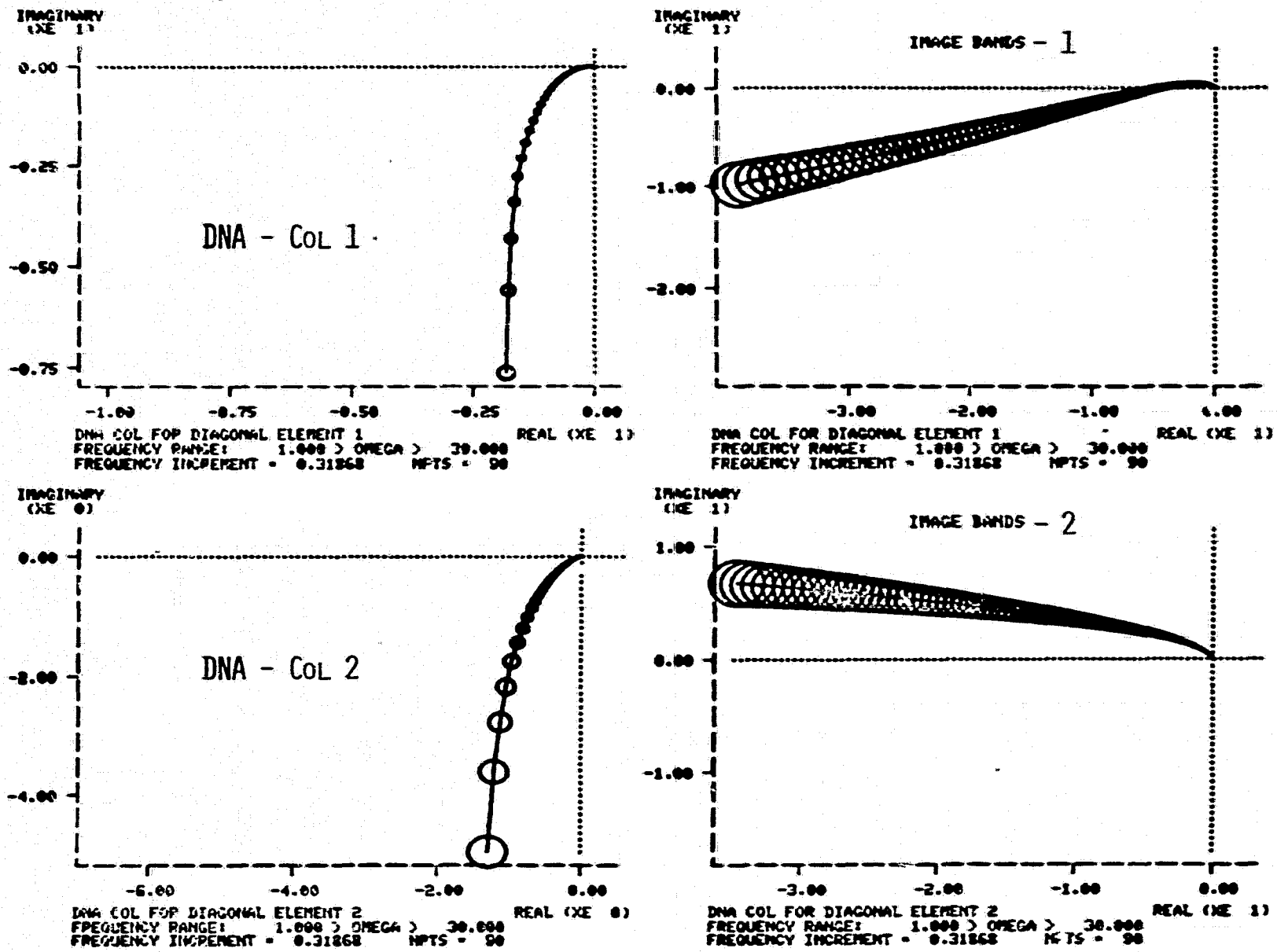

FIGURE 11: GERSHGORIN CIRCLES FOR 2x2 MNA

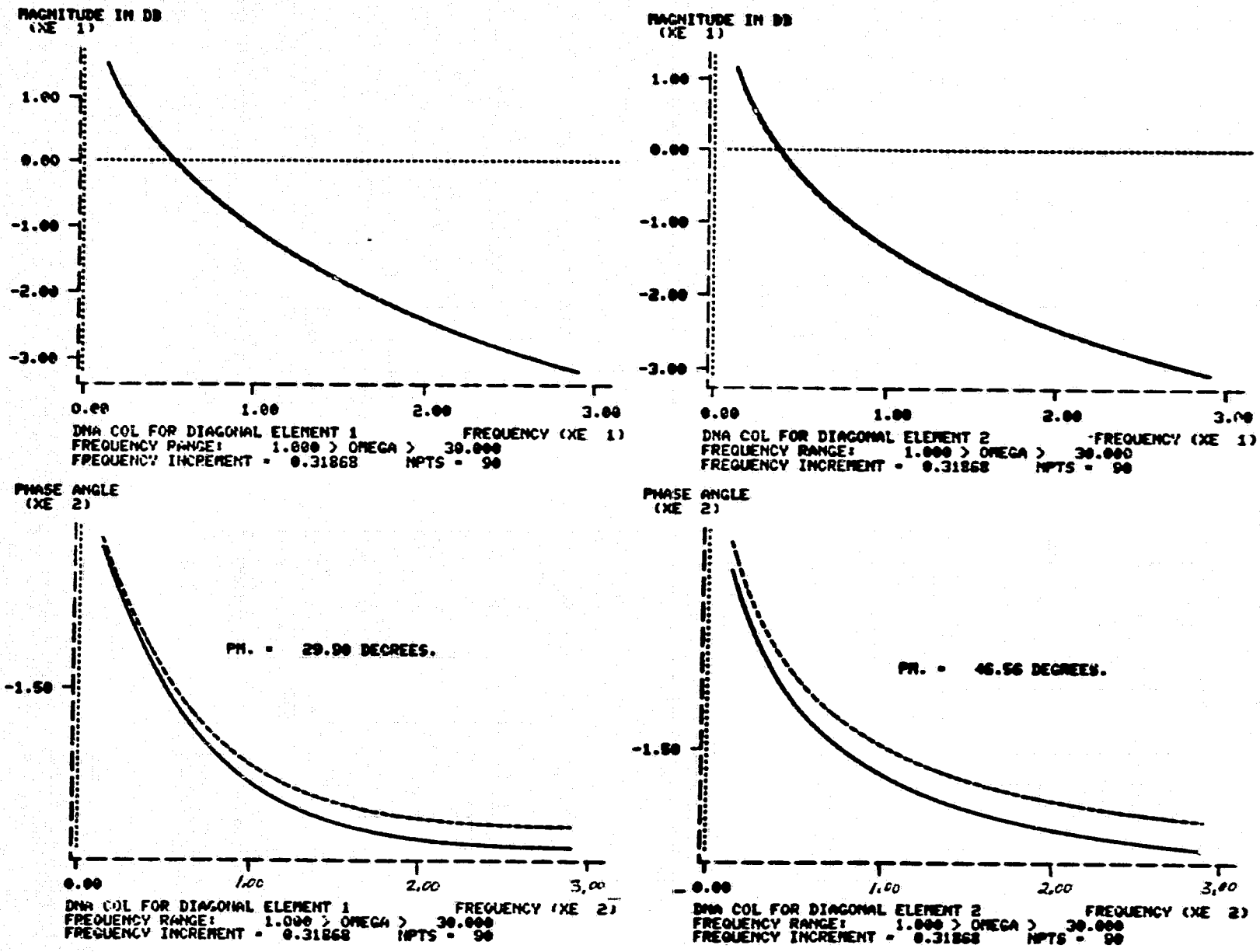

FIGURE 12: BODE PLOTS FOR 2x2 MNA

PROGRAM OPTIONS

READ AND PLOT A DATA FILE. <D>
END THIS PROGRAM. <E>
MAKE A HARD COPY. <H>
READ A FREQUENCY POINT. <F>
DRAW A "M" CONTOUR. <M>
DRAW A "N" CONTOUR. <N>
RE-START / ERASE SCREEN <R>
INSERT TEXT. <T>

ENTER FILE NAME :FTN44 ——

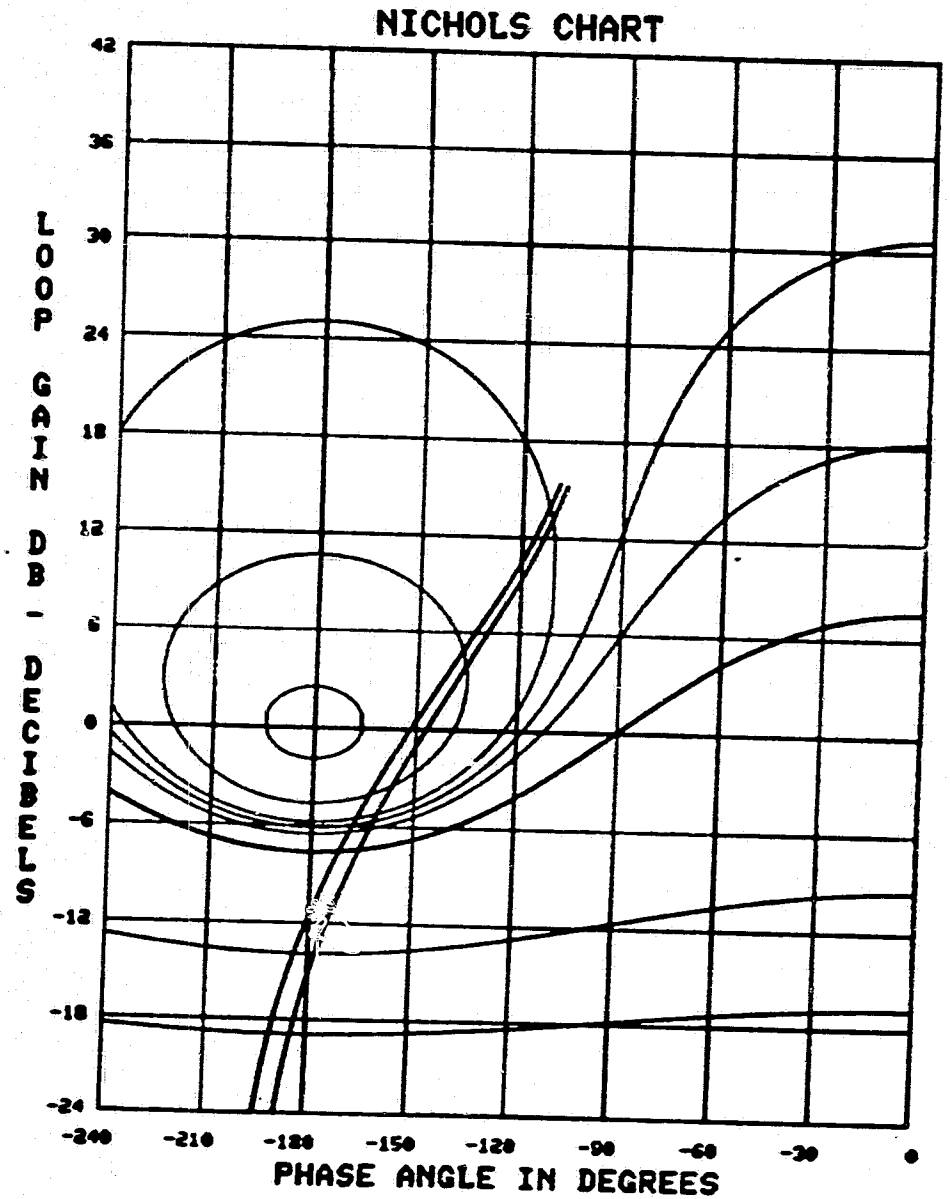

FIGURE 13: NICHOLS CHART FOR CONTROL LOOP 1

PROGRAM OPTIONS

READ AND PLOT A DATA FILE. <D>
END THIS PROGRAM. <E>
MAKE A HARD COPY. <H>
READ A FREQUENCY POINT. <F>
DRAW A "M" CONTOUR. <M>
DRAW A "N" CONTOUR. <N>
RE-START / ERASE SCREEN <R>
INSERT TEXT. <T>

ENTER FILE NAME #FTN49

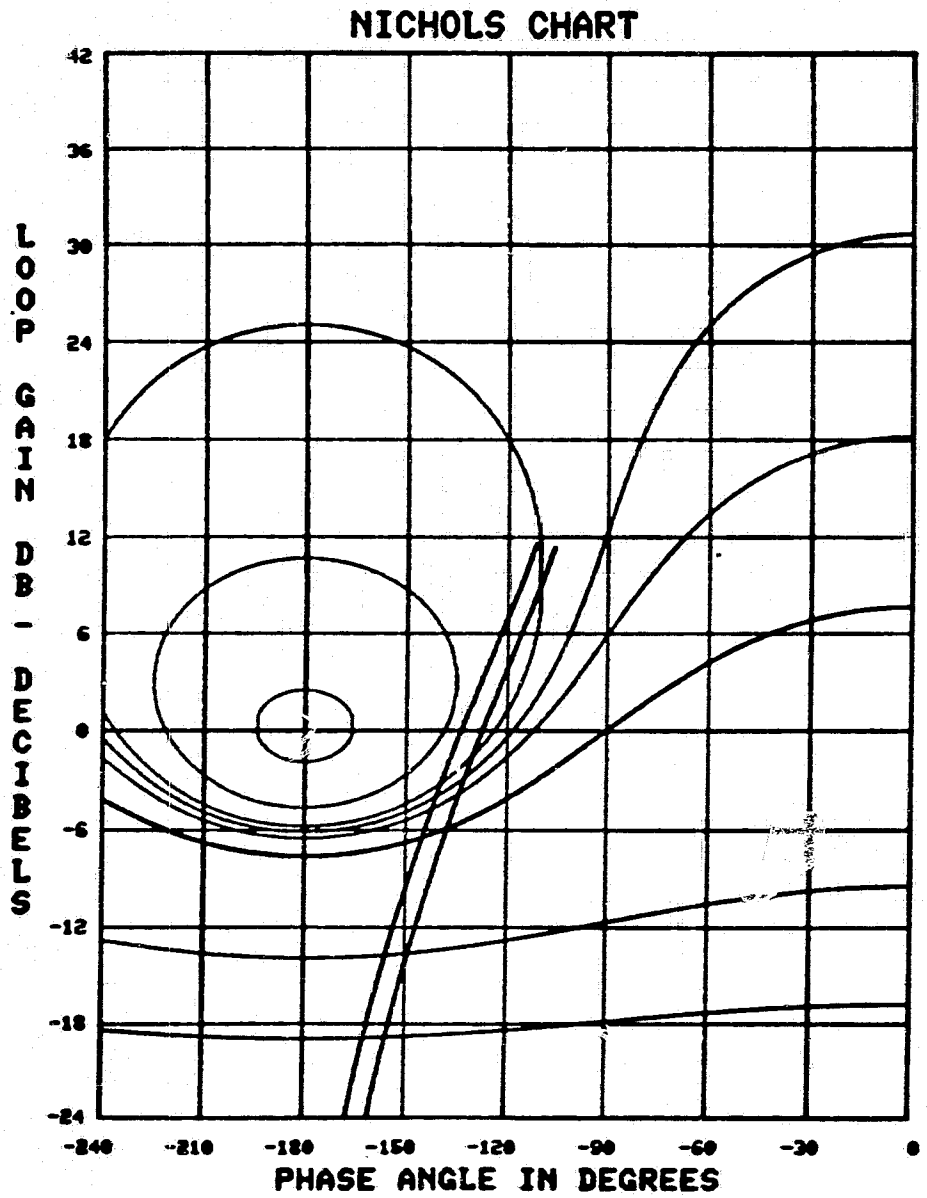

FIGURE 14: NICHOLS CHART FOR CONTROL LOOP 2

of full power are indicated in Figures 15A-15D with the two input GE control superimposed. Nozzle area was held fixed at the full open position which corresponds to the 62.5 power setting. The peak overshoots are significantly lower for the MNA design with no degradation in performance. Also total fuel consumption (area under X_{mv}) is much less for the MNA design.

For a full power slam of 62.5% to 100%, the 2x2 MNA design is compared with the two input GE control in Figures 16A-16D. In every figure, the MNA design performs very well with respect to the two input QCSEE control. A comparison of this 2x2 MNA design with the full GE QCSEE design is indicated in Figures 17A-17D. The only significant deviation is, as expected, in P_{12} and XM11. These variables are directly effected by nozzle area, X_{18}.

There is, however, a significant difference in implementation logic. This is apparent when considering the implementation of the constants in (38)-(40) versus the logic outlined in [15, 16].

To regulate inlet Mach number, a third controlled variable, inlet duct pressure (P_{12}), is introduced. Using nozzle area as the third input, a three input three output design condition exists. Although time did not permit a full scale three input three output MNA design over the full operating

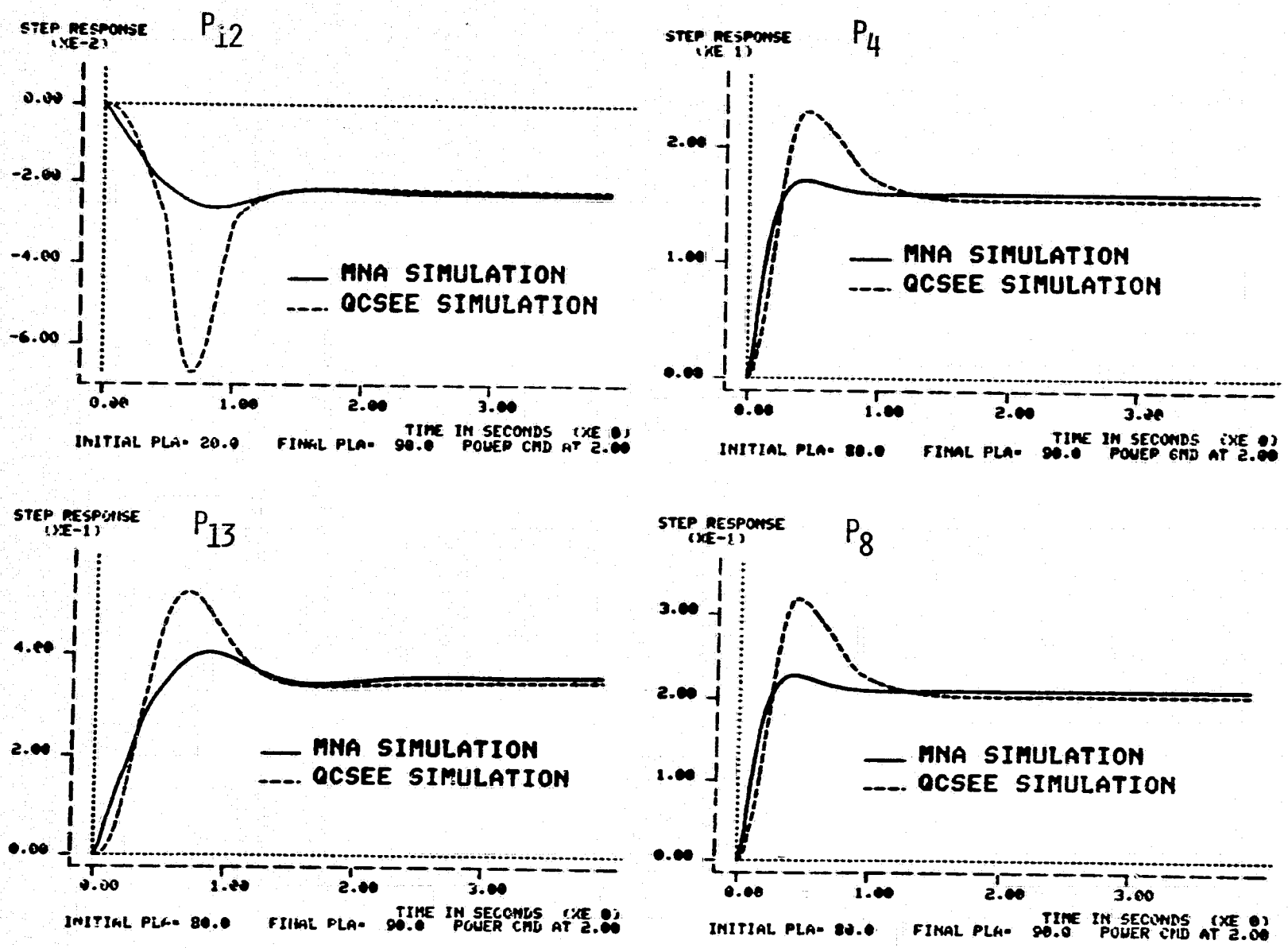

FIGURE 15A: 2x2 MNA-TWO INPUT QCSEE - 80-90%

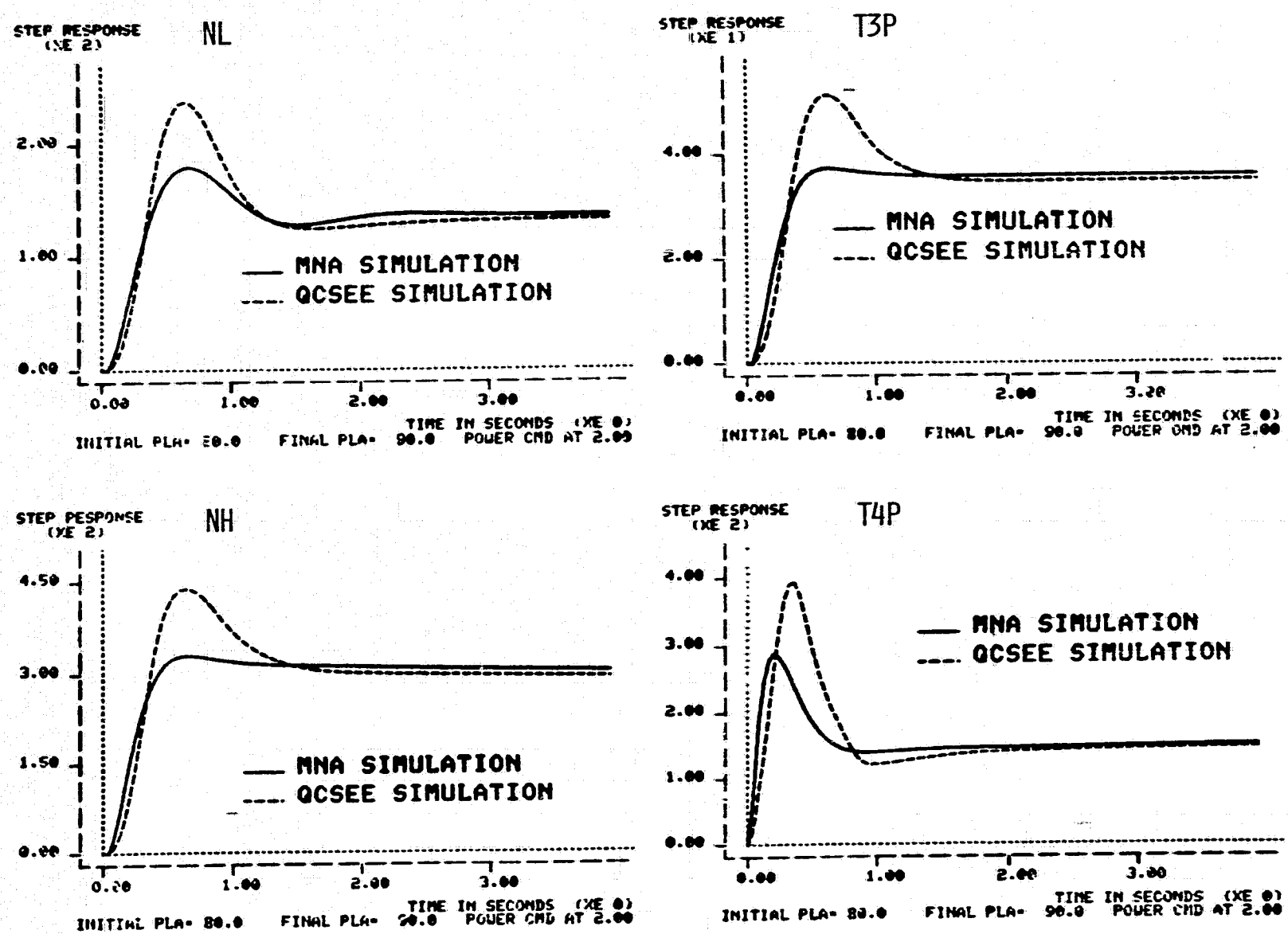

FIGURE 15B: 2x2 MNA-TWO INPUT QCSEE - 80-90%

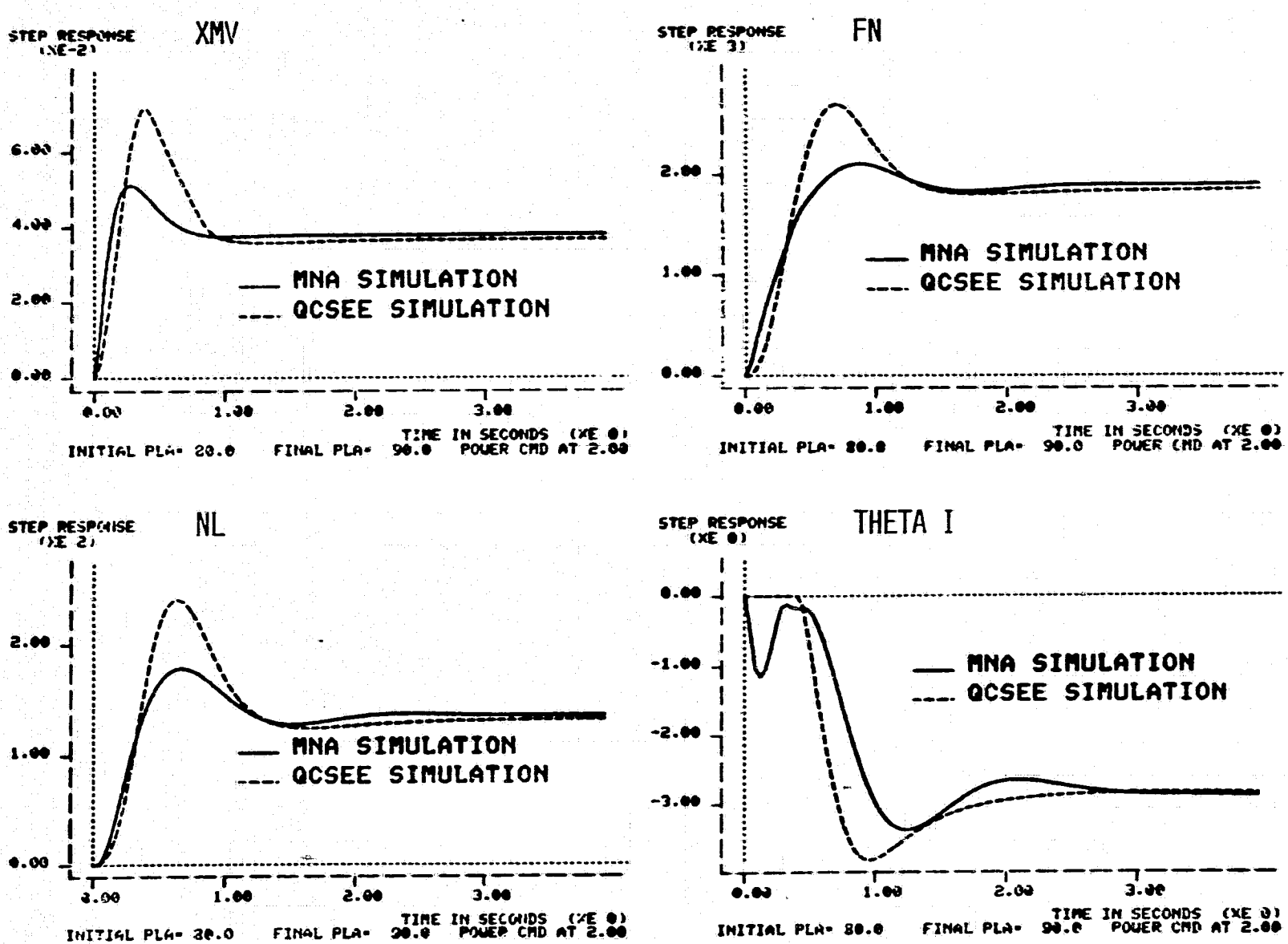

FIGURE 15C: 2x2 MNA-TWO INPUT QCSEE - 80-90%

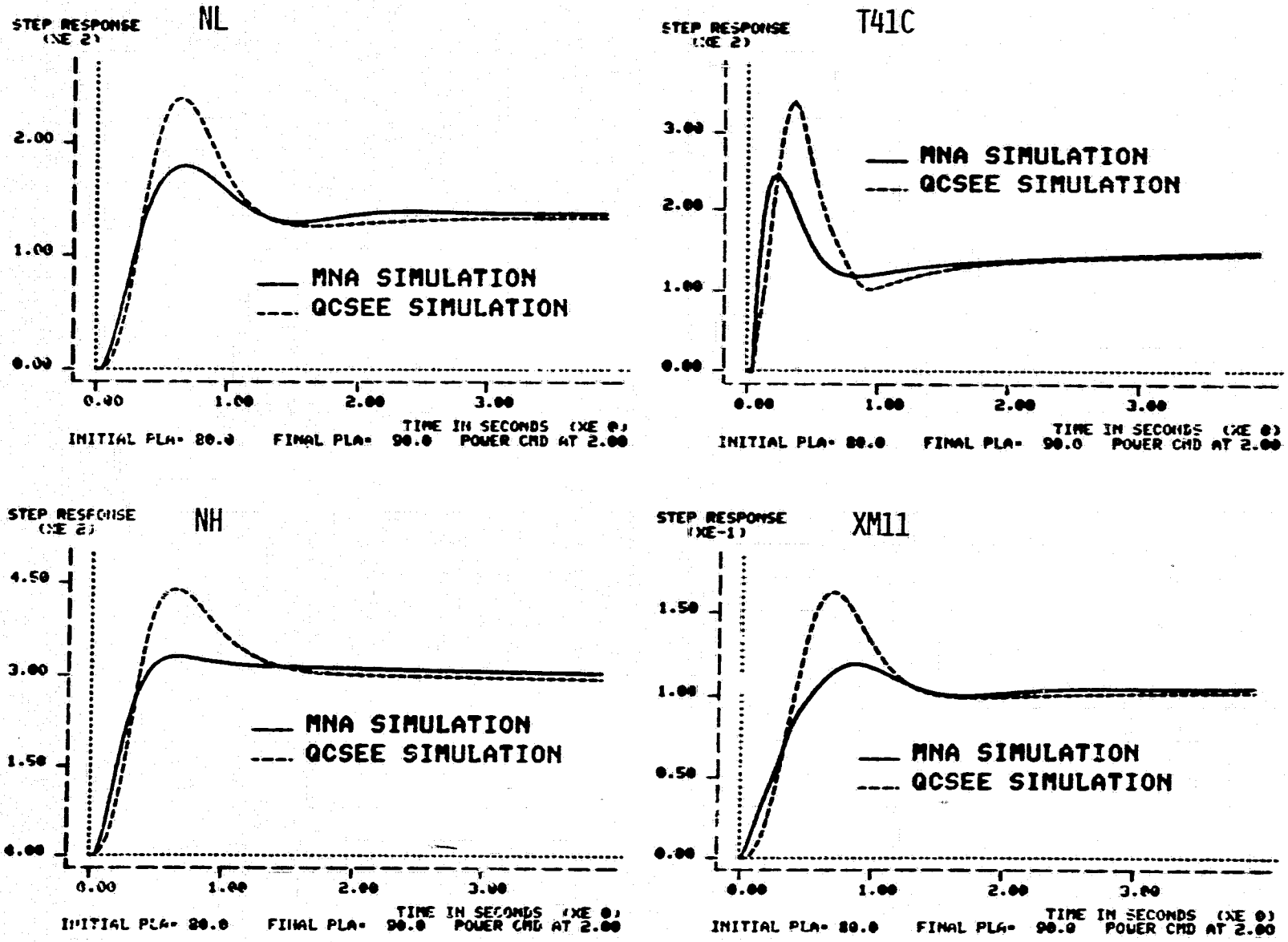

FIGURE 15D: 2x2 MNA-TWO INPUT QCSEE - 80-90%

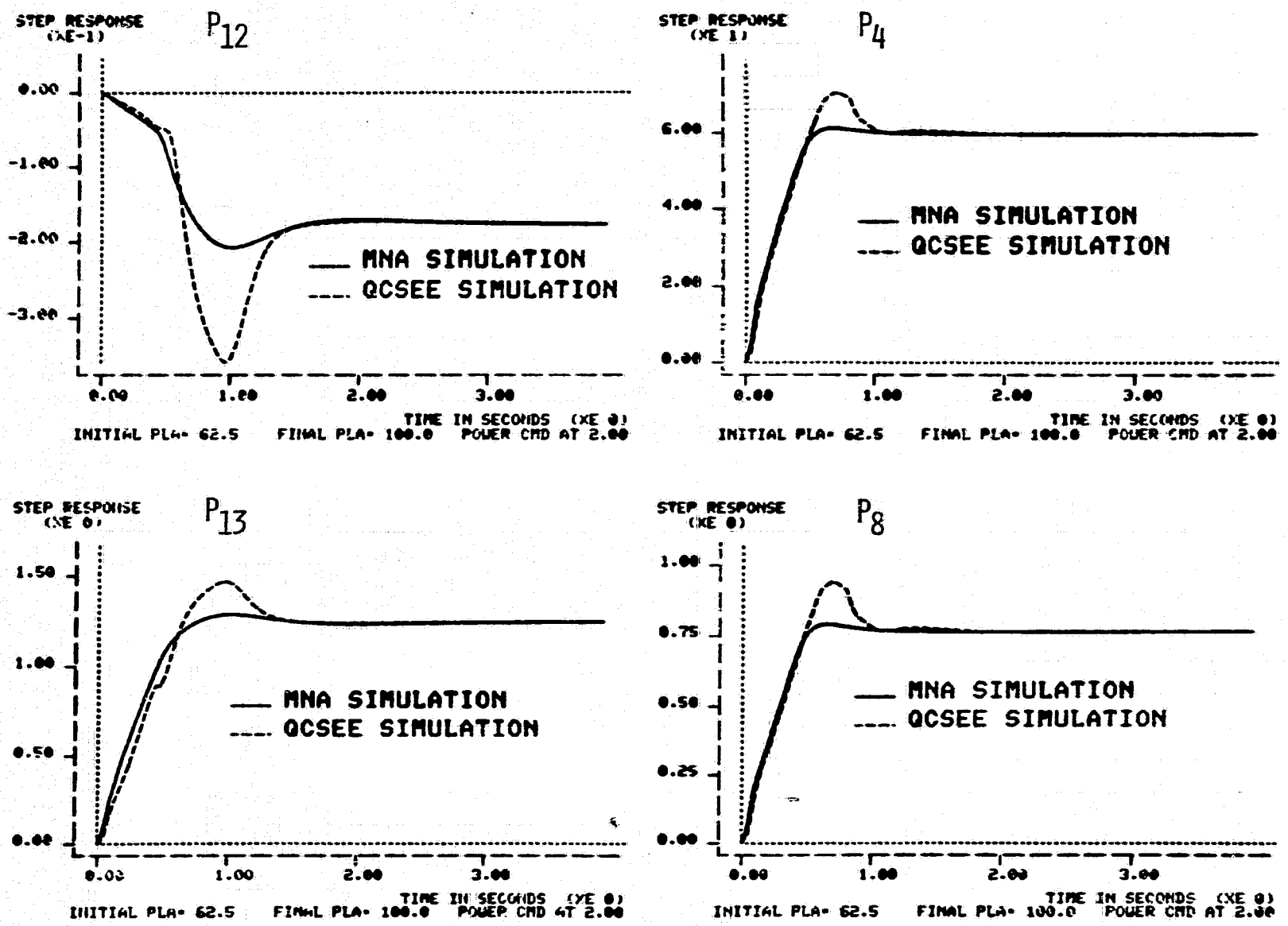

FIGURE 16A: 2x2 MNA-TWO INPUT QCSEE - 62.5-100%

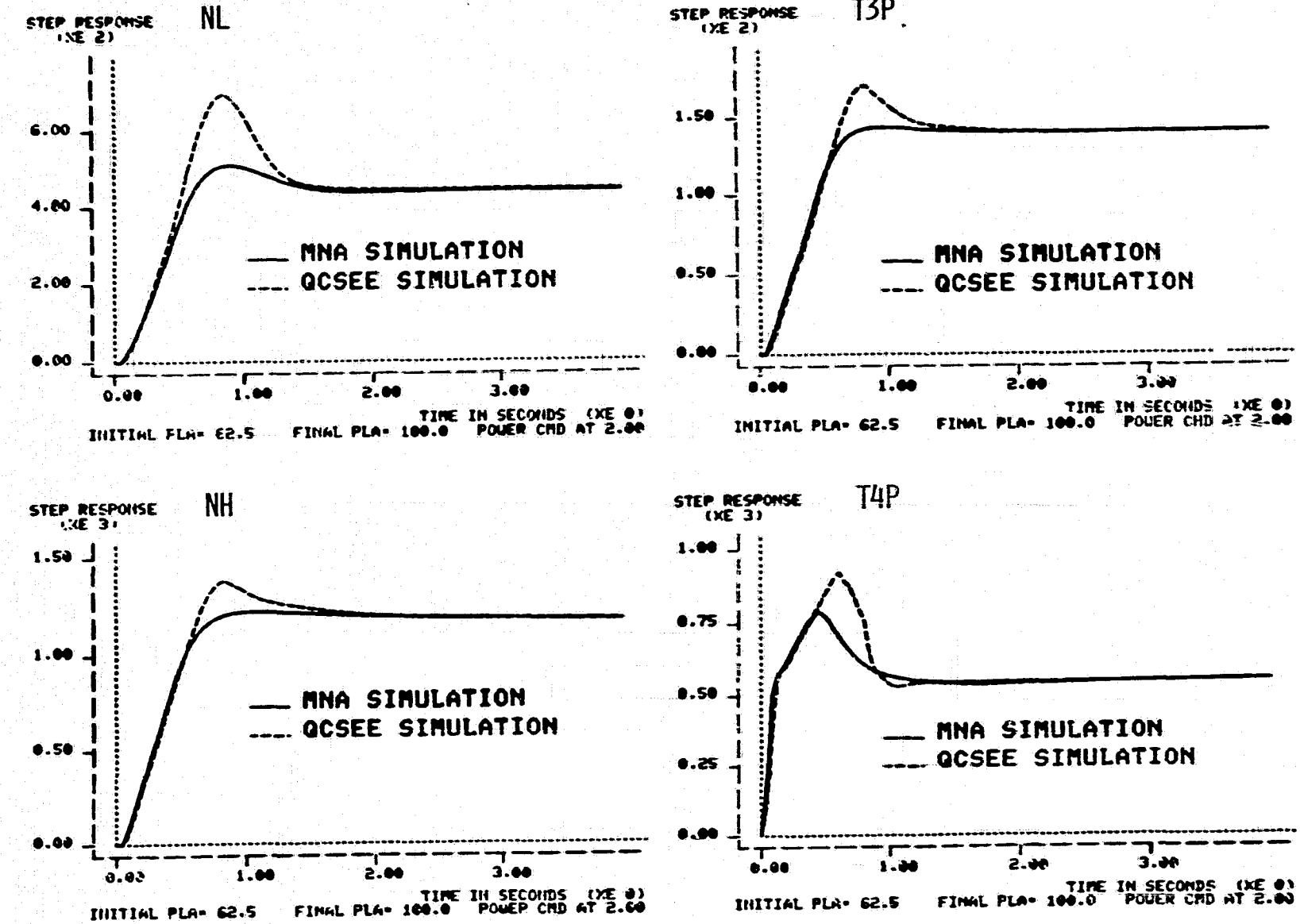

FIGURE 16B: 2x2 MNA-TWO INPUT QCSEE - 62.5-100%

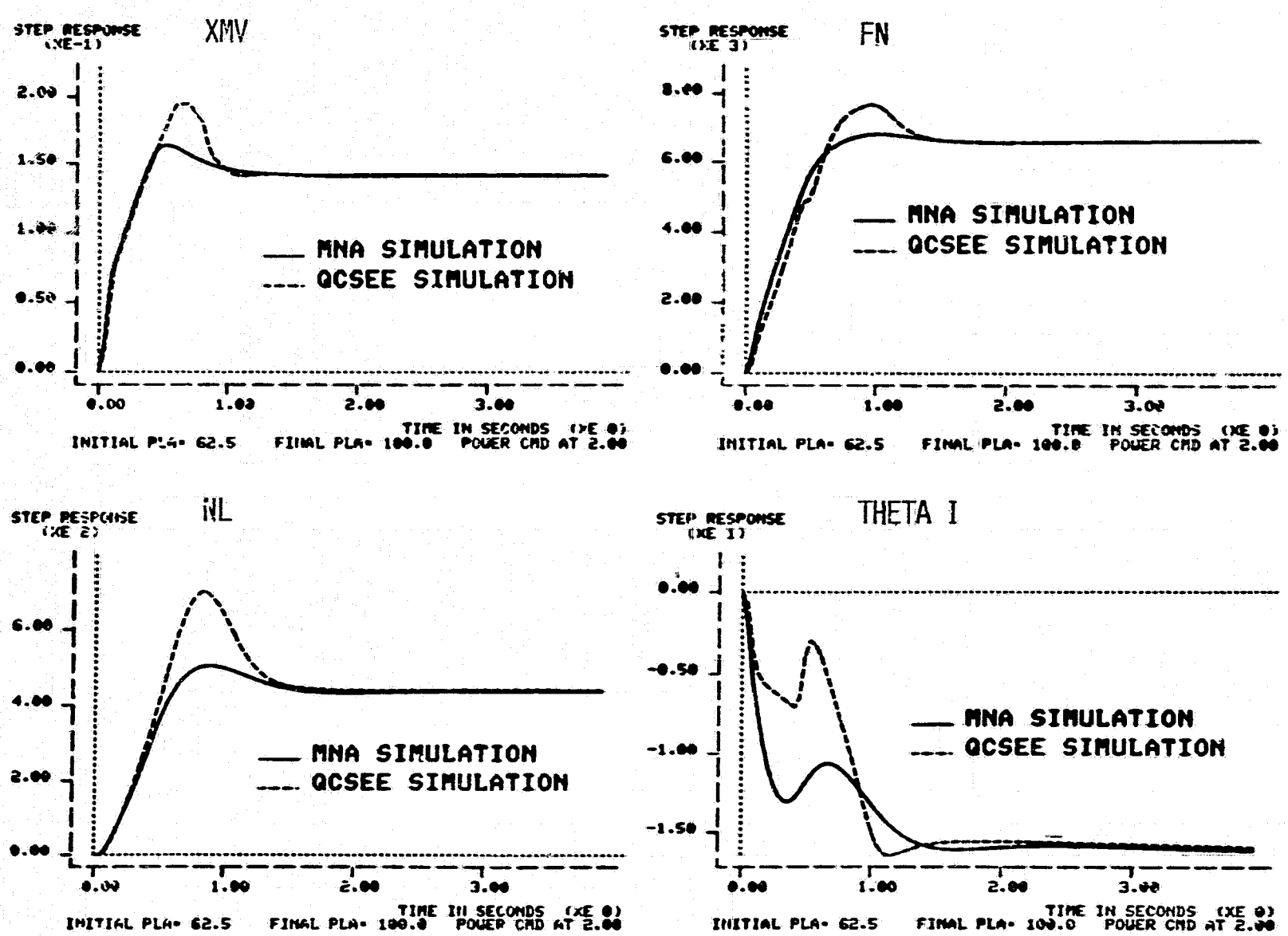

FIGURE 16C: 2x2 MNA-TWO INPUT QCSEE - 62.5-100%

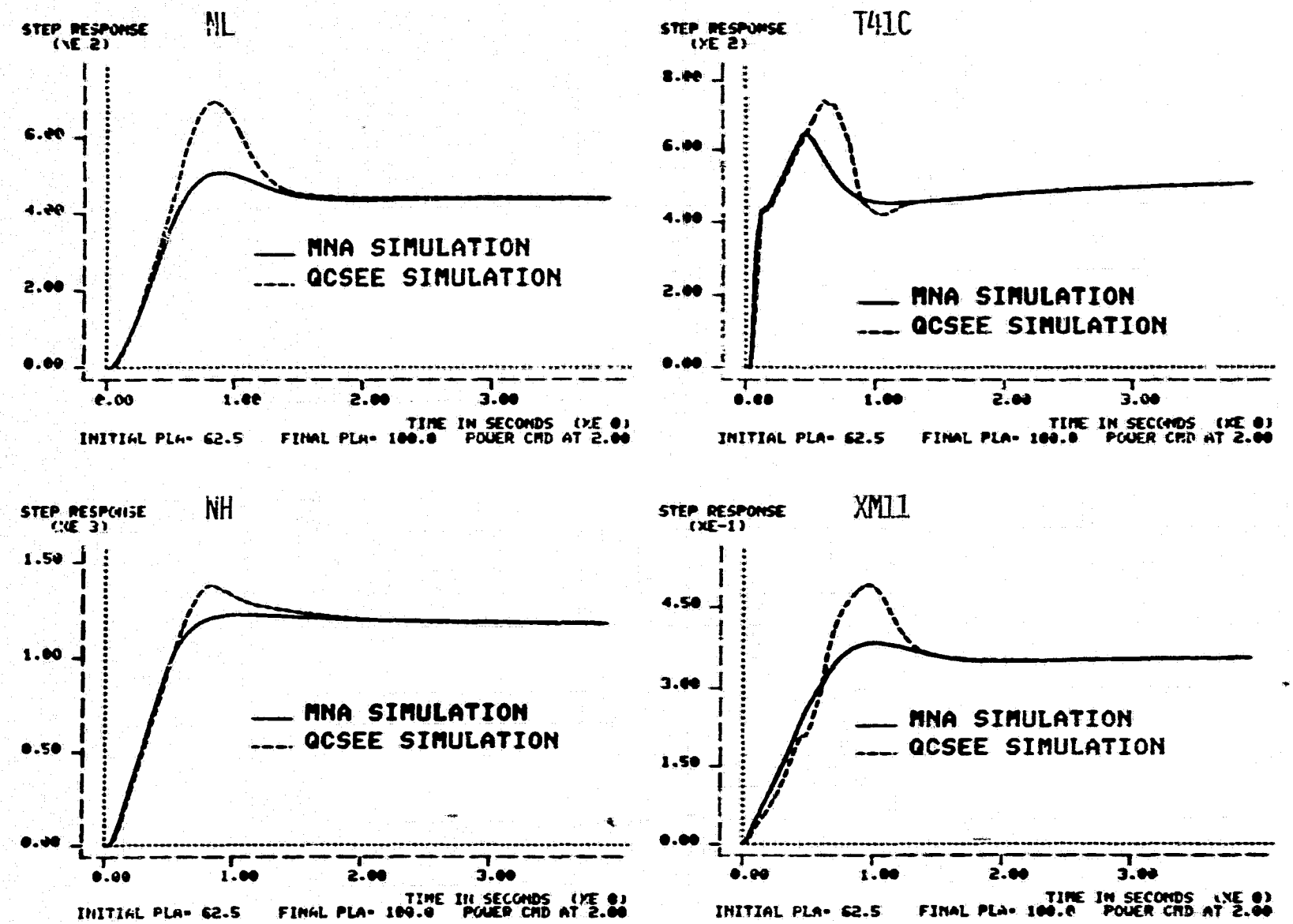

FIGURE 16D: 2x2 MNA-TWO INPUT QCSEE - 62.5-100%

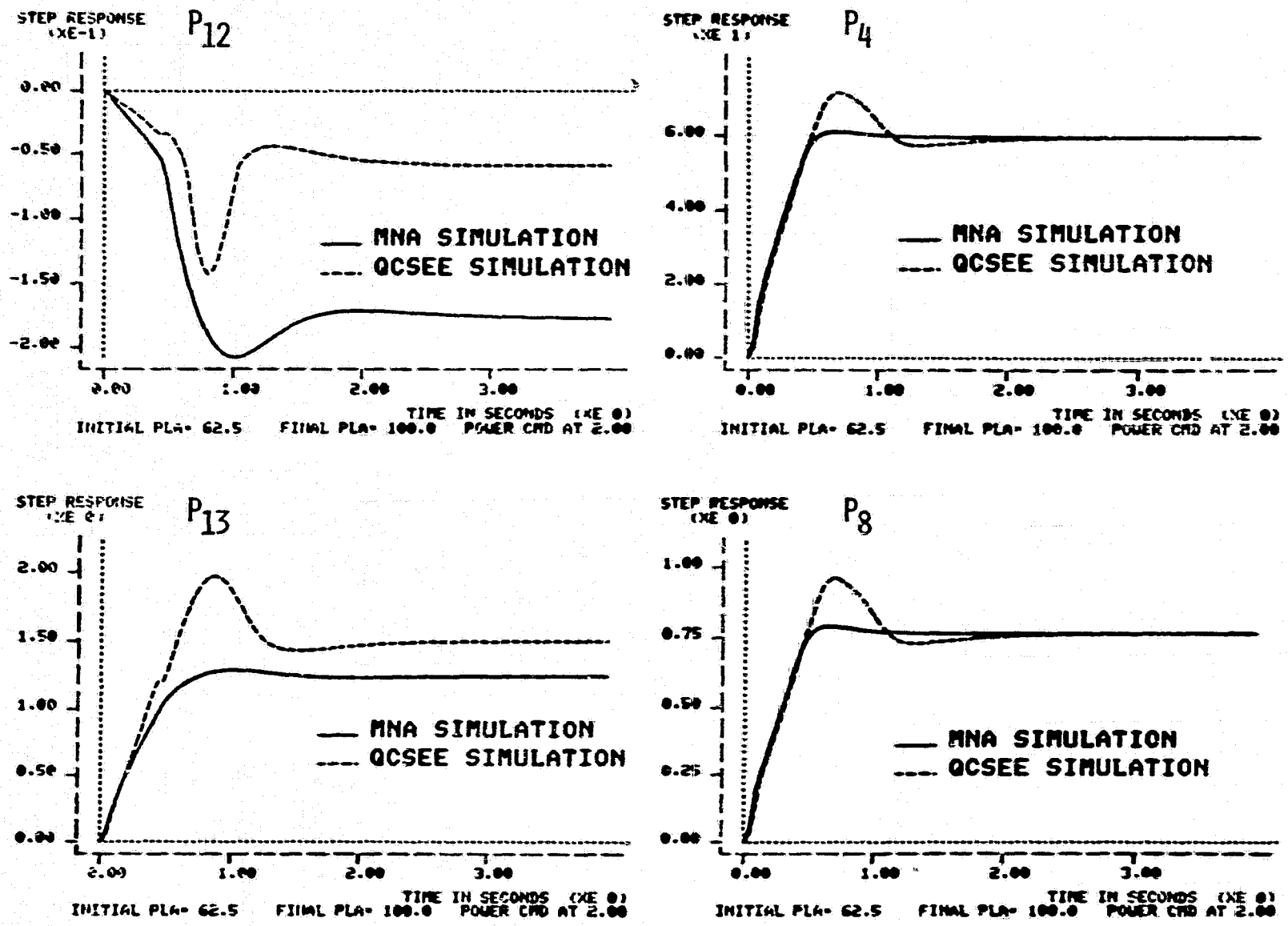

FIGURE 17A: 2x2 MNA-FULL QCSEE - 62.5-100%

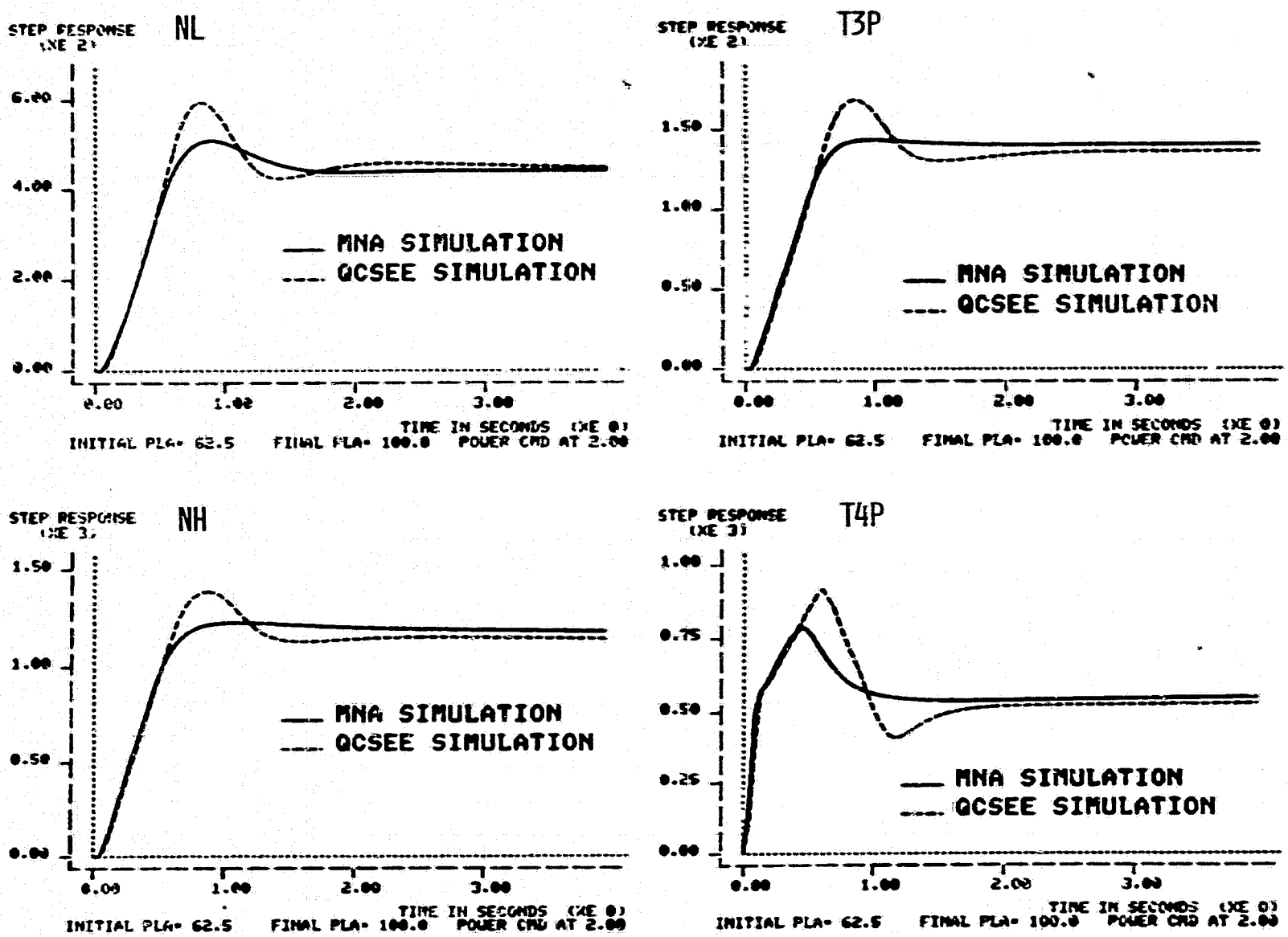

FIGURE 17B: 2x2 MNA-FULL QCSEE - 62.5-100%

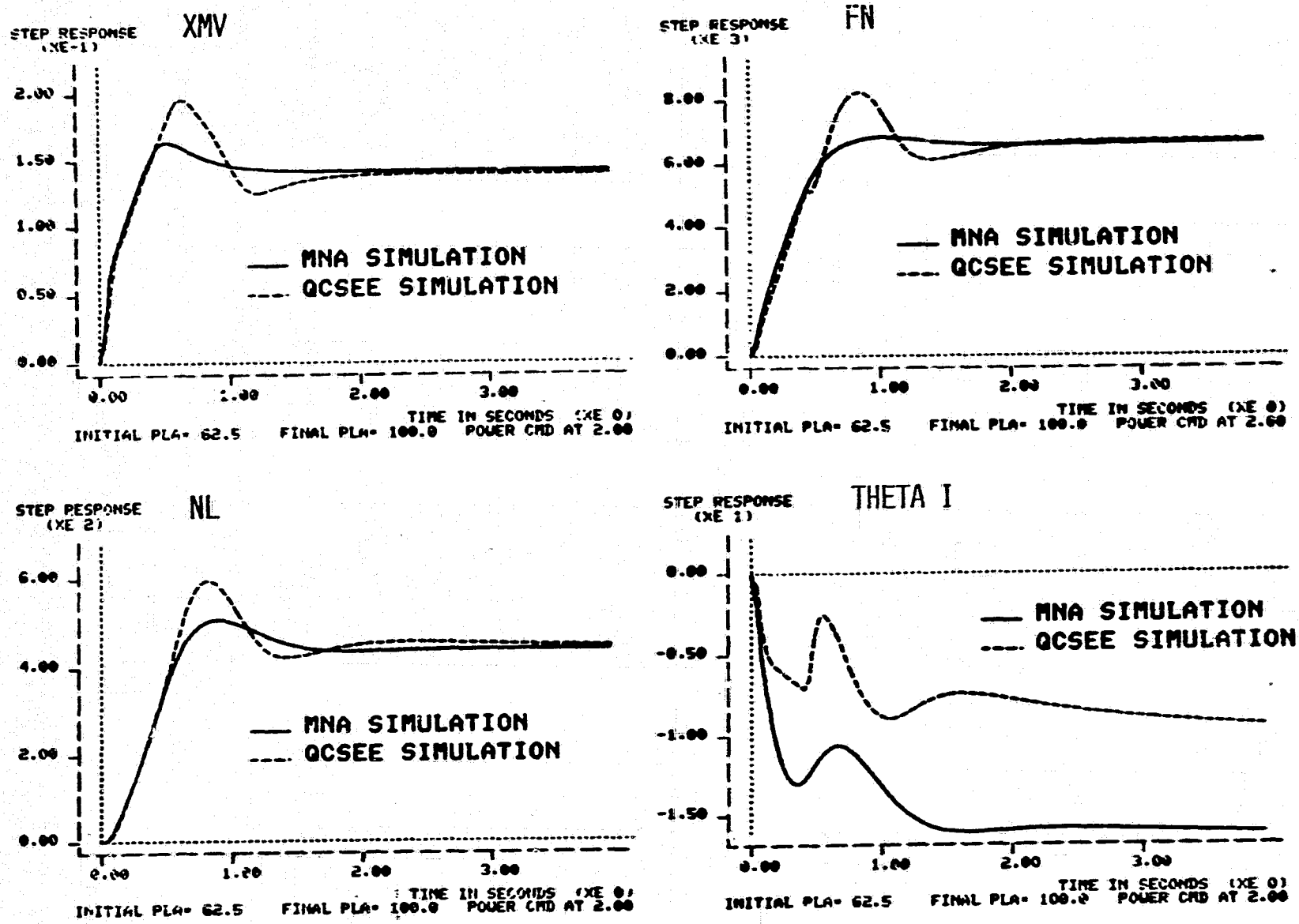

FIGURE 17C: 2x2 MNA-FULL QCSEE - 62.5-100%

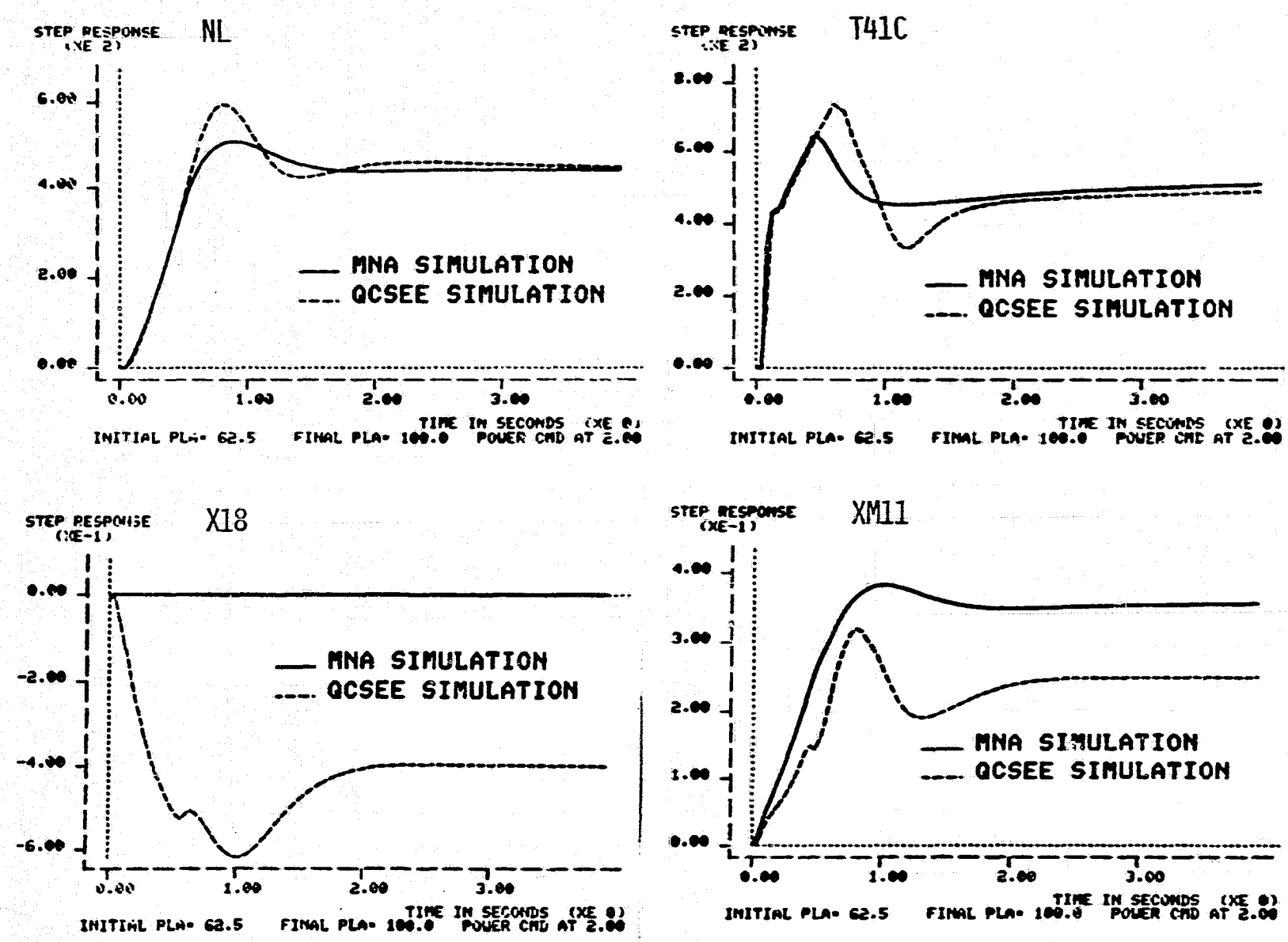

FIGURE 17D: 2x2 MNA-FULL QCSEE - 62.5-100%

range, some analysis and simulation were performed. The remainder of this section is directed to this condition.

Since the GE nozzle area control was designed using SISO methods, the SISO MNA and the 2x2 MNA designs were independently augmented with the GE nozzle area control. The first case represented in Figures 18A-18D consists of the SISO MNA with the GE X_{18} control while Theta I is fixed at the 62.5 power position. Note the rapid thrust response (same as in Figure 11C) and the respective decreases in P_{12} and XM11 from their counterparts in Figures 9A and 9D. Execept for fan speed, the Theta I curve for the full GE control has little influence on the remaining variables.

Augmenting the GE nozzle area control to the 2x2 MNA control design, results in the transient performance indicated in Figures 19A-19D. As expected, the dynamics are unchanged from the previous case except for the improved performance of P_{12} and XM11. The MNA control performs very well with the GE nozzle area control for noise suppression.

Preliminary design using MNA concepts for the three input three output case was performed using the 90% power point. The input vector u(t) and output vector y(t) were

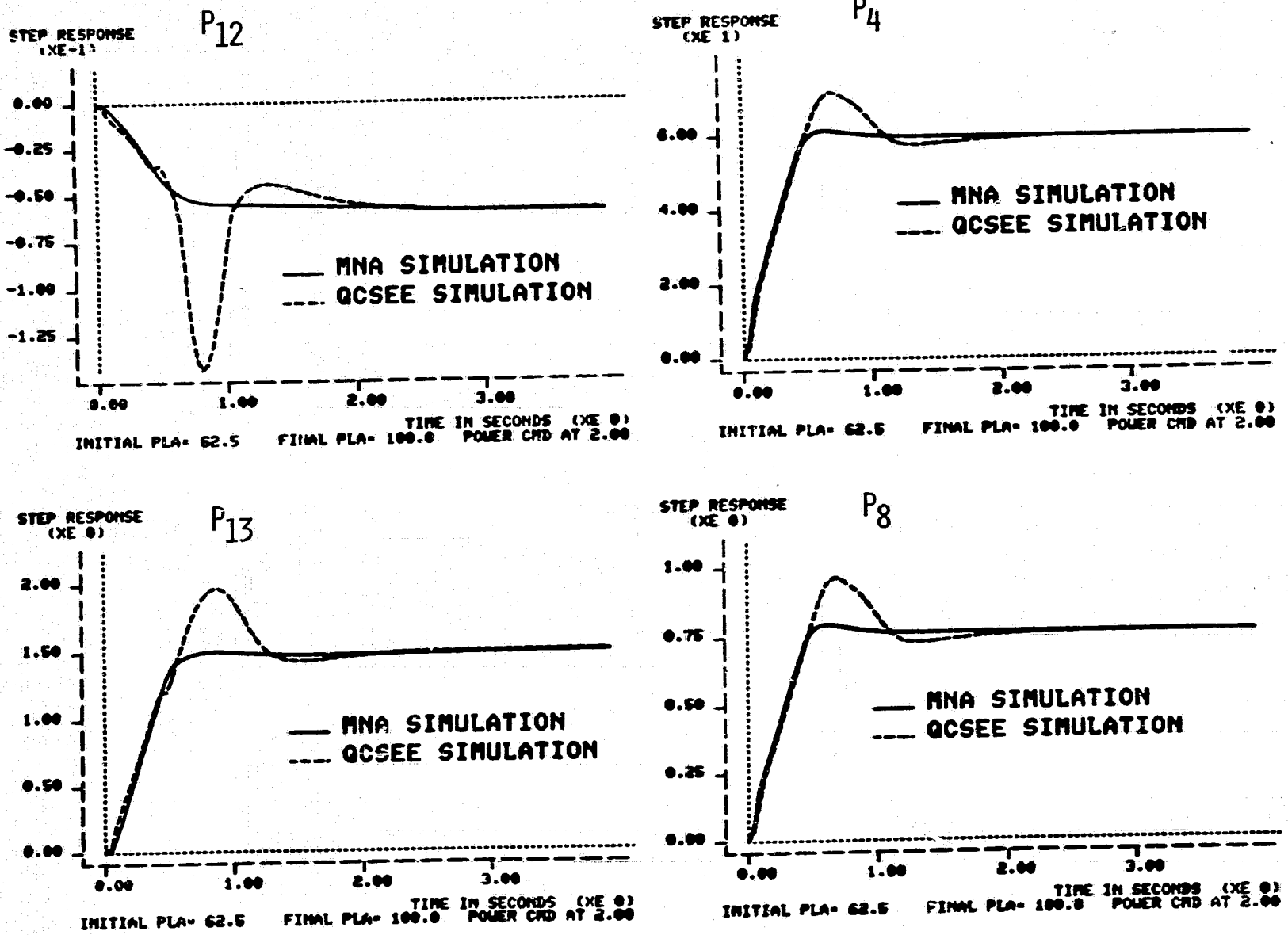

FIGURE 18A: SISO MNA WITH GE-X18 CONTROL - FULL QCSEE - 62.5-100%

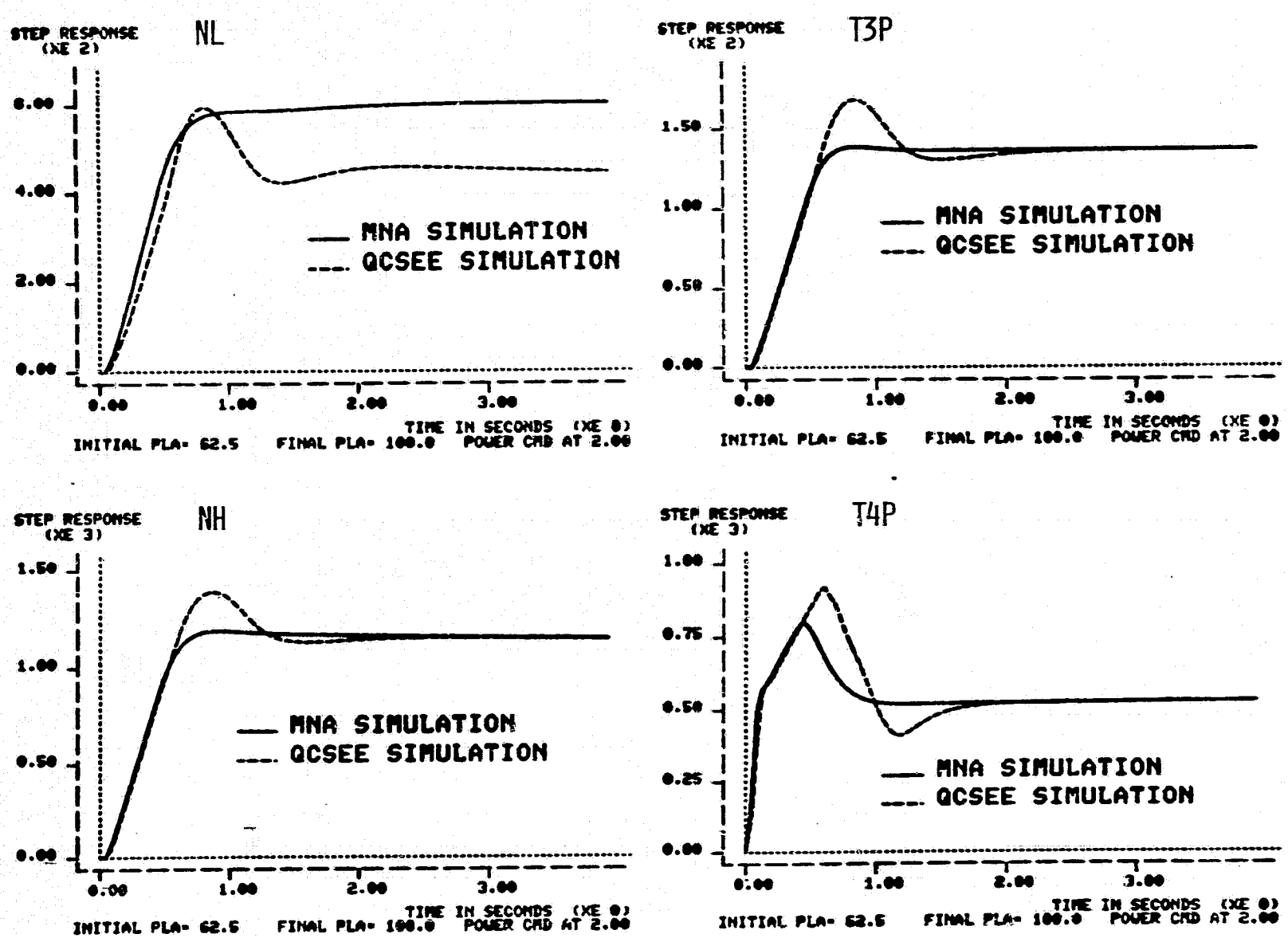

FIGURE 18B: SISO MNA WITH GE-X18 CONTROL - FULL QCSEE - 62.5-100%

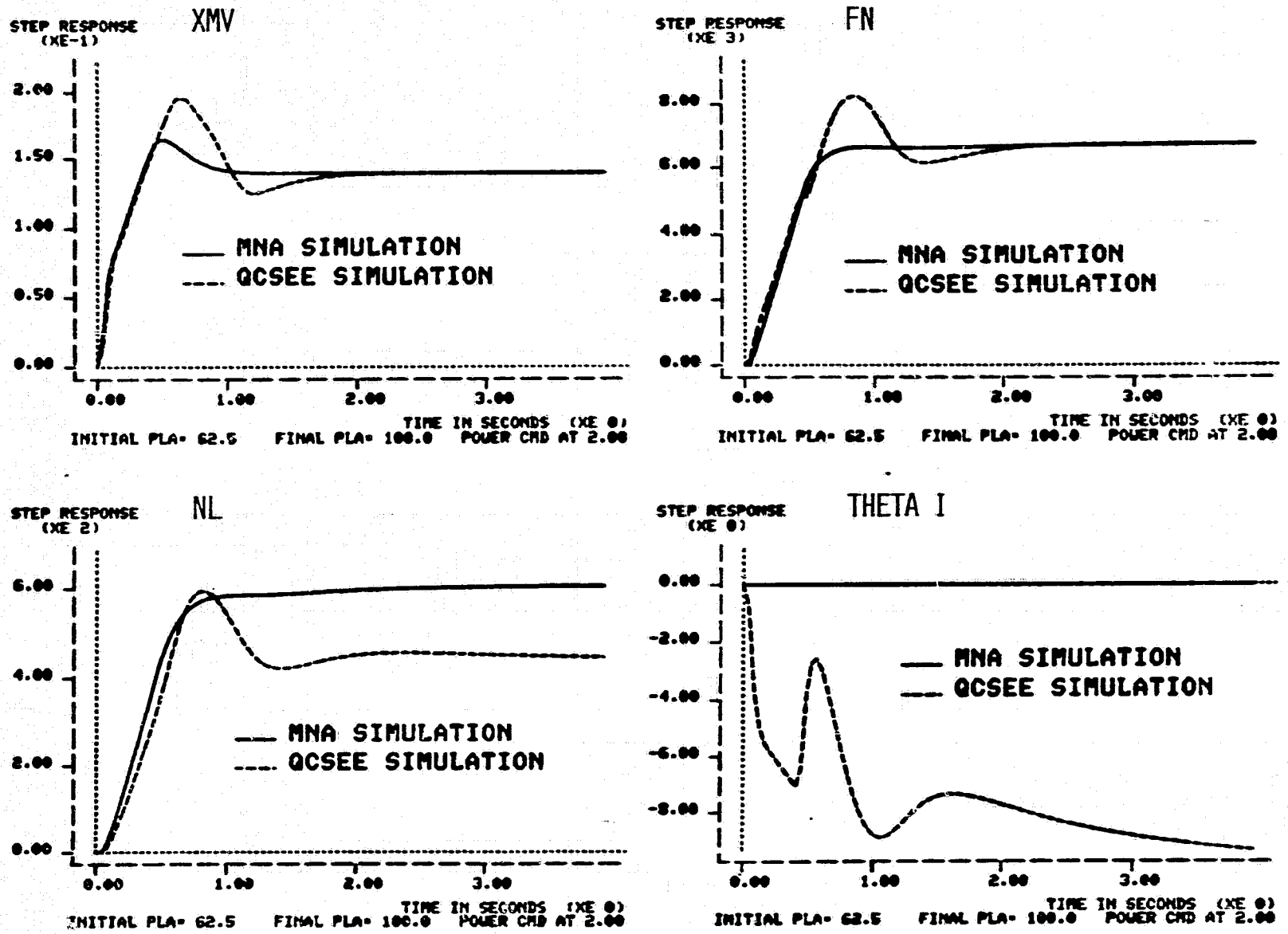

FIGURE 18C: SISO MNA WITH GE-X18 CONTROL - FULL QCSEE - 62.5-100%

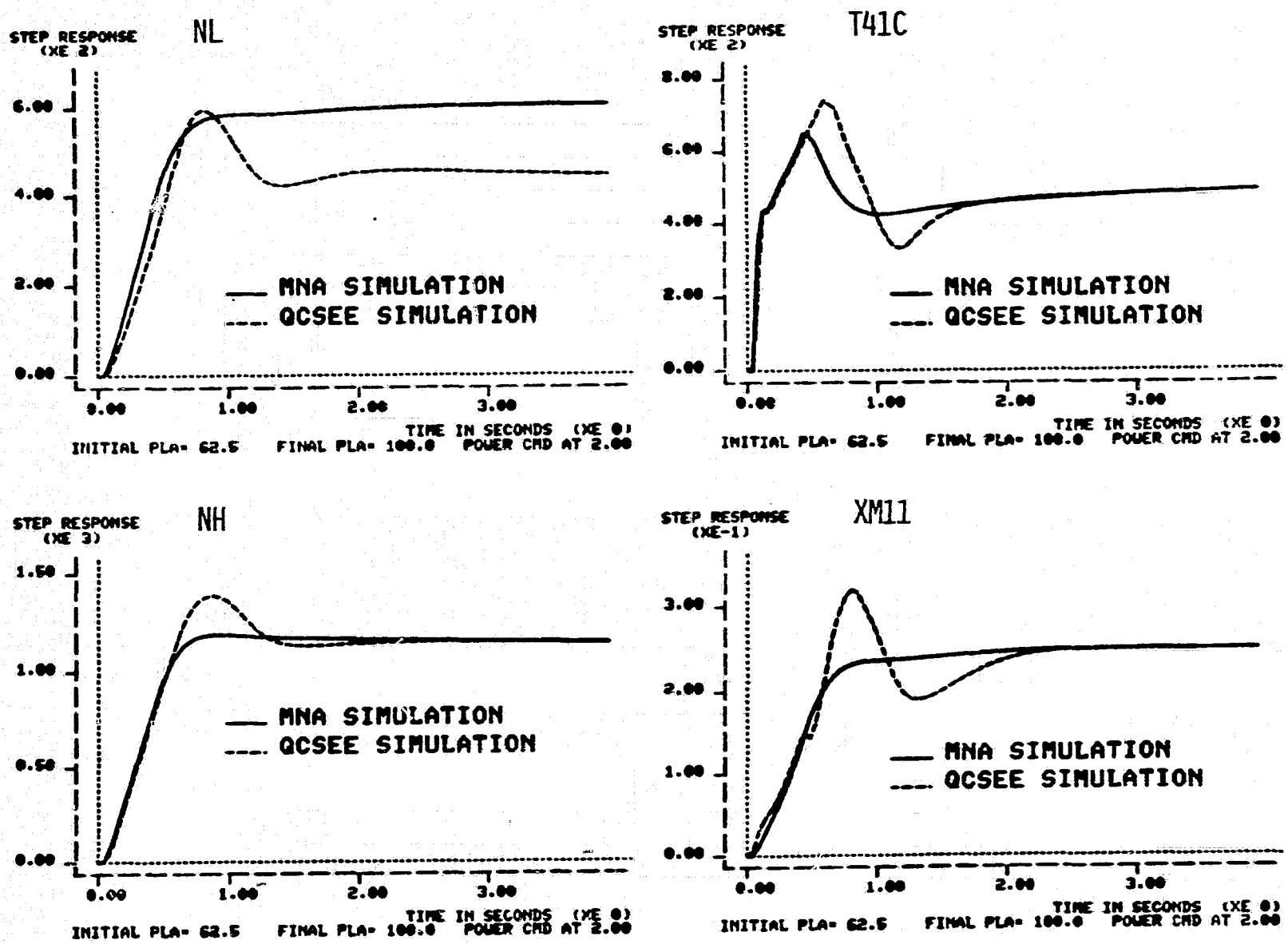

FIGURE 18D: SISO MNA WITH GE-X18 CONTROL - FULL QCSEE - 62.5-100%

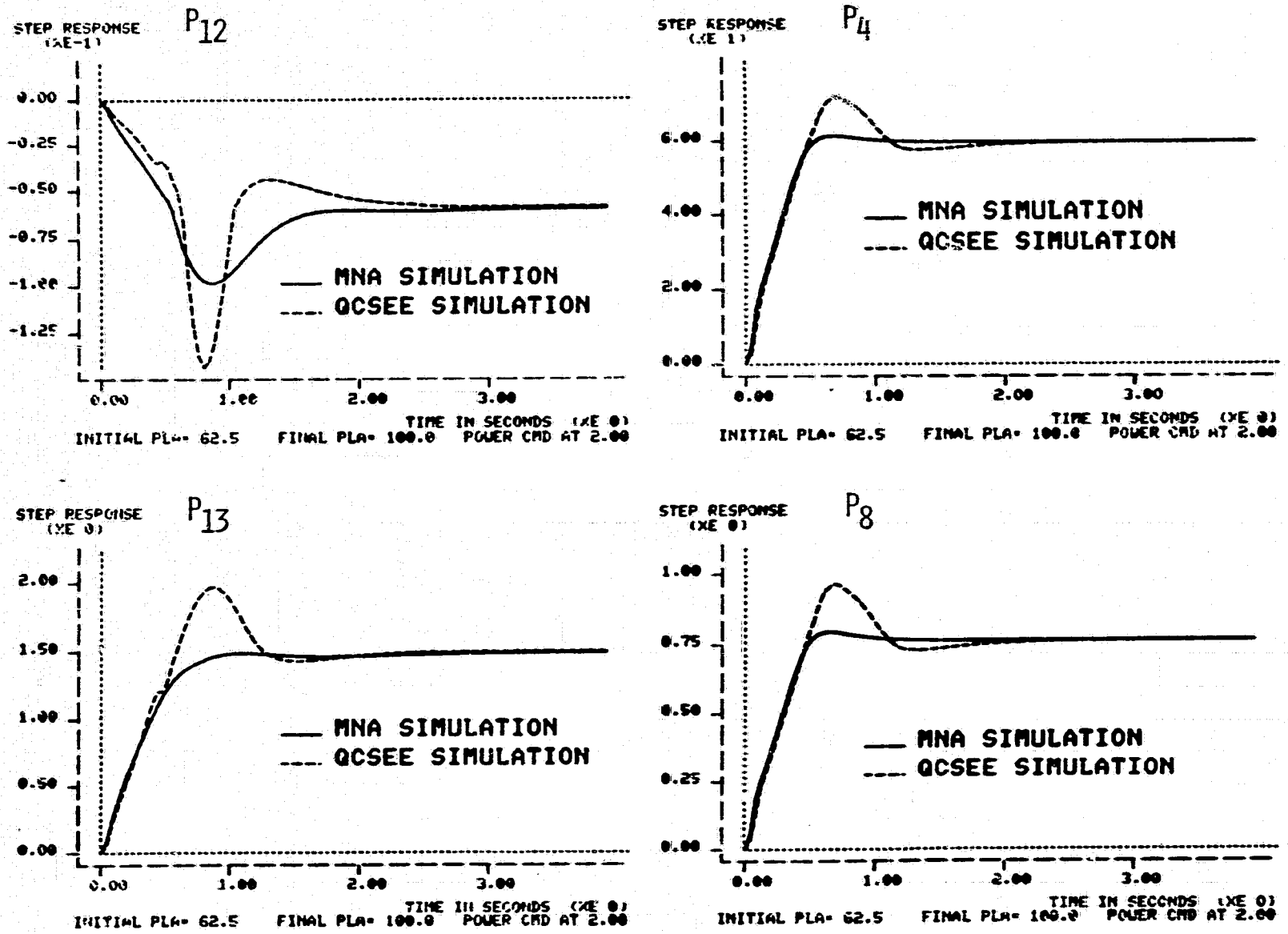

FIGURE 19A: 2x2 MNA WITH GE NOZZLE AREA - FULL GE CONTROL 62.5-100%

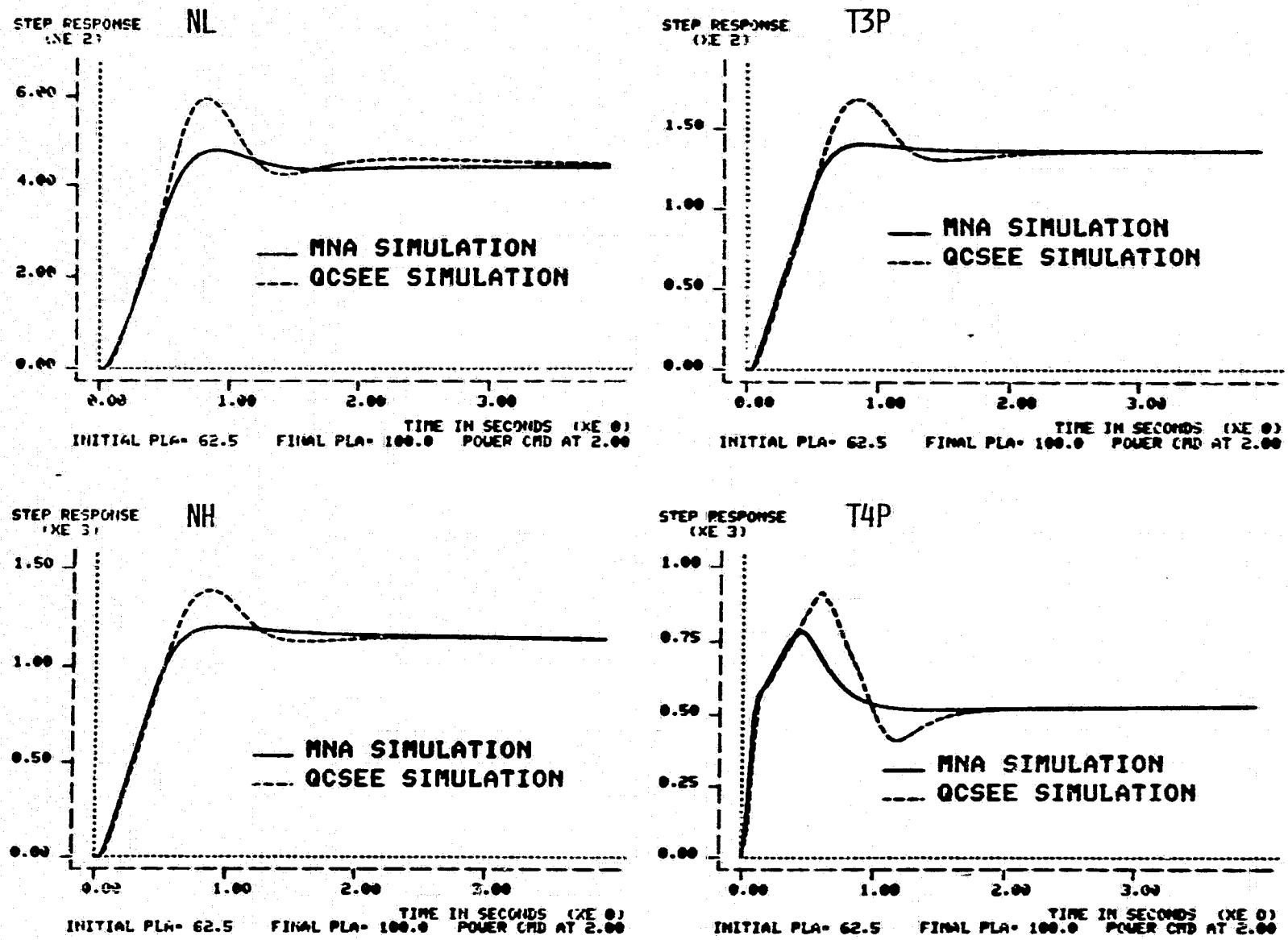

FIGURE 19B: 2x2 MNA WITH GE NOZZLE AREA - FULL GE CONTROL 62.5-100%

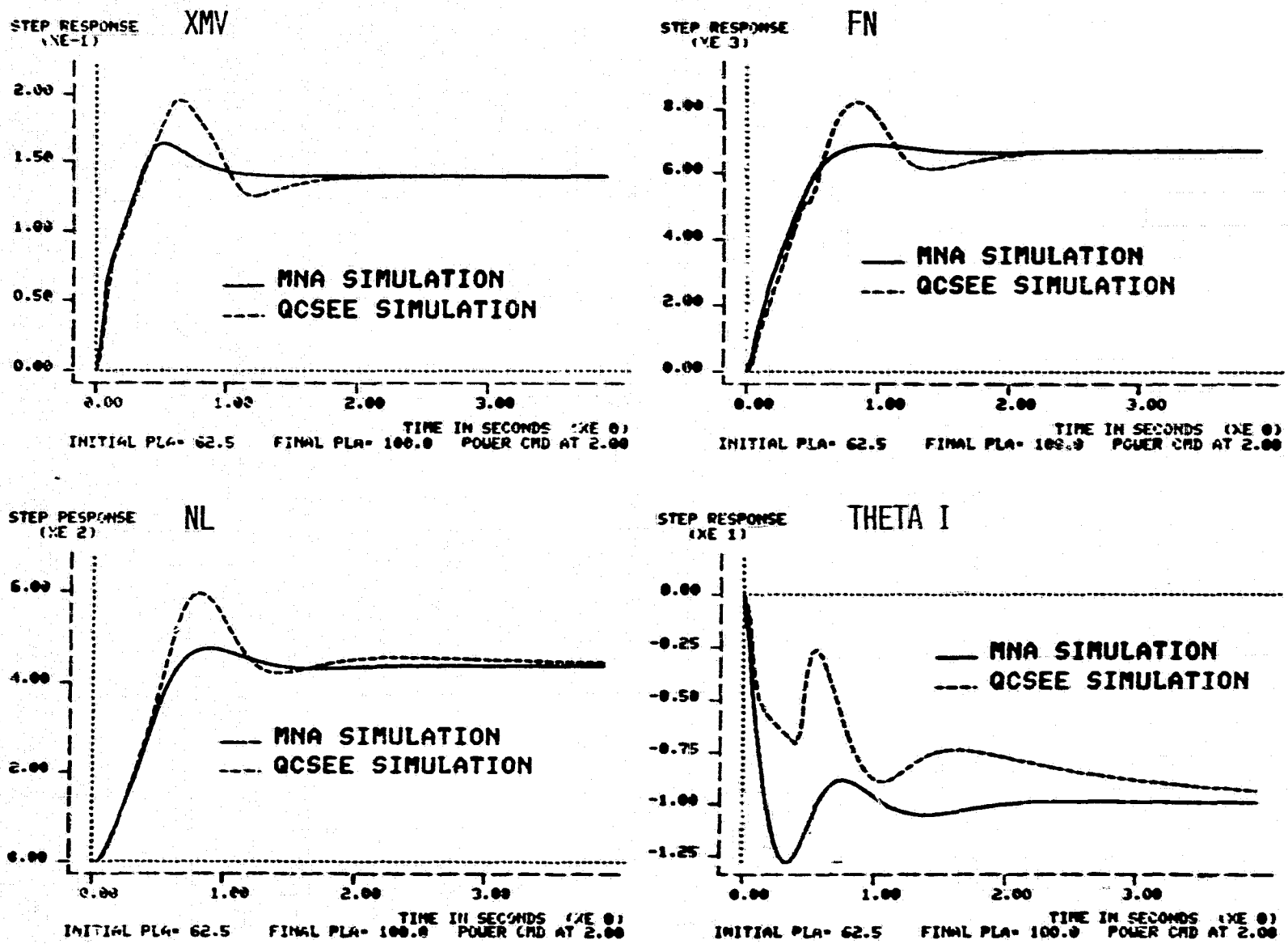

FIGURE 19C: 2X2 MNA WITH GE NOZZLE AREA - FULL GE CONTROL 62.5-100%

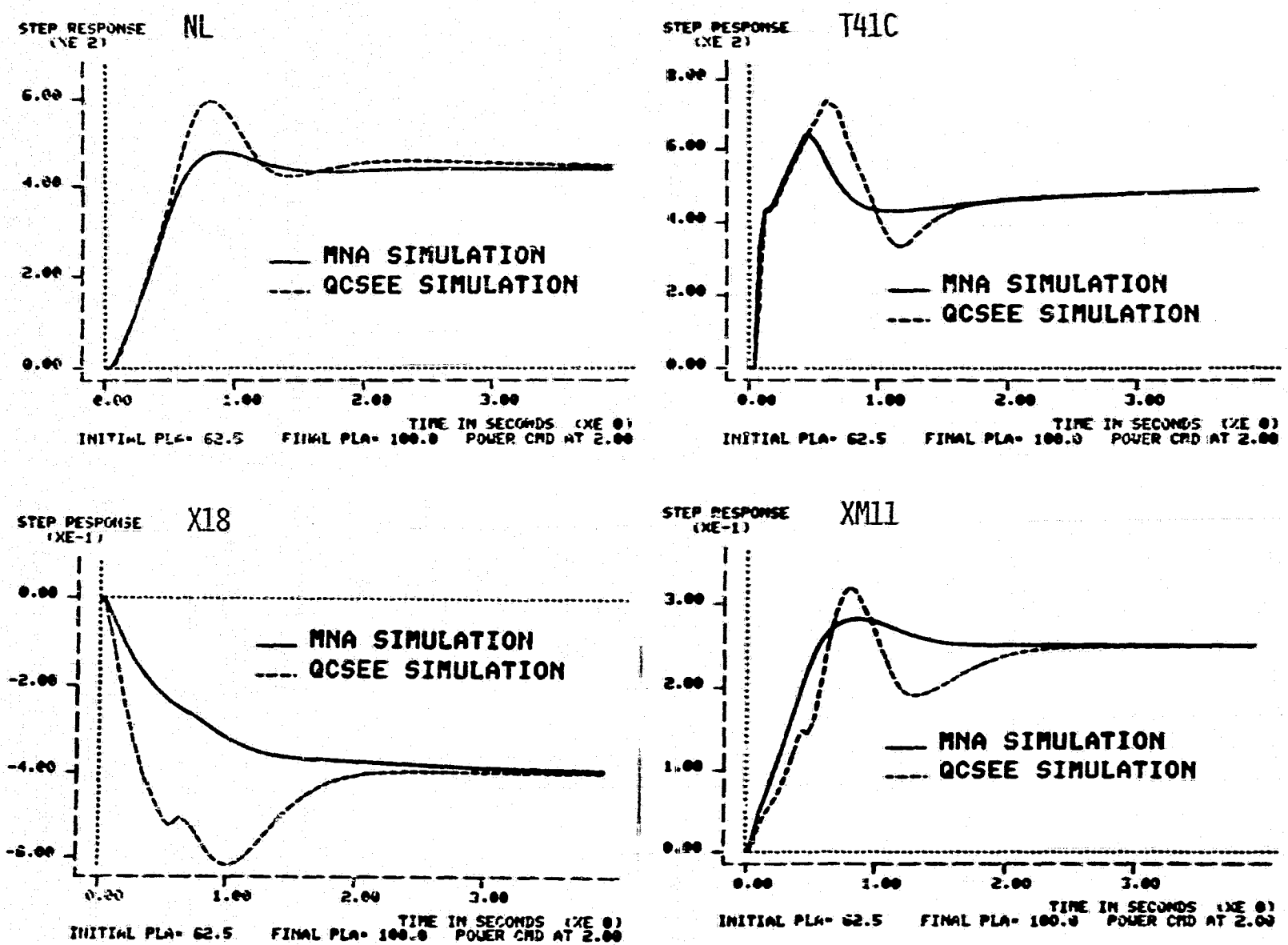

FIGURE 19D: 2x2 MNA WITH GE NOZZLE AREA - FULL GF CONTROL 62.5-100%

chosen as

$$u(t) = \begin{bmatrix} X_{mv} \\ X_{18} \\ \text{Theta I} \end{bmatrix} \qquad y(t) = \begin{bmatrix} N_L \\ P_{12} \\ P_4 \end{bmatrix}$$

where X_{18} is nozzle area and P_{12} is inlet duct pressure.

For this case, system dominance was easily obtained for each linearized operating point in Appendix A. The CAD procedure of [18, 22] resulted in the following compensators when $0.1 < \omega < 40$ radians at the 90% power point

$$K = \begin{bmatrix} .2032E\text{-}4 & -.01856 & 0.00157 \\ .0300 & -7.9359 & -.02023 \\ .0289 & 103.67 & -.001195 \end{bmatrix}$$

$$L = \text{Diag}\{0.0415,\ 71.455,\ 0.4523\}$$

$$F = \text{Diag}\{10.0,\ 0.1,\ 20.0\}$$

The corresponding DNA, Image, and Bode diagrams for this operating point are presented in Figures 20-22.

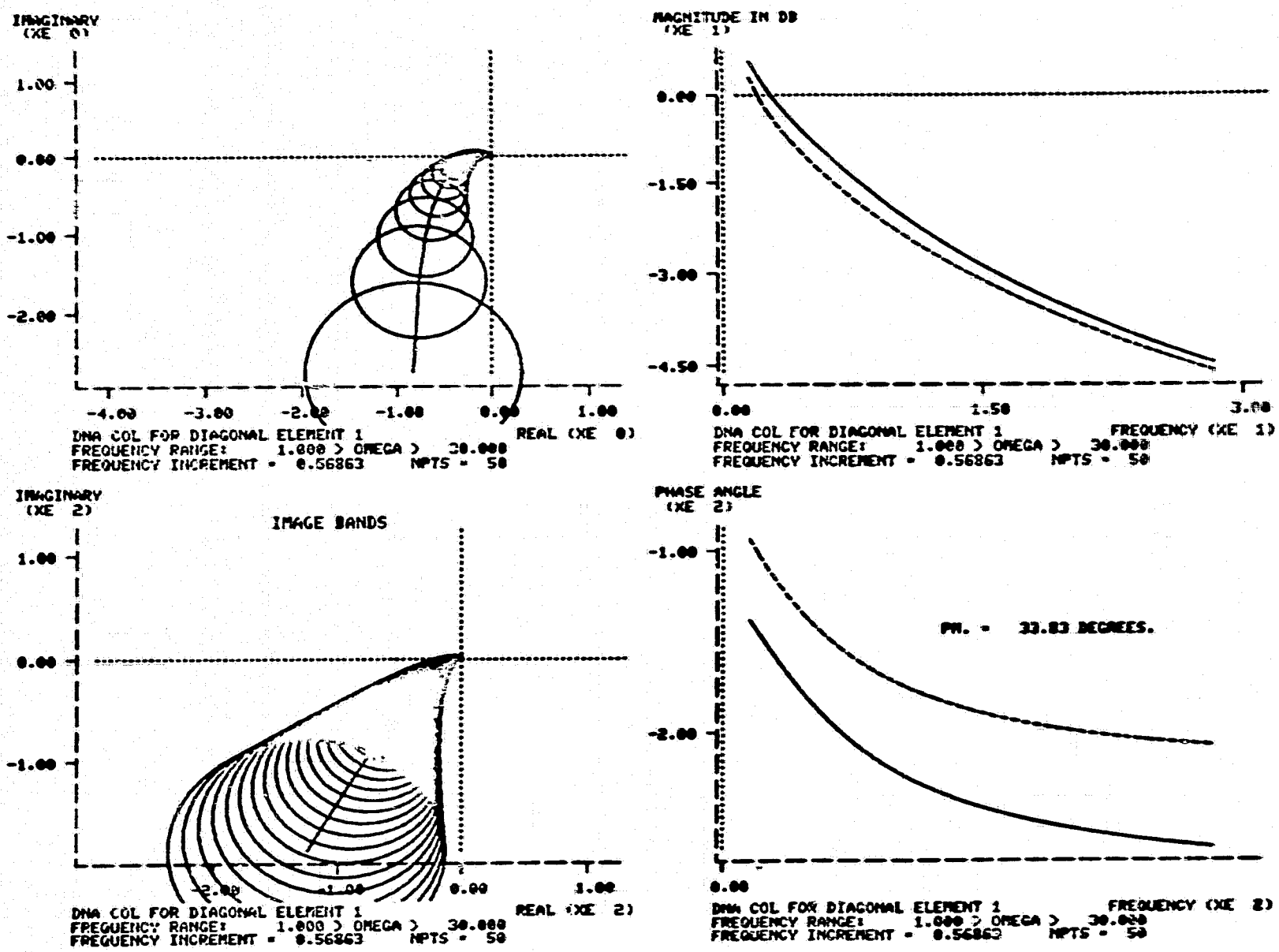

FIGURE 20: CONTROL LOOP 1

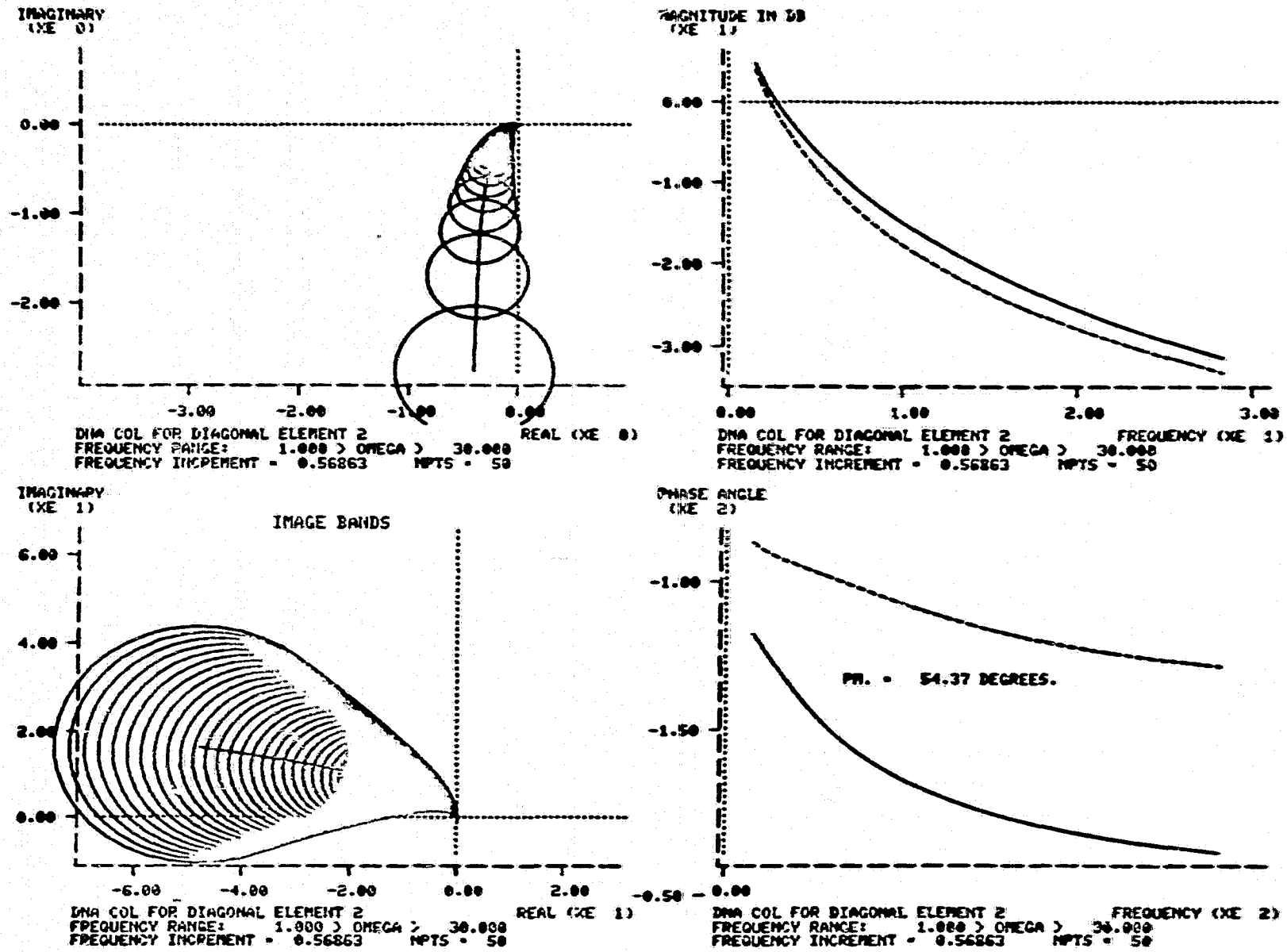

FIGURE 21: CONTROL LOOP 2

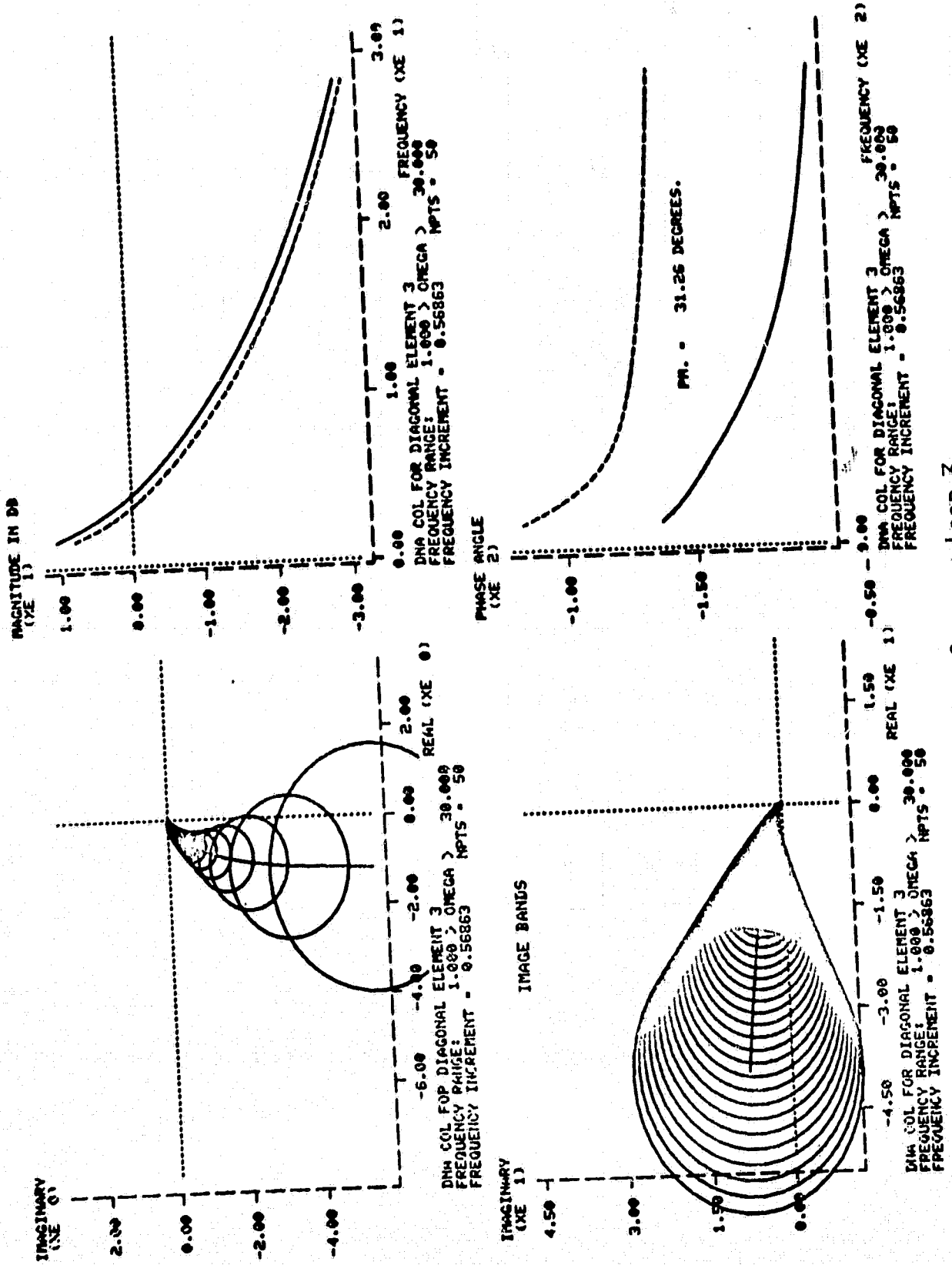

C-2

FIGURE 22: CONTROL LOOP 3

The MNA designs discussed above demonstrate the utility of the design concept in achieving good turbofan engine performance. The full potential of the Bode and Nichols concepts for multivariable plants were not fully utilized in this design application, however, as dynamic compensators were not required. In each case, appropriately determined constant compensators provided adequate closed loop system performance and feedback gain scheduling was not needed. This desirable condition is due principally to the well behaved and easily controlled dynamic system structure.

REFERENCES

1. Sobey, A. and Suggs, A., Control of Aircraft and Missile Powerplants, Wiley and Son, Inc., 1963.

2. Michael, G. and Farrar, F., "Development of Optimal Control Modes for Advanced Technology Propulsion Systems," UARL Report M9-11620-1, 1973.

3. Michael, G. and Farrar, F., "Identification of Multivariable Gas Turbine Dynamics from Stochastic Input-Output Data," UARL Report R 941620-3.

4. Stone, C., Miller, N., Ward, M., and Schmidt, R., "Turbine Engine Control Synthesis," AFAPL Report TR75, March 1975.

5. Weinberg, M., "A Multivariable Control for the F100 Engine Operating at Sea Level Static," ASD-TR-75-28, November 1975.

6. Merrill, W. and Leinginer, G., "Identification and Dual Adaptive Control of a Turbojet Engine," IFAC Symposium on Identification and System Parameter Estimation, Darmstadt, September 1979.

7. DeHoff, R. and Hall, W., "Multivariable Control Design Principles with Application to the F100 Turbofan Engine," JACC, Purdue, 1976.

8. DeHoff, R. and Hall, W., "Design of Multivariable Controller for an Advanced Turbofan Engine," 1976 CDC, Clearwater Beach, Florida.

9. DeHoff, R. and Hall, W., "Multivariable Design Procedures for the F100 Turbofan Engine," Final Report Contract Number F33615-75-C-2053, Systems Control, Inc., Palo Alto, California, January 1977.

10. DeHoff, R. and Hall, W., "A Turbofan Engine Controller Utilizing Multivariable Feedback," IFAC MVTS Symposium, Fredericton, Canada, 1977.

11. DeHoff, R. and Hall, W., "System Identification Principles Applied to the Control and Fault Diagnosis of the F100 Engine," 1977 JACC, San Francisco.

12. Lehtinen, B., Soeder, J., Costakis, W., and Seldner, K., "Altitude Tests of a Multivariable Control for the F100 Turbofan Engine," NASA Technical Report in preparation.

13. Lehtinen, B., DeHoff, R., and Hackney, R., "Multivariable Control Altitude Demonstration on the F100 Turbofan Engine," Joint Propulsion Control Conference, AIAA 79-1204, June 1979.

14. Sain, M., Peczkowski, J., and Melsa, J., Alternatives for Linear Multivariable Control, NEC. Inc., 1977.

15. QCSEE-UTW Engine Simulation Report, General Electric Company, NASA CR-134914, July 1977.

16. QCSEE-UTW Digital Control System Design Report, General Electric Company, NASA CR-134920, January 1978.

17. Mihaloew, J. and Hart, C., "Real Time Digital Propulsion System Simulation for Manned Flight Simulators," NASA TM-78958, July 1978.

18. Leininger, G., "Diagonal Dominance for Multivariable Nyquist Array Methods Using Function Minimization," Automatica, Vol. 15, pp. 339-345, 1979.

19. Leininger, G., "The Multivariable Nyquist Array - The Concept of Dominance Sharing," in Alternatives for Linear Multivariable Control, Sain et al eds., 1977.

20. Leininger, G., "New Dominance Characteristics for the Multivariable Nyquist Array Method," Int. J. Control, Vol. 30, pp. 459-475, 1979.

21. Leinginer, G. "Multivariable Compensator Design Using Bode Diagrams and Nichols Charts," IFAC CAD of Control Systems Symposium, Zurich, 1979.

22. Leininger, G., "An Interactive Design Suite for the Multivariable Nyquist Array Method," IFAC CADCS Symposium, Zurich, 1979.

23. Rosenbrock, H., "Design of Multivariable Control Systems Using the Inverse Nyquist Array," Proc. IEE, Vol. 116, 1968.

24. Rosenbrock, H., Computer Aided Design of Control Systems, Academic Press, 1974.

25. Fisher, D. G., and Kuon, J., "Comparison and Experimental Evaluation of Multivariable Frequency Domain Design Techniques," IFAC MVTS Symposium, Fredericton, Canada, 1977.

26. Ostrowski, A., "Note on Bounds for Determinants with Dominant Principal Diagonal," Proc. Am Math.Soc., Vol. 3, pp. 26-30, 1952.

27. Crossley, T. R., "Envelope Curves to Inverse Nyquist Array Diagrams," Int. J. Control, Vol. 22, 1975.

28. Daniele, C. and Krosel, S., "Generation of Linear Dynamic Models from a Digital Nonlinear Simulation," NASA Technical Paper 1388, February 1979.

APPENDIX A

LINEAR MODELS FOR THE QCSEE ENGINE

1. 62.5% power level - Model includes actuator states.
2. 70% power without actuator states.
3. 80% power without actuator states.
4. 90% power without actuator states.
5. 100% power without actuator states.

PLA = 62.5

INPUT MATRIX A=

```
-0.105E+02 0.292E+00 0.000E+00 0.000E+00-0.132E-02 0.000E+00
 0.000E+00 0.000E+00-0.608E-01 0.103E-03 0.180E-01
 0.107E-02-0.169E+02 0.000E+00 0.000E+00 0.326E-01-0.101E-02
 0.000E+00 0.000E+00 0.133E+01-0.709E+01-6.446E+00
 0.850E+02 0.588E+01-0.125E+02 0.000E+00 0.000E+00 0.431E+00
 0.401E-01 0.388E-01 0.199E+04 0.569E-02-0.391E-04
 0.102E+01 0.708E-01-0.410E-01-0.995E+01 0.000E+00 0.519E-02
 0.483E-03 0.468E-03 0.241E+02 0.632E-06-0.440E-06
 0.895E+03-0.799E+03 0.338E+01-0.144E+03-0.214E+01 0.905E+00
 0.205E+00 0.199E+00 0.101E+05 0.371E+00 0.293E+02
 0.711E+02 0.909E+02-0.633E+02-0.283E+02 0.000E+00-0.685E+02
-0.170E+01 0.643E+00 0.330E+05 0.108E+00-0.179E-02
-0.730E+01 0.177E+01 0.552E+00 0.000E+00 0.000E+00 0.118E-05
-0.276E+00 0.000E+00-0.732E+02-0.196E+00 0.342E-02
-0.138E+02 0.334E+01-0.601E+01 0.000E+00 0.000E+00 0.794E-06
 0.972E-01-0.619E+00 0.473E+04-0.214E+00 0.382E-02
 0.000E+00 0.000E+00 0.000E+00 0.000E+00 0.000E+00 0.000E+00
 0.000E+00 0.000E+00 0.000E+00 0.000E+00 0.000E+00
 0.000E+00 0.000E+00 0.000E+00 0.000E+00 0.000E+00 0.000E+00
 0.000E+00 0.000E+00 0.000E+00 0.000E+00 0.000E+00
 0.000E+00 0.000E+00 0.000E+00 0.000E+00 0.000E+00 0.000E+00
 0.000E+00 0.000E+00 0.000E+00 0.000E+00 0.000E+00
```

INPUT MATRIX B=

```
 0.000E+00 0.000E+00 0.000E+00
 0.000E+00 0.000E+00 0.000E+00
 0.000E+00 0.000E+00 0.000E+00
 0.000E+00 0.000E+00 0.000E+00
 0.000E+00 0.000E+00 0.000E+00
 0.000E+00 0.000E+00 0.000E+00
 0.000E+00 0.000E+00 0.000E+00
 0.000E+00 0.000E+00 0.000E+00
 0.100E+01 0.000E+00 0.000E+00
 0.000E+00 0.100E+01 0.000E+00
 0.000E+00 0.000E+00 0.100E+01
```

THE MATRICES FOR THIS OPERATING POINT INCLUDE THREE STATE VARIABLES ASSOCIATED WITH INTEGRAL CONTROL ACTION (I.E. ACTUATOR STATES)

PLA = 70

INPUT MATRIX A=

```
-0.105E+02 0.277E+00 0.000E+00 0.000E+00-0.147E-02 0.000E+00
 0.000E+00 0.000E+00
 0.993E+01-0.159E+02 0.000E+00 0.000E+00 0.334E-01-0.991E-03
 0.000E+00 0.000E+00
 0.881E+02 0.888E+01-0.126E+02 0.000E+00 0.000E+00 0.411E+00
 0.415E-01 0.402E-01
 0.112E+01 0.113E+00-0.440E-01-0.994E+01 0.000E+00 0.523E-02
 0.529E-03 0.512E-03
 0.970E+03-0.854E+03 0.255E+01-0.151E+03-0.220E+01 0.889E+00
 0.220E+00 0.213E+00
 0.797E+02 0.824E+02-0.639E+02-0.157E+02 0.000E+00-0.717E+00
-0.176E+01 0.668E+00
-0.777E+01 0.212E+01 0.523E+00 0.000E+00 0.000E+00 0.787E-04
-0.290E+00 0.000E+00
-0.147E+02 0.400E+01-0.620E+01 0.000E+00 0.000E+00 0.592E-04
 0.102E+00-0.651E+00
```

INPUT MATRIX B=

```
-0.579E-01 0.360E-03 0.204E-01
 0.103E+01-0.778E+01-0.463E+00
 0.201E+04-0.154E+00 0.251E-02
 0.257E+02-0.172E-02 0.283E-04
 0.106E+05-0.441E+01 0.306E+02
 0.334E+05 0.483E+01-0.755E-01
 0.496E+02-0.236E+02 0.369E+00
 0.497E+04-0.189E+02 0.294E+00
```

```
    PLA = 80


INPUT MATRIX A=
-0.105E+02 0.241E+00 0.000E+00 0.000E+00-0.166E-02 0.000E+00
 0.000E+00 0.000E+00
 0.832E+01-0.140E+02 0.000E+00 0.000E+00 0.310E-01-0.946E-03
 0.000E+00 0.000E+00
 0.934E+02 0.129E+02-0.126E+02 0.000E+00 0.000E+00 0.375E+00
 0.436E-01 0.423E-01
 0.129E+01 0.178E+00-0.479E-01-0.991E+01 0.000E+00 0.519E-02
 0.604E-03 0.585E-03
 0.112E+04-0.964E+03 0.154E+01-0.161E+03-0.205E+01 0.846E+00
 0.242E+00 0.235E+00
 0.107E+03 0.856E+02-0.679E+02 0.629E+01 0.000E+00-0.764E+00
-0.187E+01 0.703E+00
-0.896E+01 0.211E+01 0.573E+00 0.000E+00 0.000E+00 0.962E-04
-0.313E+00 0.000E+00
-0.170E+02 0.399E+01-0.634E+01 0.000E+00 0.000E+00 0.723E-04
 0.110E+00-0.702E+00
INPUT MATRIX B=
-0.446E-01 0.355E-03 0.253E-01
 0.244E+00-0.894E+01-0.471E+00
 0.204E+04-0.210E+00 0.345E-02
 0.284E+02-0.255E-02 0.424E-04
 0.114E+05-0.751E+01 0.313E+02
 0.340E+05 0.955E+01-0.148E+00
 0.102E+03-0.363E+02 0.566E+00
 0.523E+04-0.288E+02 0.449E+00
```

PLA = 90

INPUT MATRIX A=

```
-0.107E+02 0.222E+00 0.000E+00 0.000E+00-0.196E-02 0.000E+00
 0.000E+00 0.000E+00
 0.692E+01-0.124E+02 0.000E+00 0.000E+00 0.256E-01-0.875E-03
 0.000E+00 0.000E+00
 0.989E+02 0.155E+02-0.124E+02 0.000E+00 0.000E+00 0.334E+00
 0.452E-01 0.438E-01
 0.148E+01 0.231E+00-0.501E-01-0.989E+01 0.000E+00 0.499E-02
 0.677E-03 0.655E-03
 0.126E+04-0.107E+04 0.118E+01-0.172E+03-0.172E+01 0.793E+00
 0.266E+00 0.258E+00
 0.167E+03 0.112E+03-0.764E+02 0.295E+02 0.000E+00-0.787E+00
-0.195E+01 0.731E+00
-0.111E+02 0.123E+01 0.776E+00 0.000E+00 0.000E+00 0.960E-04
-0.334E+00 0.000E+00
-0.210E+02 0.231E+01-0.622E+01 0.000E+00 0.000E+00 0.721E-04
 0.117E+00-0.748E+00
```

INPUT MATRIX B=

```
-0.393E-01 0.533E-03 0.333E-01
-0.845E+00-0.101E+02-0.434E+00
 0.207E+04-0.231E+00 0.397E-02
 0.310E+02-0.303E-02 0.527E-04
 0.123E+05 0.321E+00 0.292E+02
 0.345E+05 0.154E+02-0.2[illegible]E+00
 0.122E+03-0.459E+02 0.732E+00
 0.546E+04-0.365E+02 0.582E+00
```

PLA = 100

INPUT MATRIX A=

```
-0.128E+02 0.124E+01 0.000E+00 0.000E+00-0.915E-02 0.000E+00
 0.000E+00 0.000E+00
 0.120E+02-0.158E+02 0.000E+00 0.000E+00 0.442E-01-0.887E-03
 0.000E+00 0.000E+00
 0.108E+03 0.147E+02-0.123E+02 0.000E+00 0.000E+00 0.295E+00
 0.464E-01 0.449E-01
 0.173E+01 0.236E+00-0.521E-01-0.987E+01 0.000E+00 0.474E-02
 0.745E-03 0.721E-03
 0.991E+03-0.840E+03 0.844E+00-0.190E+03-0.297E+01 0.769E+00
 0.301E+00 0.292E+00
 0.247E+03 0.127E+03-0.843E+02 0.538E+02 0.000E+00-0.848E+00
-0.202E+01 0.753E+00
-0.139E+02 0.646E+00 0.971E+00 0.000E+00 0.000E+00 0.925E-04
-0.352E+00 0.000E+00
-0.263E+02 0.122E+01-0.613E+01 0.000E+00 0.000E+00 0.669E-04
 0.124E+00-0.790E+00
```

INPUT MATRIX B=

```
-0.801E+01-0.173E+00 0.115E+00
 0.127E+00-0.133E+02-0.554E+00
 0.208E+04-0.304E+00 0.441E-02
 0.335E+02-0.425E-02 0.629E-04
 0.136E+05 0.283E-01 0.373E+02
 0.349E+05 0.313E+02-0.413E+00
 0.138E+03-0.712E+02 0.944E+00
 0.567E+04-0.543E+02 0.720E+00
```